Universidad Zaragoza
1542

Trabajo Fin de Grado

Diseño de modelos de simulación con control automático para plantas de tratamiento de aguas
Design of simulation models with automatic control of wastewater treatment plants

Autor/es

Jesús Caravaca Vilchez

Director/es

Dr. Javier Murillo Castarlenas

Escuela de Ingeniería y Arquitectura

2018

Diseño de modelos de simulación con control automático para plantas de aguas de tratamiento de aguas residuales

RESUMEN

En este trabajo de fin de grado, a través de la simulación numérica, se simula el funcionamiento transitorio de una planta de tratamiento de aguas residuales, concretamente del tratamiento secundario de la misma. Los equipos fundamentales del tratamiento secundario son: reactores biológicos, decantador secundario, línea de recirculación, línea de purga, espesador y deshidratador. Para poder reproducir la función de estos equipos se requiere de un modelo matemático hidrodinámico y biológico acoplados. Una parte fundamental de este trabajo es la comprensión de modelos biológicos que tratan de describir las reacciones que se llevan a cabo en el interior del reactor biológico. En estos modelos se detallan los componentes que están presentes en estos sistemas, así como los procesos biológicos que se llevan cabo en su interior. El elevado número de elementos químicos presentes (13), orgánicos e inorgánicos, así como el conjunto de reacciones químicas y transformaciones a modelar no lineales (8) hacen del conjunto final un sistema altamente no lineal.

Una vez elegido el modelo biológico que será empleado, conocido como modelo de lodos activados (ASM), es necesario programar el modelo hidrodinámico 0D, que permita establecer las conexiones entre los equipos mencionados. Aunque este modelo no permite apreciar las diferencias de concentración en el espacio de un mismo equipo, el principal problema es el acoplamiento entre ambos modelos, biológico e hidrodinámico, pues el número de variables a calibrar es alto, en particular cuando se tratan de definir los mecanismos de regulación de la planta.

Para llegar a un diseño que emule la realidad, en esta memoria se procede a la simulación de varias configuraciones de plantas de tratamiento aguas residuales, a las cuales se irán añadiendo cada uno de los equipos mencionados anteriormente hasta completar el diseño final. Cada equipo aporta una variación en el funcionamiento de la planta que será estudiado con detalle, haciendo hincapié en las relaciones entre componentes. A su vez, se realizará una comparativa entre los resultados de una de las configuraciones y los proporcionados por el programa comercial Linx ASM1. El modelo aquí desarrollado tendrá prestaciones superiores ya que cuenta con la simulación de los procesos en el decantador secundario.

Parte del trabajo de fin de grado se centra en la simulación de una planta de tratamiento de aguas residuales con control automático, reproduciendo la complejidad de los mecanismos de oxigenación gobernados por la velocidad de rotación de los equipos de aireación. En esta parte del trabajo, la regulación de la purga y el control automático amonio-oxígeno se incluirán en los modelos desarrollados de la parte anterior. A continuación, se realizará una comparativa entre la información proporcionada por la planta de tratamiento de aguas residuales Río Huerva y los resultados proporcionados por la simulación del modelo con control automático. El realismo en la simulación se aumentará al incluir en la simulación anterior un modelo de decantador secundario más sofisticado, donde el flujo y las especies transportadas serán calculadas asumiendo variaciones temporales y espaciales en la vertical mediante un modelo 1D. También se realizará de nuevo la comparativa con la información anterior.

A este trabajo de fin de grado le acompañan una serie de anexos que desarrollan con detalle el modelo matemático necesario para simular el funcionamiento de la planta de tratamiento de aguas residuales. En primer lugar, incluye una descripción del modelo biológico aplicado. Posteriormente, describe con detalle cada una de las configuraciones empleadas en la primera parte del trabajo. A su vez, incluye toda la información proporcionada por la planta de aguas residuales Río Huerva. Seguidamente, describe con detalle los modelos de simulación con control automático, incluyendo el modelo del decantador más sofisticado. Por último, incluye las conclusiones de ambas partes de trabajo.

TRABAJOS DE FIN DE GRADO / FIN DE MÁSTER

Escuela de Ingeniería y Arquitectura Universidad Zaragoza

DECLARACIÓN DE AUTORÍA Y ORIGINALIDAD

(Este documento debe acompañar al Trabajo Fin de Grado (TFG)/Trabajo Fin de Máster (TFM) cuando sea depositado para su evaluación).

D./Dª. Jesús Caravaca Vilchez,

con nº de DNI 48621206B en aplicación de lo dispuesto en el art. 14 (Derechos de autor) del Acuerdo de 11 de septiembre de 2014, del Consejo de Gobierno, por el que se aprueba el Reglamento de los TFG y TFM de la Universidad de Zaragoza,

Declaro que el presente Trabajo de Fin de (Grado/Máster) Grado, (Título del Trabajo) Diseño de modelos de simulación con control automático para plantas de tratamiento de aguas residuales,

es de mi autoría y es original, no habiéndose utilizado fuente sin ser citada debidamente.

Zaragoza, 27 de Agosto de 2018

Fdo: Jesús Caravaca Vilchez

AGRADECIMIENTOS

Tras de siete meses de trabajo y dedicación, hoy escribo este apartado de agradecimientos para finalizar mi trabajo de fin de grado. Ha sido un periodo de aprendizaje en el ámbito de la investigación, así como de enriquecimiento personal. La realización del presente trabajo supone el mayor proyecto al que me he enfrentado en mi vida académica. Por ello, me gustaría agradecer a todas aquellas personas que me han acompañado y apoyado durante este periodo.

En primer lugar, me gustaría agradecer al grupo de hidráulica computacional de la Universidad de Zaragoza, en concreto a Pilar García Navarro, por concederme una beca de colaboración extracurricular en actividades de investigación. Además, me gustaría dar las gracias a mi tutor, J. Murillo, y a A. Navas por su extraordinaria ayuda y por brindarme todas las herramientas necesarias para completar el trabajo. Me gustaría agradecer a la empresa Aguas de Valencias S.A. y a la Estación Depuradora de Aguas Residuales Río Huerva por asesorarme y facilitarme información útil para el desarrollo del trabajo.

Por último, me gustaría agradecer a mi padre y a mi madre por el incesante apoyo y el cariño que me demuestran día a día. Sin ellos nada de esto hubiera sido posible.

¡Muchas gracias a todos!

Índice general

1. Introducción **9**

1.1. Estado del arte 9

1.2. Motivación 10

1.3. Contenidos del trabajo 10

1.4. Objetivos 12

2. Modelo biológico **13**

2.1. Cinética de los procesos de crecimiento microbiano 13

2.2. ASM1 14

3. Simulación de 5 configuraciones de planta de tratamiento de aguas residuales **17**

3.1. Modelos de simulación 17

3.1.1. Resultados y conclusiones de las simulaciones 20

3.2. Comparativa con el programa comercial Linx ASM1 22

4. Simulación de plantas de tratamiento de aguas residuales con control automático **25**

4.1. Control de la planta de tratamiento de aguas residuales Río Huerva 25

4.1.1. Regulación de la purga 25

4.1.2. Control oxígeno-amonio 26

4.2. Modelos de simulación con control automático 29

4.3. Conclusiones generales 32

5. Conclusiones **35**

Bibliografía **35**

Lista de imágenes **39**

Lista de tablas **43**

A. Biological modelling **45**

A.1. Kinetics of the microbial-growth processes . . . 45

A.2. The Activated Sludge Model No. 1 (ASM1) model . . . 46

A.2.1. Type of components in the model . . . 46

A.2.2. Measurement of the components . . . 46

A.2.3. Definition of the components . . . 46

A.2.4. Equations of the ASM1 model . . . 47

B. Modelling of the water treatment plant vs. Linx ASM1 **51**

B.1. Model 1 . . . 51

B.2. Model 2 . . . 52

B.3. Model 3 . . . 54

B.4. Model 4 . . . 56

B.5. Model 5 . . . 59

B.6. ASM1 results . . . 65

B.6.1. Influent analysis . . . 65

B.6.2. Test case 1: Model 1 ($r = 0$) . . . 67

B.6.3. Test case 2: Model 2 ($r = 1$) . . . 69

B.6.4. Test case 3: Model 3 ($r = 1$, $p = 0{,}02$) . . . 72

B.6.5. Test case 4: Model 4 ($r = 1$, $p = 0{,}02$, $\eta_s = 0{,}96$, $f_{el} = 0{,}8$) . . . 75

B.6.6. Test case 5: Model 5 ($r = 1$, $p = 0{,}02$, $\eta_s = 0{,}96$, $f_{el} = 0{,}8$, $\eta_d = 0{,}96$, $f_d = 0{,}8$) . . . 78

B.6.7. Effluent analysis . . . 82

B.7. Analysis of the results . . . 84

B.7.1. Analysis of models . . . 84

B.7.2. General conclusions . . . 84

B.8. Comparison with Linx ASM1 example Model . . . 86

B.8.1. Characterization of the example model . . . 86

B.8.2. Results of the example Model 87
B.8.3. Numerical comparison 93
B.9. Study on the sensitivity of the concentration of dissolved oxygen in the reactors and purge flow 94

C. Wastewater treatment plant simulation with automatic control **97**
C.1. Experimental data 97
C.2. Purge regulation 101
C.3. Oxygen-ammonium automatic control 103
C.3.1. Oxygen-ammonium alternative control 108
C.4. Models with automatic control 108
C.4.1. Model simulation including mass storage 109
C.4.2. Model simulation including mass storage and ASM1 processes in the clarifier . . . 112
C.4.3. Model simulation taking into account clarifier characterization 115
C.5. Initial conditions 125
C.6. Results 127
C.7. Conclusions 135

Capítulo 1

Introducción

1.1. Estado del arte

El proceso de lodos activados es ampliamente usado en plantas de tratamiento de aguas residuales para reducir los niveles de sustancias contaminantes del efluente, las cuales provienen fundamentalmente del sector industrial y municipal [1]. En el proceso de lodos activados aparecen una gran variedad de microorganismos capaces de degradar la materia orgánica, disminuir el contenido de nutrientes y transformar componentes tóxicos en productos inocuos. Por tanto, en el diseño de plantas de tratamiento de aguas residuales es fundamental entender la estructura microbiana y los procesos más importantes del tratamiento de lodos activados.

Durante las últimas décadas, muchos autores han intentado desarrollar modelos biológicos para caracterizar la estructura y función de los procesos microbianos, así como de los microorganismos fundamentales que los gobiernan [2]. En 1987, el Modelo Lodos Activados No. 1 (ASM1) fue presentado por la IAWQ (International Association on Water Quality). Este modelo describe la demanda de nitrógeno y oxígeno en los procesos de crecimiento microbiano, incluyendo los mecanismos de nitrificación, desnitrificación y eliminación de la materia orgánica [3]. Posteriormente, el conocimiento básico de las bacterias que eliminan el fósforo se incluyó en el modelo $ASM1$ y los parámetros se ajustaron en consecuencia, de manera que en 1995 se publicó el modelo $ASM2$ [4]. Los modelos $ASM1$ y $ASM2$, o modelos basados en ASM, están incluidos en la mayoría de los programas de simulación comercial y no comercial de la actualidad.

Para representar estos procesos biológicos se requiere de la utilización y diseño de programas informáticos de simulación que permitan obtener mejoras en los procesos y automatizar el diseño de las plantas de tratamiento de aguas residuales. Los modelos matemáticos de lodos activados, como ASM1, se centran principalmente en la microbiología, a menudo ignorando la hidrodinámica del sistema. El diseño de modelos hidrodinámicos que permitan ser acoplados a modelos de lodos activados sigue siendo una cuestión poco desarrollada en la actualidad [5].

La mayoría de los autores se centran en la simulación de uno de los equipos de las plantas de tratamiento de aguas residuales, sobretodo de los decantadores secundarios [6] [7] y de los reactores biológicos [9]. Otros autores, en cambio, describen de forma general los principios teóricos y procedimientos de diseño de las operaciones bioquímicas presentes en los procesos de tratamiento de aguas residuales [10]. En este trabajo se llevan a cabo simulaciones de todos los equipos del tratamiento secundario en conjunto, poniendo en práctica los procedimientos de diseño que describen autores como [4] o [7]. Por ejemplo, la línea de recirculación y purga de fangos son elementos tratados en este trabajo que no suelen incluirse en las simulaciones, pese a que son de especial importancia para el control de los sólidos en suspensión y nivel de bacterias en los reactores biológicos. Una parte del presente trabajo ha sido documentada con información proporcionada por la planta de tratamiento de aguas residuales Río Huerva, con objeto de simular el funcionamiento real de la planta completa y así predecir su comportamiento frente a situaciones transitorias y situaciones extremas de vertido, rotura de equipos, etc.

1.2. Motivación

El modelado es una parte inherente del diseño de plantas de tratamiento de aguas residuales. Estos modelos son meramente conceptuales, con el fin de reducir la complejidad del sistema. Para un diseño óptimo de plantas de aguas residuales es fundamental comprender los procesos hidrodinámicos y biológicos, así como su interacción, que tienen lugar en el circuito de lodos activados y en el decantador. Para ello, es interesante desarrollar en primer lugar una herramienta matemática con lenguaje C++ que permita modelizar estos sistemas de la manera más clara posible. Esta herramienta permitirá comprender y optimizar los procesos que se llevan a cabo en los equipos que conforman la planta de aguas residuales, con objeto de mejorar el funcionamiento global de la misma.

1.3. Contenidos del trabajo

En este trabajo se modelizarán los elementos que forman parte del tratamiento secundario de una planta de aguas residuales, de manera que se acerque de la mejor manera posible a la realidad. Entre los elementos que se simularán se encuentran:

- Los reactores biológicos, que son los que principalmente se encargan de reducir los niveles de materia orgánica, componentes nitrogenados y componentes fosforosos [1]. Existen numerosas geometrías para este equipo, aunque la más usual es la geometría ovalada. Las plantas de aguas residuales suelen constar de tres de estos reactores. El primero de ellos, el exterior, consta de un vehiculador, el cual se encarga de asegurar la homogenización de la mezcla. El segundo y el tercero, medio e interior, constan de equipos Orbal, los cuales se encargan de aportar el oxígeno necesario para evitar que la concentración de bacterias autótrofas y heterótrofas decrezca y así asegurar que los procesos de eliminación de materia orgánica y nitrificación se sigan llevando a cabo. De la misma forma que el vehiculador, los Orbal también tienen la función de asegurar la homogenización de la mezcla.

- El decantador secundario, situado tras los reactores, de manera que el flujo que abandona del reactor interior entra al decantador. Su función principal es la de separar los componentes particulados o sólidos en suspensión, gracias a la acción de la gravedad [6]. Los sólidos en suspensión, así como los flóculos que se han formado en los reactores, sedimentan en la parte inferior del decantador, mientras que por la parte superior se produce la descarga del efluente o agua tratada. Como se detallará más adelante, parte del caudal que abandona el decantador por su parte inferior es recirculado de nuevo al reactor exterior, con objeto de evitar que la concentración de bacterias autótrofas y heterótrofas decrezca en los reactores.

- El espesador de fangos y el deshidratador, que tienen como función principal eliminar gran porcentaje del agua contenida en el flujo que abandona el decantador por su parte inferior, con objeto de facilitar el transporte del fango sobrante [8].

Se abordarán dos cuestiones bien diferenciadas.

La primera de ellas es la necesidad de desarrollar un modelo acoplado hidrodinámico y biológico de una planta de aguas residuales, con objeto de comprender las relaciones entre especies y determinar la sensibilidad de las variables que lo gobiernan. Inicialmente se desarrollará un modelo hidrodinámico 0D donde se considerará mezcla perfecta en los reactores biológicos y en el decantador, es decir, las concentraciones del licor mezcla son iguales en todo el volumen.

En el reactor, la posición de los elementos auxiliares mencionados anteriormente, como los Orbal, afecta en términos biológicos, pero la mezcla se considera homogénea ya que la sedimentación de sólidos se intenta evitar mediante la presencia de vehiculadores o elementos rotatorios que incrementan el nivel de agitación del fluido para evitar la sedimentación de la materia particulada. La mezcla perfecta en el decantador se considera a través de un modelo conceptual definido a través de un rendimiento. Hay que destacar que, en la realidad, en el decantador, existe una variabilidad entre las concentraciones de la parte superior e inferior del mismo, debido a la sedimentación de los sólidos.

Pese a las simplificaciones, el modelo 0D permite unos tiempos de simulación mucho menores en comparación con modelos 2D más sofisticados, permitiendo la realización de un mayor número de pruebas para su calibración incluyendo procesos transitorios y estacionarios abarcando desde días hasta años. Una vez desarrollado y calibrado el modelo hidrodinámico, el modelo biológico es acoplado. El modelo ASM1, el cual consta de 13 concentraciones y 8 procesos [13], será empleado como modelo biológico. Como se ha comentado anteriormente, los mecanismos fundamentales que incluye este modelo son la eliminación de materia orgánica y la desnitrificación. En una primera aproximación, se asumirá que los procesos del modelo ASM1 únicamente son llevados a cabo en el interior de los reactores. Se ha elegido el modelo biológico más sofisticado posible con el mínimo número de incógnitas, ya que la calibración del modelo completo acoplado de la planta no es trivial. El número de pruebas experimentales necesarias para la implementación de un modelo biológico más sofisticado, como ASM2, sobrepasa el alcance de este trabajo de fin de grado.

Una vez acoplados ambos modelos, hidrodinámico y biológico, se simularán 5 configuraciones de plantas de aguas residuales. Partiendo de la configuración inicial, en la que se incluyen 3 reactores y 1 decantador secundario, se irá añadiendo un elemento adicional en cada configuración, de manera que la quinta configuración constará de 4 elementos adicionales. Entre los elementos adicionales se encuentra la línea de recirculación de fangos, cuya función ya se ha comentado, la línea de purga, cuya función es evitar la acumulación excesiva del particulado en los reactores, el espesador y el deshidratador, cuyas funciones también han sido detalladas. Los resultados de todas las configuraciones serán comparados entre sí, así como correlados con el programa de simulación biológica comercial Linx ASM1, el cual utiliza las mismas hipótesis hidrodinámicas y biológicas que el empleado en esta parte del trabajo.

La segunda de las cuestiones es la necesidad de implementar al modelo anterior un sistema de control automático próximo a la realidad, con objeto de simular y predecir el funcionamiento de una planta de tratamiento de aguas residuales real. Para simular en detalle el decantador secundario se modelizó la sedimentación de los sólidos en el interior del mismo, mediante un modelo transitorio 1D que permite calcular el flujo y la distribución de la materia particulada en la vertical y la sedimentación de materia en el fondo.

Para poder calibrar la simulación de la planta, la empresa Aguas de Valencia proporcionó la siguiente información:

- Datos reales de la planta de aguas residuales Rio Huerva, como algunas concentraciones del efluente, influente (entrada al primer reactor) y reactores. Estos datos sirvieron como condiciones iniciales de las simulaciones que posteriormente se lanzaron. A su vez, sirvieron como valores reales con los que comparar los resultados de estas simulaciones.

- Información relacionada con el control automático y manual que es llevado a cabo en la planta. Esta información permitió la programación de la operación de los Orbal, cuyo objetivo era realizar un control fundamentalmente ligado al proceso de desnitrificación, y de la purga, fundamentalmente ligado al proceso de eliminación de materia orgánica.

- Datos relacionados con la calidad del fango del decantador, con los que posteriormente se modelizó la sedimentación de los sólidos en el interior del mismo.

En esta segunda parte del trabajo, una vez definidas las condiciones iniciales e implementado el control de la planta, se definen 3 modelos diferentes, cuyos resultados posteriormente serán comparados con los datos reales mencionados. Debido a la falta de información real del espesador y deshidratador, no se tendrán en cuenta el agua de retorno a la planta de estos elementos. En cualquier caso, es un aporte despreciable frente a total de la recirculación y no tiene efector sobre el funcionamiento de la planta.

En el primero de los modelos se aplicarán las mismas hipótesis que en la etapa anterior del trabajo. En el segundo de ellos, se considera que los procesos ASM1 también se llevan a cabo en el interior del decantador secundario. En el tercer modelo, se llevará a cabo una discretización espacial en capas del decantador. En este modelo se tendrá en cuenta que los procesos ASM1 se llevan a cabo en cada una de las capas del mismo. A su vez, se modelizará la propagación del flujo en el interior del decantador mediante la aplicación de la teoría de flujo de sólidos [24]. El esquema de volúmenes finitos de primer

orden de Godunov será empleado para resolver la ecuación diferencial definida por la teoría de flujo de sólidos [32]. Para aplicar el método de Godunov es necesario en primer lugar resolver un problema de Riemann de forma explícita para la parte convectiva e ímplicita para la difusiva [34]. Los resultados de las simulaciones se compararán entre sí y con los valores reales medidos en la estación depuradora de aguas residuales Río Huerva.

1.4. Objetivos

Este trabajo debe servir como una primera etapa de la implementación y calibración del modelo $ASM1$ y su acoplamiento hidrodinámico, desarrollado en el Departamento de Mecánica de Fluidos de la Universidad de Zaragoza (MFC-T21) y con el apoyo de la empresa Aguas de Valencia S.A., formando parte del proyecto de investigación *Estudio hidrodinámico del reactor biológico. Estudio metabólico e hidrodinámico de la decantación secundaria para la optimización de la eliminación de fósforo en la EDAR de rio Huerva*. Los anexos han sido escritos en inglés a petición de Aguas de Valencia S.A. para dar una mayor difusión al proyecto.

A través este de este trabajo es posible comprender el comportamiento de las plantas de aguas residuales, la función y operación de los equipos que la conforman, incluyendo las relaciones biológicas entre especies, así como en la hidrodinámica que los gobierna en casos transitorios a diferencia de los modelos comerciales habituales, capaces de trabajar exclusivamente en régimen estacionario. La posibilidad de introducir entradas transitorias al sistema de depuración es una gran ventaja a la hora de modelar/mejorar los procesos de regulación que deben aplicarse ante los cambios continuos que experimentan las aguas residuales a depurar, ya sea por vertidos puntuales, lluvias o cambios estacionales a corto y largo plazo.

Para este fin, este trabajo tiene como objetivo diseñar e implementar un modelo acoplado hidrodinámico y biológico que incluya un sistema de regulación automática fiel a la realidad. Este modelo permitirá reproducir la operación de una planta de aguas residuales de forma autónoma, sirviendo de apoyo para la empresa Aguas de Valencia a la hora de plantear estrategias de ahorro energético en el funcionamiento de la planta.

Capítulo 2

Modelo biológico

En este Capítulo, se describirán de forma breve las directrices en la que se basan los modelos biológicos comúnmente utilizados, haciendo hincapié en el modelo objeto de este trabajo, ASM1. En la Sección 2.1, se presentará la cinética de los procesos de lodos activados. En la Sección 2.2, se describirá el modelo biológico ASM1.

2.1. Cinética de los procesos de crecimiento microbiano

La variación en el tiempo debido a un proceso químico de un componente arbitrario i, que denotaremos como ϕ_i, se expresa como una función r_i de la forma

$$\frac{d\phi_i}{dt} = r_i \tag{2.1}$$

La función r_i depende fundamentalmente de tres parámetros

- $r_{i,max}$: máximo ratio de variación del componente i.
- ϕ_j: concentración de la sustancia limitante.
- K_j: constante de velocidad de reacción media, definida como el valor de ϕ_j cuando $\frac{r_i}{r_{i,max}} = 0{,}5$.

En los modelos ASM, los procesos de crecimiento microbiano, r_i, se clasifican en

- Aquellos en los que el crecimiento microbiano o aumento de la concentración de una sustancia i sólo ocurre en presencia de la sustancia limitante, ϕ_j. En este caso, el ratio o proceso de crecimiento se denota como ecuación de Monod [11] y se define como

$$r_i = r_{i,max} \frac{\phi_j}{K_j + \phi_j} \,. \tag{2.2}$$

- Aquellos en los que el crecimiento microbiano o aumento de la concentración de una sustancia i sólo ocurre en ausencia de la sustancia limitante, ϕ_j. En este caso, el ratio o proceso de crecimiento se define como

$$r_i = r_{i,max} \frac{K_j}{K_j + \phi_j} \,. \tag{2.3}$$

2.2. ASM1

Los procesos biológicos que se llevan a cabo en el reactor serán simulados a través del modelo de lodos activados número 1 (ASM1). El modelo brinda una buena descripción del proceso de lodos activados siempre que el agua residual sea de origen doméstico o municipal, no industrial [12]. Incluye 8 procesos de crecimiento microbiano [13], denotados como ρ_j. La mayor parte de ellos presentan la forma de las Ecuaciones 2.2 y 2.3, en algunos casos de forma individual y en otros de forma acoplada. Entre los 8 procesos se incluyen

- Crecimiento aeróbico y anóxico de la biomasa heterótrofa, necesaria para que se produzca la eliminación de la materia orgánica y se lleve a cabo el proceso de desnitrificación.
- Decaimiento de la biomasa heterótrofa, la cual se transforma en otros componentes particulados.
- Crecimiento aeróbico de la biomasa autótrofa, necesaria para que se lleve a cabo el proceso de nitrificación.
- Decaimiento de la biomasa autótrofa, la cual se transforma en otros componentes particulados.
- Amonificación, que lleva a cabo la transformación del nitrógeno orgánico soluble en amonio y amoníaco.
- Hidrólisis de componentes particulados orgánico y nitrogenados, que los transforma en solubles.

Por otra parte, el modelo ASM1 incluye 13 componentes [15], ϕ_i, los cuales se clasifican en solubles o particulados de la siguiente forma

Símbolo	Nombre del componente	Dimensiones
S_S	Materia orgánica rápidamente biodegradable	$M(DQO)L^{-3}$
S_I	Materia inorgánica soluble	$M(DQO)L^{-3}$
S_O	Oxígeno disuelto	$M(O_2)L^{-3}$
S_{NO}	Nitritos y nitratos	$M(N)L^{-3}$
S_{NH}	Amonio y amoníaco	$M(N)L^{-3}$
S_{ND}	Nitrógeno orgánico biodegradable soluble	$M(N)L^{-3}$
S_{ALK}	Alcalinidad de las aguas residuales	$mol(HCO_3^-)L^{-3}$

Cuadro 2.1: Componentes solubles, $S_{(\cdot)}$.

Símbolo	Nombre del componente	Dimensiones
X_I	Materia inorgánica particulada	$M(DQO)L^{-3}$
X_S	Materia orgánica lentamente biodegradable	$M(DQO)L^{-3}$
$X_{B,H}$	Biomasa heterótrofa activa	$M(DQO)L^{-3}$
$X_{B,A}$	Biomasa autótrofa activa	$M(DQO)L^{-3}$
X_P	Productos de decaimiento no biodegradables	$M(DQO)L^{-3}$
X_{ND}	Nitrógeno orgánico biodegradable particulado	$M(N)L^{-3}$

Cuadro 2.2: Componentes particulados, $X_{(\cdot)}$.

Las unidades de DQO, demanda química de oxígeno, se emplean debido a que permiten la unión entre electrones equivalentes del sustrato orgánico, la biomasa y el oxígeno utilizados [14].

La variación en el tiempo de un componente ϕ_i es expresada como una función r_i [17] de la forma

$$r_i = \sum_{j=1}^{N_{proc}} \nu_{ji} \cdot \rho_j \,, \tag{2.4}$$

siendo N_{proc} el número de procesos en los que interviene el componente i y ν_{ji} los coeficientes estequiométricos del modelo, los cuales están recogidos en la Tabla A.4 del Anexo A. En la tabla mencionada también se recogen los parámetros cinéticos que gobiernan el modelo, algunos de los cuales varían con la temperatura según la ecuación modificada de Arrhenius [19]

$$P(T) = P(20°C)\theta_p^{T-20}, \tag{2.5}$$

siendo $P(20°C)$ el valor nominal del parámetro P a $20°C$ y θ_p el factor de corrección de temperatura de cada parámetro, incluido también en la Tabla A,4.

Por último, en la siguiente tabla se recogen todos los procesos, componentes y parámetros del modelo ASM1, con el fin de ilustrar las relaciones que existen entre especies

Cuadro 2.3: Porcesos cinéticos y estequiométricos de la oxidación del carbono, nitrificación y desnitrificación en ASM1.

Proceso j → Componente i ↓	*Crecimiento aeróbico de heterótrofos*	*Crecimiento anóxico de heterótrofos*	*Crecimiento aeróbico de autótrofos*	*Decaimiento de heterótrofos*	*Decaimiento de autótrofos*	*Amonificación del nitrógeno orgánico soluble*	*Hidrólisis del particulado orgánico*	*Hidrólisis del nitrógeno orgánico*
S_I	0	0	0	0	0	0	0	0
S_S	$-\frac{1}{Y_H}$	$-\frac{1}{Y_H}$	0	0	0	0	1	0
X_I	0	0	0	0	0	0	0	0
X_S	0	0	0	1-f_P	1-f_P	0	-1	0
$X_{B,H}$	1	1	0	-1	0	0	0	0
$X_{B,A}$	0	0	1	0	-1	0	0	0
X_P	0	0	0	f_P	f_P	0	0	0
S_O	$-\frac{1-Y_H}{Y_H}$	0	$-\frac{4,57-Y_A}{Y_A}$	0	0	0	0	0
S_{NO}	0	$-\frac{1-Y_H}{2,86Y_H}$	$\frac{1}{Y_A}$	0	0	0	0	0
S_{NH}	$-i_{XB}$	$-i_{XB}$	$-i_{XB}-\frac{1}{Y_A}$	0	0	1	0	0
S_{ND}	0	0	0	0	0	-1	0	1
X_{ND}	0	0	0	$-i_{XB}-f_P i_{XP}$	$-i_{XB}-f_P i_{XP}$	0	0	-1
S_{ALK}	$-\frac{i_{XB}}{14}$	$\frac{1-Y_H}{14\cdot 2,86Y_H}-\frac{i_{XB}}{14}$	$\frac{i_{XB}}{14}-\frac{1}{7Y_A}$	0	0	$\frac{1}{14}$	0	0
Process rate $\rho_j\,[ML^{-3}T^{-1}]$	$\hat{u}_H\left(\frac{S_S}{K_S+S_S}\right)\left(\frac{S_O}{K_{O,H}+S_O}\right)X_{B,H}$	$\hat{u}_H\left(\frac{S_S}{K_S+S_S}\right)\left(\frac{K_{O,H}}{K_{O,H}+S_O}\right)\left(\frac{S_{NO}}{K_{NO}+S_{NO}}\right)\eta_g X_{B,H}$	$\hat{u}_A\left(\frac{S_{NH}}{K_{NH}+S_{NH}}\right)\left(\frac{S_O}{K_{O,A}+S_O}\right)X_{B,A}$	$b_H X_{B,H}$	$b_A X_{B,A}$	$k_a S_{N,D} X_{B,H}$	$k_h\frac{X_S/X_{B,H}}{K_X+(X_S/X_{B,H})}[\left(\frac{S_O}{K_{O,H}+S_O}\right)+$ $+\eta_b\left(\frac{K_{O,H}}{K_{O,H}+S_O}\right)\left(\frac{S_{NO}}{K_{NO}+S_{NO}}\right)]X_{B,H}$	$\rho_7\left(\frac{X_{ND}}{X_S}\right)$

Capítulo 3

Simulación de 5 configuraciones de planta de tratamiento de aguas residuales

En este Capítulo, se describirán y compararán los modelos de simulación, cuyas simplificaciones son similares a las del programa comercial Linx ASM1. En la Sección 3.1, se detallarán 5 configuraciones de plantas de tratamiento de aguas residuales, concluyendo con una comparativa entre las mismos. En la Sección 3.2, se realizará una comparativa entre los resultados proporcionados por el programa comercial Linx ASM1 y los proporcionados por uno de los modelos de simulación.

3.1. Modelos de simulación

Debido a la complejidad que supone modelizar una planta de aguas residuales en su conjunto, en esta sección únicamente se tendrán en cuenta los equipos presentes en el tratamiento secundario de la misma. Las configuraciones que se plantearán en esta sección constan desde 3 reactores biológicos y 1 decantador en la primera configuración, hasta 3 reactores biológicos, 1 decantador, 1 línea de recirculación, 1 línea de purga, 1 espesador y 1 deshidratador en la quinta configuración. Estos elementos se irán añadiendo uno a uno a la primera configuración, hasta formar la última. En las Figuras 3.1 y 3.2, se muestra la primera y la quinta configuración, respectivamente.

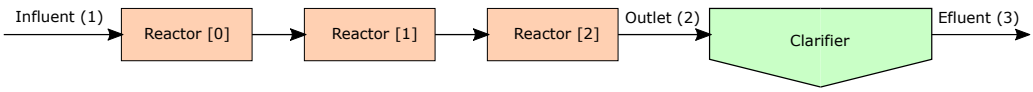

Figura 3.1: Primera configuración de la planta de aguas residuales.

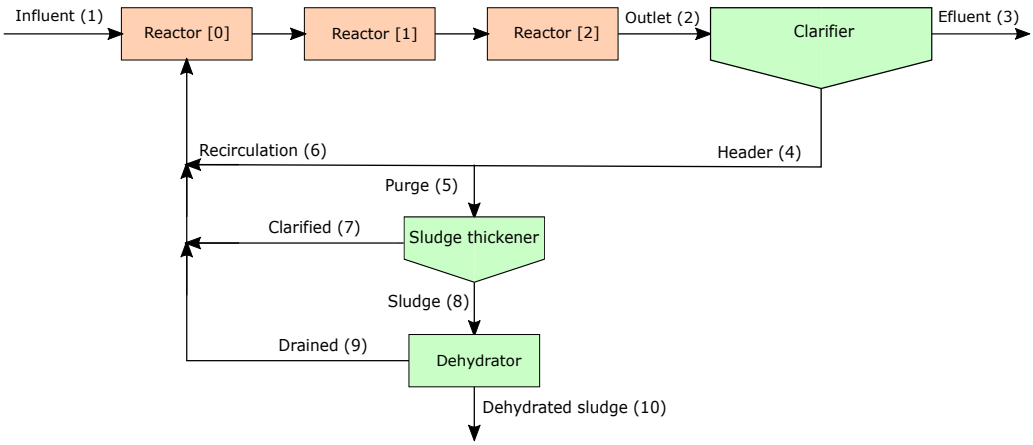

Figura 3.2: Quinta configuración de la planta de aguas residuales.

Cuya notación es la que se indica a continuación

Concentración	Caudal	Descripción
X_1, S_1	q_1	Influente de la planta
X_2, S_2	q_2	Salida del reactor
X_3, S_3	q_3	Efluente de la planta
X_4, S_4	q_4	Cabecera
X_5, S_5	q_5	Purga
X_6, S_6	q_6	Recirculación
X_7, S_7	q_7	Clarificado
X_8, S_8	q_8	Fango hidratado
X_9, S_d	q_9	Escurrido
X_{10}, S_{10}	q_{10}	Fango deshidratado

Cuadro 3.1: Variables de los modelos

Las características de cada uno de los equipos, así como las simplificaciones que se tendrán en cuenta, serán explicadas a continuación. Los reactores biológicos tienen las siguientes características

- En el interior de los reactores se llevan a cabo todos los procesos biológicos del ASM1, descritos en la Sección 2.2.
- Son considerados con 0 dimensiones, es decir, las concentraciones de cada uno de los reactores son las mismas en todo su volumen. En los modelos ASM no existe ningún parámetro que sea capaz de describir el nivel de homogenización de las concentraciones en el licor mezcla. Sin embargo, en la realidad existen elementos, como el vehiculador o los discos Orbal, que tratan de asegurar la homogeneidad de todas las especies.
- Los reactores están conectados entre sí a través de compuertas laterales sumergidas que, por diferencia de nivel, permiten el paso del fluido de un reactor al siguiente. La ecuación que describe este fenómeno es la siguiente

$$Q_{br} = 0{,}611 b_g h_g \sqrt{2g|l_2 - l_1|}, \tag{3.1}$$

donde l_2 y l_1 son los niveles de reactores consecutivos, b_g es la anchura de la compuerta lateral, h_g es la apertura de la compuerta y g es la aceleración de la gravedad.

- El primer reactor opera en condiciones anaeróbias, es decir, en ausencia de oxígeno. El segundo y tercer reactor opera en condiciones aerobias, es decir, con una concentración de oxígeno disuelto constante y de valor 1 $M(-COD)L^{-3}$

Los decantadores secundarios tienen las siguientes características

- En el interior del decantador secundario no se llevan a cabo los procesos biológicos del ASM1.
- Se modelizan imponiendo un rendimiento de decantación, η_c, constante y de valor 99.5 %, aplicado únicamente a los componentes particulados. Los componentes solubles permanecen invariantes a su paso por el decantador, lo que implica que la concentración de especies solubles a la entrada del decantador, efluente, cabecera, recirculación y purga es la misma. En el caso de los componentes particulados, se aplica el rendimiento antes mencionado, de forma que la concentración de componentes particulados en el efluente se define como

$$X_3 = X_2(1 - \eta_c), \tag{3.2}$$

La definición de la concentración de los componentes particulados de la cabecera, recirculación y purga es diferente para cada modelo, pues cada elemento que añadimos al primer modelo induce una variación a priori no despreciable. A continuación, se presenta la definición antes mencionada para cada una de las configuraciones, obtenidas a partir de los balances de masa planteados en el Anexo B.

$$\begin{cases} N/A & \text{Modelo sin recirculación (1)} \\ X_4 = \frac{X_2(r+\eta_c)}{r} & \text{Modelo con recirculación (2)} \\ X_4 = \frac{X_2(r+\eta_c - r\eta_c p)}{r} & \text{Modelo con recirculación y purga (3)} \\ X_4 = \frac{X_2(r+\eta_c - r\eta_c p + \eta_c f_{cl} r p)}{r} & \text{Modelo con recirculación, purga y espesador (4)} \\ X_4 = \frac{X_2(r+\eta_c + r\eta_c p(f_{cl}+f_d(1-f_{cl})-1))}{r} & \text{Modelo con recirculación, purga, espesador y deshidratador (5)} \end{cases} \tag{3.3}$$

donde r representa el factor de recirculación, $r = \frac{q_4}{q_1}$, p representa el factor de purgado, $p = \frac{q_5}{q_4}$, f_{cl} representa el factor de clarificado, $f_{cl} = \frac{q_7}{q_5}$, y f_d representa el factor de deshidratado, $f_d = \frac{q_9}{q_8}$. Los valores de los parámetros mencionados empleados en los modelos descritos en esta Sección son los valores por defecto del programa comercial Linx ASM1, de forma que

Parámetro	Valor
r	1.0
p	0.02
f_{cl}	0.8
f_d	0.8

Cuadro 3.2: Parámetros de caudales de la planta

- El tercer reactor está conectado con el decantador secundario a través de un aliviadero lateral que, por rebosamiento, permite el paso del fluido del tercer reactor al decantador. El decantador secundario también consta de un aliviadero cuya definición es la misma que la del aliviadero lateral. En este caso, permite la descarga de caudal de efluente por la parte superior del mismo. La ecuación que describe el fenómeno de rebosamiento es la siguiente

$$Q_{sp} = F_r \sqrt{g H_w} H_w L_{sp}, \tag{3.4}$$

donde F_r es el número adimensional de Froude de valor 1, L_{sp} es la longitud del aliviadero, H_w es la altura de la lámina de agua y g es la aceleración de la gravedad.

El espesador y el deshidratador son modelados de igual forma. Las características de ambos equipos se detallarán a continuación.

- En el interior estos equipos no se llevan a cabo los procesos biológicos del ASM1.
- Ambos equipos se consideran de tipo centrífugo [20]. La mayor parte del fango que se extrae de estos equipos queda concentrado en la periferia de los mismos. El fango que abandona el deshidratador de esta forma se recoge y se almacena, mientras que la fracción de fango que no se concentra en la periferia es retornada al primer reactor. De la misma forma que el decantador segundario, la concentración de componentes solubles a la entrada y salida de estos equipos es la misma. La operación de estos equipos centrífugos se puede definir como un rendimiento, el cual simula la variación de las concentraciones de los componentes particulados de las corrientes de ambos equipos, como sigue

$$\eta_s = 1 - \frac{X_7(X_8 - X_5)}{X_5(X_8 - X_7)}, \tag{3.5}$$

  El rendimiento de estos equipos en las simulaciones de esta Sección de nuevo corresponde con los valores por defecto del programa Linx ASM1, de forma que

Parámetro	Valor
η_s	0.96
η_d	0.96

Cuadro 3.3: Parámetros de equipos centrífugos de la planta

- El reparto de caudales de estos dos equipos se lleva a cabo mediante los factores de clarificado, f_{cl}, y escurrido, f_d, que aparecen en la definición de las concentraciones de los componentes particulados de la recirculación, purga y cabecera 3.3.

3.1.1. Resultados y conclusiones de las simulaciones

Los resultados gráficos presentados en esta Subsección representan la evolución en el tiempo de alguna de las concentraciones de los componentes de los reactores o del efluente. El tiempo de simulación es de 10.000 horas.

La evolución en el tiempo de la concentración de materia orgánica lenta y rápidamente biodegradable en el efluente es presentada en la Figura 3.3. La suma de ambas concentraciones corresponde con la concentración de DBO del efluente, parámetro fundamental en el diseño de estaciones depuradoras de aguas residuales, que permite cuantificar el nivel de materia orgánica presente en la planta [21].

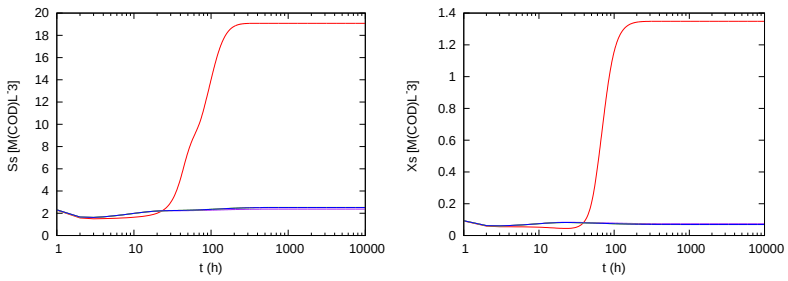

Figura 3.3: Concentración de la materia orgánica presente en el efluente del Modelo 1 (—), Modelo 2 (—), Modelo 3 (—), Modelo 4 (—), Modelo 5 (—).

Como se puede observar, los valores de materia orgánica alcanzados en el primer modelo, sin recirculación, son muy superiores a los alcanzados por los modelos posteriores. Esta discrepancia se debe a que los

valores de bacterias heterótrofas en los reactores del primer modelo, necesarias para la eliminación la materia orgánica del licor mezcla a partir de reacciones de oxidación, son casi despreciables en comparación con los modelos posteriores, como puede observarse en la Figura 3.4. Gracias a la línea de recirculación, gran parte de las bacterias que abandonan el decantador retornan al primer reactor, evitando que los niveles de biomasa no decaigan.

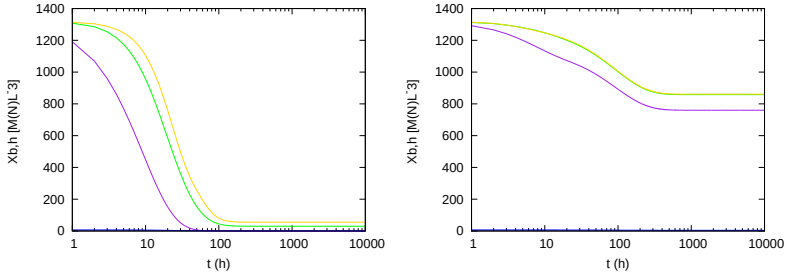

Figura 3.4: Concentración de biomasa heterótrofa en los reactores [0] (—), reactor[1] (—), reactor[2] (—) y efluente (—) del Modelo 1 (izquierda) y 3 (derecha).

La evolución en el tiempo de la concentración de amonio y amoníaco en el efluente es presentada en la Figura 3.5. Esta concentración es crítica en el diseño y operación de plantas de tratamiento de aguas residuales por su toxicidad [22].

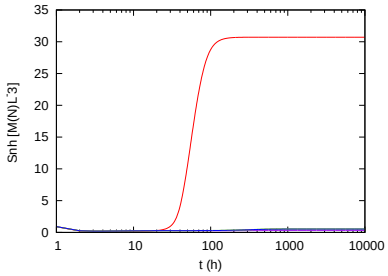

Figura 3.5: Concentración del amonio y amoníaco presente en el efluente del Modelo 1 (—), Modelo 2 (—), Modelo 3 (—), Modelo 4 (—), Modelo 5 (—).

Como se puede observar, los valores de amonio y amoníaco alcanzados en el primer modelo, sin recirculación, son muy superiores a los alcanzados por los modelos posteriores. Esta discrepancia se debe a que los valores de bacterias autótrofas en los reactores del primer modelo, necesarias para la transformación de amonio y amoníaco en nitritos y nitratos a partir de la reacción de nitrificación, son casi despreciables en comparación con los modelos posteriores, como puede observarse en la Figura 3.6, debido a la ausencia de línea de recirculación.

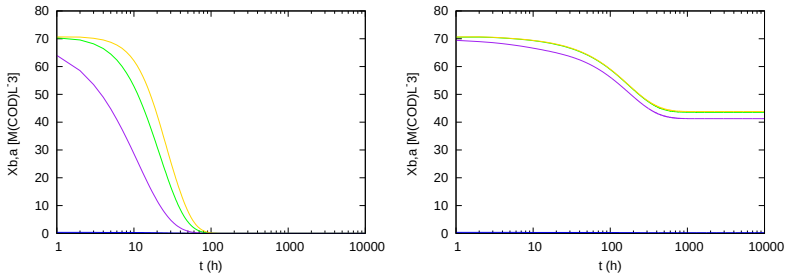

Figura 3.6: Concentración de biomasa autótrofa en los reactores [0] (—), reactor[1] (—), reactor[2] (—) y efluente (—) del Modelo 1 (izquierda) y 3 (derecha).

La evolución en el tiempo de la concentración de los productos inertes del decaimiento de la biomasa y los particulados inertes en el efluente es presentada en la Figura 3.7.

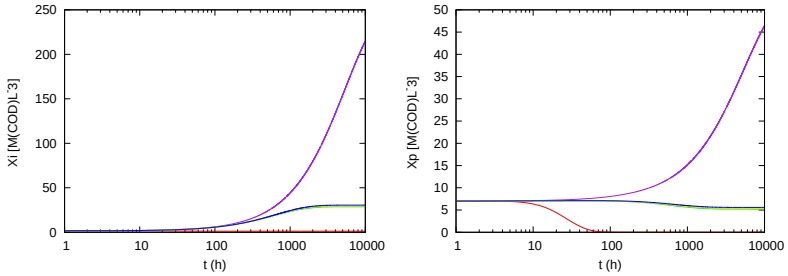

Figura 3.7: Concentración de productos inertes presentes en el efluente del Modelo 1 (—), Modelo 2 (—), Modelo 3 (—), Modelo 4 (—), Modelo 5 (—).

Como se puede observar, los valores de X_p y X_i alcanzados en el segundo modelo, sin purga, son muy superiores a los alcanzados por el resto de modelos. De hecho, mientras que en los modelos con purga o sin recirculación alcanzan un estacionario, la evolución en el tiempo del modelo sin purga presenta una pendiente positiva tras 10.000 horas. Esto se debe a que la línea de recirculación sin purga provoca una acumulación de componentes particulados indeseable en los reactores. Como se detallará en la Subsección 4.1.1, la línea de purga es un elemento fundamental en el diseño de estaciones depuradoras de aguas residuales, ya que permite controlar los niveles de sólidos en suspensión de la planta. En la Sección B.9 del Anexo A, se lleva a cabo un análisis de sensibilidad del factor de purgado.

Por último, cabe destacar que no existe una variación significativa entre las concentraciones de los componentes del efluente de los modelos con purga (3), espesador (4) y deshidratador (5), como se puede observar en las Figuras de la presente Subsección. Esto es debido a que las líneas adicionales de clarificado y escurrido no introducen una cantidad excesiva de bacterias en los reactores. La existencia de equipos de espesamiento y deshidratación únicamente está relacionada con la mejora en el transporte y almacenamiento de los fangos sobrantes de la planta [8].

3.2. Comparativa con el programa comercial Linx ASM1

El programa comercial Linx ASM1 permite obtener resultados de simulación de forma sencilla y simular plantas de tratamiento de aguas residuales con infinitas configuraciones. Es un software comercial comúnmente empleado en el diseño de este tipo de sistemas. En esta Sección se llevará a cabo una comparativa entre resultados de este software comercial y los proporcionados por el programa desarrollado con lenguaje C++.

El modelo que será comparado consta de 1 reactor, 1 clarificador, 1 espesador y 1 deshidratador, tal y como se muestra en la Figura 3.8

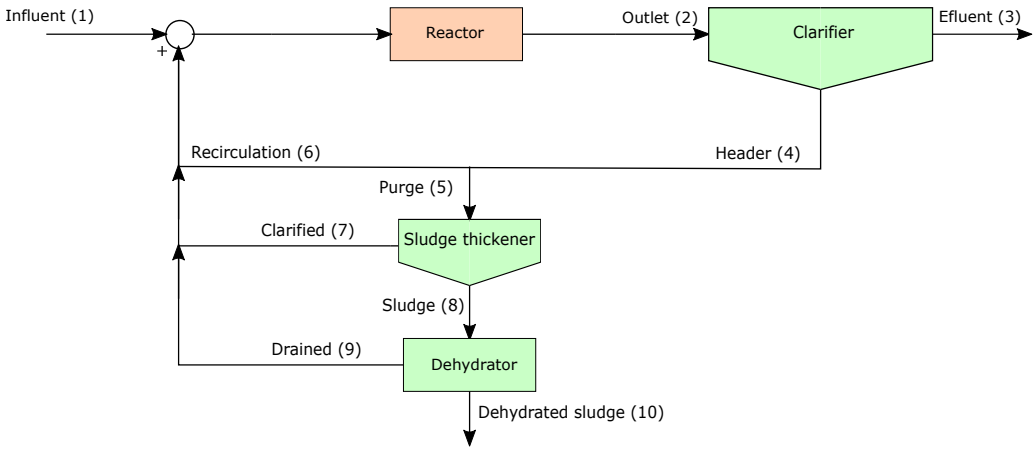

Figura 3.8: Esquema de la planta.

Las características de cada uno de los equipos son las mismas que las descritas en la Sección 3.1, a excepción de la concentración de oxígeno disuelto en el reactor, que toma un valor de 1.5 $M(-COD)L^3$ constante. Los parámetros de la planta elegidos para esta simulación corresponden con los empleados en un ejemplo de la planta de tratamiento de aguas residuales Río Huerva, de forma que

Parámetro	Valor
r	0.9771167
p	0.0234192037
f_{cl}	0.9
f_d	0.96
η_c	0.89
η_s	0.96
η_d	0.96

Cuadro 3.4: Parámetros de la planta

Tras un tiempo de simulación de 12.000 horas, los resultados proporcionados por Linx ASM1 y los del software desarrollado son presentados en la Tabla siguiente

Componente	Linx ASM1	Software desarrollado	Dimensiones
S_S	2.443	2.443	$M(COD)L^{-3}$
S_I	12.720	12.720	$M(COD)L^{-3}$
S_O	1.500	1.500	$M(O_2)L^{-3}$
S_{NO}	19.373	19.377	$M(N)L^{-3}$
S_{NH}	0.408	0.408	$M(N)L^{-3}$
S_{ND}	0.764	0.764	$M(N)L^{-3}$
S_{ALK}	97.065	97.055	$mol(HCO_3^-)L^{-3}$
X_I	1.003	1.003	$M(COD)L^{-3}$
X_S	0.029	0.029	$M(COD)L^{-3}$
$X_{B,H}$	2.617	2.622	$M(COD)L^{-3}$
$X_{B,A}$	0.122	0.122	$M(COD)L^{-3}$
X_P	3.966	3.964	$M(COD)L^{-3}$
X_{ND}	0.002	0.002	$M(N)L^{-3}$

Cuadro 3.5: Resumen de resultados

Como puede observarse, los resultados de ambas simulaciones son idénticos. Por tanto, se puede afirmar que el software desarrollado sea ajusta a las características del programa comercial Linx ASM1.

Capítulo 4

Simulación de plantas de tratamiento de aguas residuales con control automático

En este Capítulo, se describirán y compararán los resultados de 3 modelos de simulación de plantas de tratamiento de aguas residuales con control automático. En la Sección 4.1, se detallarán los controles que se aplican en la planta de tratamiento de aguas residuales Río Huerva. En la Sección 4.2, se describirán los 3 modelos de simulación. En la Sección 4.3, se realizará una comparativa entre los resultados porporcionados por los modelos de simulación descritos en la Sección 4.2 y los datos reales de la planta de tratamiento de aguas residuales Río Huerva.

4.1. Control de la planta de tratamiento de aguas residuales Río Huerva

Los métodos de control aplicados en la planta de aguas residuales Río Huerva son fundamentalmente de dos tipos. El primero de ellos es un control del caudal de la línea de purga, el cual lleva a cabo el coordinador de la planta a través de una estimación de la materia orgánica eliminada por la planta. El segundo de ellos es un control automático y manual de los niveles de amonio y amoníaco presentes en el tercer reactor, llevado a cabo gracias a la información proporcionada por una sonda de amonio y a la operación de los discos Orbal.

4.1.1. Regulación de la purga

El caudal de la línea de purga de la planta es regulado mediante una bomba controlada con un sistema marcha/paro. El coordinador de la planta determina, mediante un cálculo bisemanal, el tiempo de operación de la bomba para controlar los niveles de sólidos en suspensión de la planta. El parámetro fundamental que debe ser medido para llevar a cabo este control es la concentración de DBO del influente y del efluente.

El primer paso para calcular el tiempo de operación de la bomba de purga es determinar la masa de DBO eliminada por la planta de aguas residuales durante 3 días, como sigue

$$\frac{\Delta KgDBO}{3day} = \frac{(\frac{gDBO}{m^3})_e - (\frac{gDBO}{m^3})_s}{1000\frac{g}{Kg}} Q_{inlet}[\frac{m^3}{3day}], \tag{4.1}$$

A continuación, es necesario estimar la relación que existe entre la masa de sólidos en suspensión y la masa de DBO ($\frac{KgSS}{\Delta KgDBO}$), con objeto de determinar la producción biológica de fango de la planta. La

relación mencionada fue determinada por el coordinador de la planta mediante el método de Chudoba [23], tomando un valor de 0.8 para la planta de tratamiento de aguas residuales Río Huerva. Por tanto, la masa de sólidos en suspensión eliminada por la planta cada 3 días se calcula como

$$\frac{\Delta KgSS}{3day} = (\frac{\Delta KgDBO}{3day})(\frac{KgSS}{\Delta KgDBO}), \tag{4.2}$$

Este parámetro es empleado para estimar el volumen de fluido que debe ser purgado durante los 3 días. Para ello, deben conocerse los niveles de sólidos en suspensión de la propia línea de purga, que se estiman a través del ratio entre el DQO y los sólidos en suspensión de la línea de recirculación. Considerando que la relación antes mencionada, medida por el coordinador de la planta periódicamente, es de 0.873, el volumen fluido que debe ser purgado durante los 3 días se calcula como

$$Q_{purge}[\frac{m^3}{3day}] = \frac{\frac{\Delta SS}{3day}}{SS_{recirculation}[\frac{kg}{m^3}]}, \tag{4.3}$$

Considerando a su vez que el caudal nominal de la bomba (Q_{pump}) es de $48\frac{m^3}{h}$, el tiempo de operación total de la misma durante 3 días se calcula como

$$t_{pump}[\frac{s}{3day}] = \frac{Q_{purge}[\frac{m^3}{day}]}{Q_{pump}[\frac{m^3}{s}]}, \tag{4.4}$$

El tiempo de operación total de la bomba se repartirá de forma equitativa durante los 3 días (t_{bc}), de manera que la bomba trabajará realizando ciclos marcha/paro de misma duración. Considerando que el tiempo máximo de operación en continuo de la bomba es de 1 hora (t_{om}), el tiempo de operación de la bomba por ciclo se calcula como

$$t_o[\frac{s}{h}] = \frac{t_{pump}[\frac{s}{3day}]}{t_{bc}[\frac{s}{3day}]} t_{om}[\frac{s}{h}], \tag{4.5}$$

Como puede observarse, cuanto menor es la diferencia de DBO entre influente y efluente, menor es el tiempo de purga de la planta. Una diferencia de DBO baja entre ambas corrientes implica que no se está llevando a cabo la eliminación de materia orgánica correctamente. Como ha sido detallado en la Subsección 3.1.1, este hecho puede deberse a unos niveles de biomasa heterótrofa bajos en los reactores. Disminuyendo el tiempo de purga se consigue un aumento de concentración de biomasa heterótrofa en los reactores, dando como resultado una mejora en el funcionamiento del sistema.

4.1.2. Control oxígeno-amonio

El control de oxígeno-amonio se basa en la optimización de la eliminación de nutrientes. Este control permite establecer un valor objetivo de amonio (NH_4^+, NH_3) en el tercer reactor. Para ello, una sonda de amonios colocada en el tercer reactor manda una señal al convertidor de frecuencia de los Orbal para ajustar su velocidad rotacional. Los Orbal son equipos que se encargan de aportar oxígeno al segundo y tercer reactor para evitar un aumento excesivo de la concentración de amonio-amoníaco.

La planta de tratamiento de aguas residuales Río Huerva consta de un vehiculador en el primer reactor, cuya función se detalló en el capítulo anterior, y 4 pares de Orbal. Cada par de Orbal está formado por 2 conjuntos de discos, uno de ellos colocado en el segundo y otro en el tercer reactor, de manera que la velocidad de giro de ambos es la misma. La distribución de cada par de Orbal en los reactores es representada en la siguiente Figura

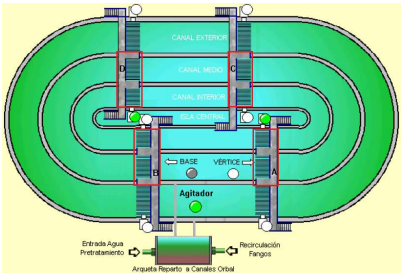

Figura 4.1: Esquema de la planta

Los parámetros de la regulación que pueden ser modificados por el coordinar de la planta son

- Punto de regulación (S_{NH}^{ref}). Es el valor de amoníaco-amonio buscado y suele fijarse en 7 g/m3.
- Punto de paro (S_{NH}^{stop}). Si la concentración de amoníaco-amonio se encuentra por debajo de este valor, el variador de frecuencia de cada par de Orbal establece su velocidad rotacional mínima. Este parámetro suele fijarse en 6.4 g/m3.
- Banda muerta (S_{NH}^{band}). Cuando el valor de amonio-amoníaco se encuentra en el rango $S_{NH}^{ref} \pm S_{NH}^{band}$, la velocidad de rotación los pares de Orbal se mantiene constante. Este parámetro suele fijarse en 0.2 g/m3.
- Tiempo entre correcciones. Es el tiempo que el variador de frecuencia emplea para aumentar o disminuir la velocidad de rotación de los Orbal desde el valor actual hasta el porcentaje de corrección, descrito a continuación. Este parámetro suele fijarse en 300 s.
- Corrección. Es el porcentaje de velocidad de rotación de los Orbal que aumenta o disminuye entre el tiempo de correcciones. Este parámetro suele fijarse en 2 %.
- Máximo número de rotores activados. Determina el número de pares de Orbal deben actuar en la regulación. Actualmente son 3 los rotores que actúan.

Teniendo en cuenta que un 0 % de velocidad de rotación implica que el rotor está parado y que un 100 % de velocidad de rotación implica que el rotor funciona a su máxima capacidad, la secuencia de funcionamiento de los Orbal es presentada en la Figura 4.2. En esta Figura se representa un ciclo completo de funcionamiento, alcanzando finalmente la misma velocidad rotacional que al inicio.

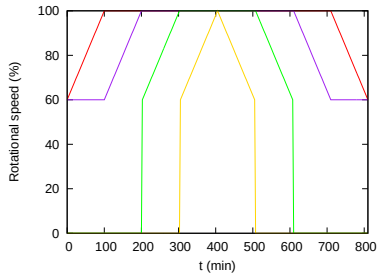

Figura 4.2: Velocidad de rotación del rotor A (—), D (—), B (—) y C (—) durante el ciclo de subida-bajada

Como puede observarse, la velocidad mínima de los rotores A y D es del 60 %, mientras que la de los rotores B y C es del 0 %. El aporte de oxígeno y la potencia consumida de los Orbal para cada velocidad de rotación es presentada en la Tabla C.1 de la Sección C.3 del Anexo C. La secuencia de operación de los pares de Orbal es A, D, B y C, de manera que 2 pares de Orbal no pueden variar su velocidad de giro de forma simultánea.

La Figura 4.3 trata de ilustrar el control automático de la planta, una vez descritos los parámetros y la secuencia de operación de los Orbal. Es necesario tener en cuenta que existen dos estados diferenciados del control: aumento y disminución de la concentración amonio-amoníaco. Para cada estado se aplica una secuencia de decisión diferente, representada en la siguiente Figura como

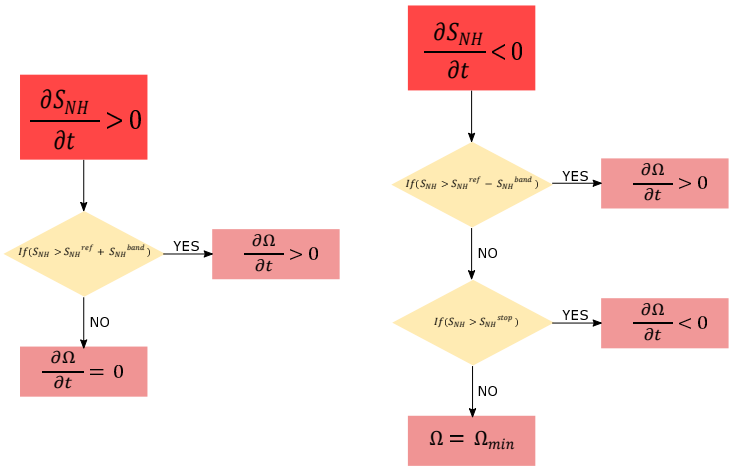

Figura 4.3: Secuencia de decisión cuando la concentración de amonio-amoníaco aumenta (izquierda) o disminuye (derecha) en el tercer reactor.

Como puede observarse, cuando los valores de amonio en el tercer reactor se encuentran por encima de $S_{NH}^{ref} + S_{NH}^{band}$, se incrementa la velocidad rotacional de los Orbal, produciendo un aumento en la concentración de oxígeno disuelto en el segundo y tercer reactor. El oxígeno es necesario para que se lleve a cabo la reacción de nitrificación, pues el amonio debe reaccionar con el oxígeno para transformarse en nitritos y nitratos. La biomasa autótrofa es también necesaria para que la reacción en cuestión se lleve a cabo. Un aumento del oxígeno disuelto en el reactor también favorece el crecimiento de estas bacterias.

El coordinador de la planta lleva a cabo el control automático que acaba de ser resumido en la Figura 4.3 y que, por tanto, será aplicado a los modelos de simulación descritos en la Sección 4.2. Sin embargo, hay momentos en los que este control no es suficiente y es necesario aplicar un control manual en la planta real. Puede ocurrir que la carga del influente sea tan alta que los Orbal no sean capaces de reducir la concentración de amonio-amoníaco por debajo de los valores objetivo. En este caso, la velocidad rotacional de los Orbal alcanza un máximo de forma prolongada, que puede derivar en un aumento excesivo de la concentración de nitritos y nitratos en los reactores. Es necesario tener en cuenta que la planta de aguas residuales Río Huerva tiene como restricción una concentración máxima de nitrógeno total en efluente de 15 g/m3, de manera que el coordinador de la planta debe asegurar que nunca se sobrepase. Por ello, en esta situación el coordinar de la planta puede decidir parar los Orbal, de manera que la concentración de nitrógeno total disminuya, pues la sensibilidad de los nitritos y nitratos es mayor que la de los amonios y amoníacos.

Este control podría mejorarse si en lugar de parar completamente los Orbal cuando la concentración de nitrógeno total exceda los 15 g/m3, se aplicara un algoritmo de control de reducción de la velocidad rotacional de los Orbal. En este caso, cuando la concentración de nitrógeno total exceda los 15 g/m3, la velocidad rotacional de los Orbal decrecerá de la misma forma que en el control automático de la planta. De esta forma el impacto del aumento o disminución de la concentración de oxígeno disuelto será menor. A su vez, será necesario fijar un valor de concentración de nitritos y nitratos mínimos, con objeto de limitar la disminuación de la velocidad rotacional de los Orbal. Esta limitación debe estar presente para que la concentración de amonio-amoníaco no aumente en exceso.

Los resultados presentados a continuación permiten apreciar la mejora del control alternativo presentado respecto al control manual aplicado actualmente por la planta. Ambos gráficos corresponden con la evolución de la concentración de nitrógeno total en el mes de Marzo.

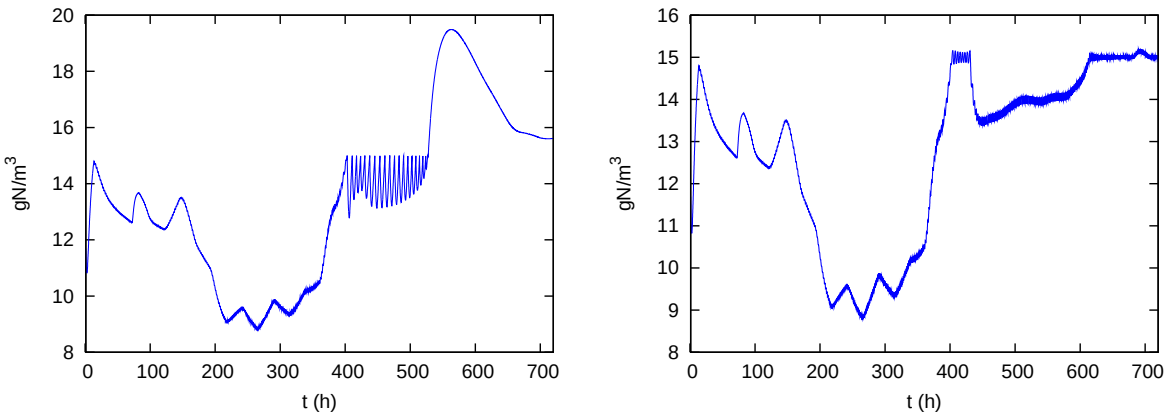

Figura 4.4: Concentración de nitrógeno total en el tercer reactor empleando el método de control manual (izquierda) y el método de control alternativo (derecha).

Como puede observarse, con el control manual la concentración de nitrógeno total excede al valor límite durante aproximadamente 200 horas. Sin embargo, con el método alternativo la concentración de nitrógeno total se mantiene prácticamente durante todo el periodo por debajo del valor límite. Por tanto, podemos concluir que el control alternativo supone una mejora sustancial en la regulación de los niveles de nitrógeno total en la planta.

4.2. Modelos de simulación con control automático

Los 3 modelos de simulación que serán comparados con resultados reales de la planta de tratamiento de aguas residuales Río Huerva tratan de simular un sistema de depuración de aguas residuales con el control automático descrito en las Subsecciones 4.1.1 y 4.1.2. Consta de 3 reactores, 1 decantador secundario, 1 línea de recirculación y 1 de purga, como el Modelo 3 descrito en la Sección 3.1. El espesador y el deshidratador no serán incluidos en ninguno de los modelos de esta Sección, debido a la falta de información real de los mismos. A diferencia de los modelos de simulación detallados en el Capítulo 3, las diferencias entre los 3 modelos de simulación descritos en esta sección se basan en la definición y características del clarificador. En las Figura 4.5, se muestra la configuración del sistema evaluado en los 3 modelos.

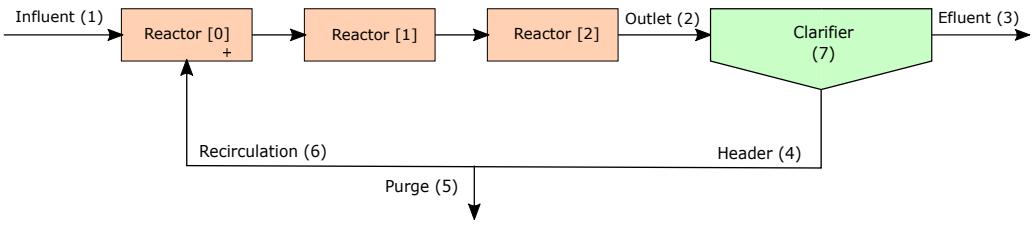

Figura 4.5: Configuración de la planta.

Cuya notación es la que se indica a continuación

Concentración	Caudal	Descripción
X_1, S_1	q_1	Influente de la planta
X_2, S_2	q_2	Salida del reactor
X_3, S_3	q_3	Efluente de la planta
X_4, S_4	q_4	Cabecera
X_5, S_5	q_5	Purga
X_6, S_6	q_6	Recirculación
X_7, S_7	V_7	Decantador

Cuadro 4.1: Variables de los modelos

Las características de cada uno de los equipos, así como las simplificaciones que se tendrán en cuenta, serán explicadas a continuación. Los reactores biológicos tienen las siguientes características en los 3 Modelos

- En el interior de los reactores se llevan a cabo todos los procesos biológicos del ASM1, descritos en la Sección 2.2.
- Las concentraciones de los componentes de los reactores son las iguales en todo su volumen.
- Los reactores están conectados entre sí a través de compuertas laterales sumergidas. La definición del caudal que las atraviesa corresponde a la Ecuación 3.1.
- El primer reactor opera en condiciones anaeróbias, es decir, en ausencia de oxígeno. El segundo y tercer reactor opera en condiciones aerobias gracias al oxígeno aportado por los discos Orbal, cuya operación resulta del control automático presentado en la Figura 4.3.

Los decantadores secundarios tienen las siguientes características

- En el Modelo 1, no se llevan a cabo los procesos biológicos del ASM1 en el interior del decantador secundario. En el Modelo 2 y 3, sí se llevan a cabo.
- Los Modelos 1 y 2 simulan la operación del decantador con un rendimiento, η_c, constante y de valor 99.5 %, aplicado únicamente a los componentes particulados. En el Modelo 1, los componentes solubles permanecen invariantes a su paso por el decantador, lo que implica que la concentración de especies solubles a la entrada del decantador, efluente, cabecera, recirculación y purga es la misma. En el caso de los componentes particulados, se aplica el rendimiento antes mencionado, de forma que la concentración de componentes particulados en el efluente se define como

$$\begin{cases} X_3 = X_2(1-\eta_c) & \text{Modelo 1} \\ X_3 = X_7(1-\eta_c) & \text{Modelo 2} \end{cases} \tag{4.6}$$

  En los Modelos 1 y 2, la definición de la concentración de los componentes particulados de la cabecera, recirculación y purga se determina a partir de los balances de masa planteados en la Sección C.4 del Anexo C, de forma que se define como

$$\begin{cases} X_4 = X_2\left(\frac{r+\eta_c(1-p-rp)}{r}\right) & \text{Modelo 1} \\ X_4 = \frac{X_2(1-p)(1+r)-X_7(1-\eta_c)(1-p-rp)}{r} & \text{Modelo 2} \end{cases} \tag{4.7}$$

  donde r representa el factor de recirculación, $r = \frac{q_6}{q_1}$, p representa el factor de purgado, $p = \frac{q_5}{q_4}$.
- En los 3 Modelos, el tercer reactor está conectado con el decantador secundario a través de un aliviadero lateral que, por rebosamiento, permite el paso del fluido del tercer reactor al decantador. En los Modelos 1 y 2, el decantador secundario también consta de un aliviadero cuya definición es la misma que la del aliviadero lateral. La ecuación que describe el fenómeno de rebosamiento es Ecuación 3.4. En el Modelo 3, el volumen del decantador secundario se supone constante, debido a

la gran discrepancia que existe entre las variaciones de volumen y el volumen total del mismo. Esto implica que el caudal del efluente en el Modelo 3 se define directamente como

$$q_3 = q_2 - q_4, \tag{4.8}$$

- El Modelo 3 se basa en la teoría de flujo de sólidos [24], que permite simular tanto la propagación del flujo como la sedimentación continua de los sólidos en el decantador secundario. La ecuación diferencial en la que se basa esta teoría es presentada a continuación

$$\frac{\partial(SS)}{\partial t} = -V\frac{\partial(SS)}{\partial z} + \frac{\partial(V_s \cdot SS)}{\partial z} + D_a \cdot \frac{\partial^2(SS)}{\partial^2 z}. \tag{4.9}$$

donde SS es la concentración de cualquiera de los componentes particulados en el decantador; V es la velocidad del flujo, que depende de la coordenada Z como se detalla en la Ecuación C.39 del Anexo C; V_s es la velocidad de sedimentación de cada especie del decantador, definida de forma exponencial con los modelos de Vesilind y Takacs detallados en la Subsubsección C.4.3 del Anexo C; D_a es el coeficiente de difusión, que según la literatura [25] toma un valor constante de 0.54 m2/h, pero que en nuestro caso es un parámetro que deberá ser calibrado, Sección C.6.

El decantador es dividido en un número N de celdas de igual espesor Δz. Según la literatura [31], el número de celdas N es un parámetro fundamental para asegurar la convergencia del problema, tomando un valor de 100. El esquema de la discretización del clarificador es presentado en la siguiente Figura

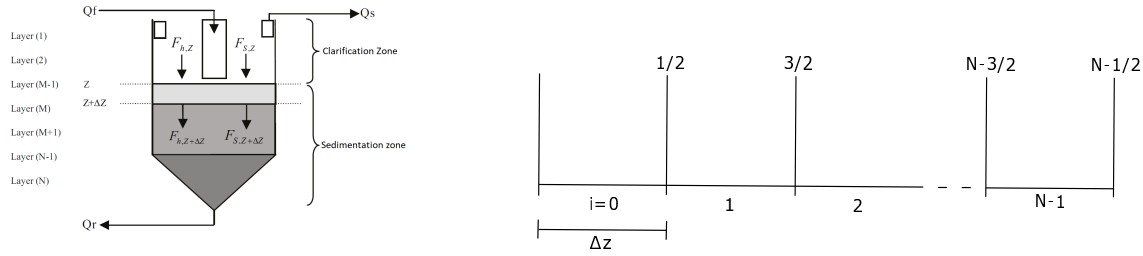

Figura 4.6: Discretización del clarificador

La Ecuación 4.9 se resolverá aplicando un método implícito para el término difusivo y explícito para el resto de términos de la ecuación. En primer lugar, se plantea un problema 1D de Riemann [32] que se resuelve integrando los términos no difusivos de la Ecuación 4.9, de forma que la concentración de particulado de la celda i en un tiempo igual a $n+1$ queda

$$SS_i^{n+1} = SS_i^n - \frac{\Delta t}{\Delta z}\left(F_{i+1/2}^- - F_{i-1/2}^+\right), \tag{4.10}$$

donde $F_{i+1/2}^-$ y $F_{i-1/2}^+$ son los flujos numéricos, ambos definidos en la Ecuación C.45 del Anexo C. En este caso, los flujos numéricos son conocidos, pues están evaluados en un tiempo igual a n, por lo que el método de integración es explícito. Sin embargo, en el caso la integración del término difusivo, los flujos numéricos también dependen de variables evaluadas en un tiempo igual a $n+1$, como se puede observar en la Ecuación C.48 del Anexo C, de manera que la ecuación a resolver es la siguiente

$$-\Delta t\frac{(D_a)_{i-1/2}}{\Delta x^2}SS_{i-1}^{n+1} + \left(1 + \Delta t\frac{(D_a)_{i+1/2}}{\Delta x^2} + \Delta t\frac{(D_a)_{i-1/2}}{\Delta x^2}\right)SS_i^{n+1} - \Delta t\frac{(D_a)_{i+1/2}}{\Delta x^2}SS_{i+1}^{n+1} = SS_i^n \tag{4.11}$$

Esta ecuación puede escribirse de forma matricial, C.52, y resolverse empleando el algoritmo de Thomas [34], detallado en la Subsubsección C.4.3. Este algoritmo permite, a partir de una matriz tridiagonal, resolver la Ecuación 4.11 de forma implícita.

La descripción detallada de la discretización del decantador es presentada en la Subsubsección C.4.3

Las condiciones de contorno de las simulaciones de este Capítulo, así como las simplificaciones aplicadas a las condiciones iniciales, son detalladas en la Sección C.5 del Anexo C. Por último, en la Sección C.1 del Anexo C se puede encontrar la información real que ha sido empleada en las simulaciones, porporcionada por la planta de tratamiento de aguas residuales Río Huerva. En esta Sección, se incluyen los datos de la planta durante los días en los que no se llevó a cabo el control manual oxígeno-amonio, que serán comparados con los resultados de las simulaciones en la Sección 4.3. Entre la información que se incluye en la Sección C.1 del Anexo C se encuentra la evolución en el tiempo de alguna de las concentraciones del efluente, así como de los caudales de entrada, efluente y purga de la planta.

4.3. Conclusiones generales

En las conclusiones serán comparados los resultados proporcionada por los Modelos 1, 2 y 3 descritos en este Capítulo con la información real de la planta de tratamiento de aguas residuales Río Huerva. Entre los datos que se compararán se encuentra los niveles de DBO, DQO y nitrógeno total del efluente.

El primer modelo que será comparado con la información real es el Modelo 1. La evolución en el tiempo de las 3 especies antes mencionadas es representada en la Figura 4.7

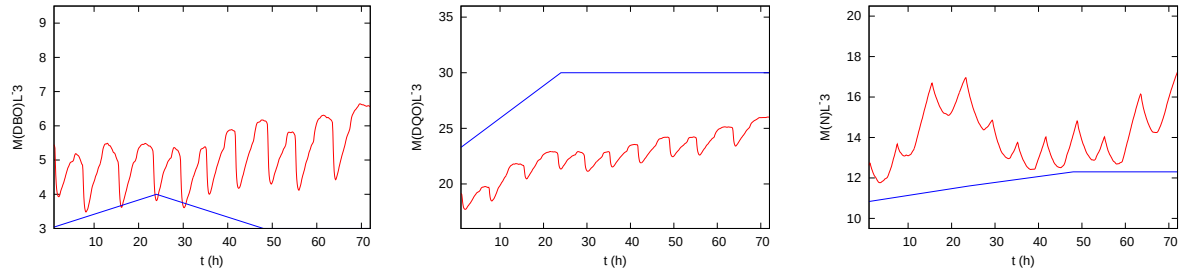

Figura 4.7: Resultados del Modelo 1 (—) y concentraciones reales en el efluente (—).

Como puede observarse, la evolución en el tiempo de las concentraciones proporcionada por la simulación no se ajusta a la realidad. En el caso de la concentración de DBO, mientras que en la realidad oscila entre 3 y 4 g/m^3, en el Modelo 1 oscila entre 4 y 7 g/m^3. En cuanto a la concentración de DQO, pese a que ambas tendencias son ascendentes, los valores alcanzados por ambas evoluciones en el tiempo son significativamente distintos. Por último, la concentración de nitrógeno total del Modelo 1 es superior en todo momento a la real.

A continuación, el Modelo 2 será comparado con la información real. La evolución en el tiempo de las 3 especies antes mencionadas es representada en la Figura 4.8

En este caso los valores de las concentraciones alcanzados en la simulación están más próximos a la realidad que en el Modelo 1. La concentración de DBO de la simulación oscila entre 3 y 4 g/m^3, de la misma forma que la real, aunque la evolución en el tiempo de ambas es diferente. En cuanto a la concentración de DQO, ambas tendencias son ascendentes y los valores alcanzados son similares. Por último, los valores de concentración de nitrógeno total de la simulación son menores que los alcanzados en la realidad.

La evolución en el tiempo de las 3 especies antes mencionadas del Modelo 3, empleando la definición de Takacs para la velocidad de sedimentación, es representada en la Figura 4.9

En este caso las concentraciones presentadas son significativamente diferentes a las reales. En cuanto al DBO, mientras que en la realidad oscila entre 3 y 4 g/m^3, en el Modelo 3 (Takacs) oscila entre 6 y 9

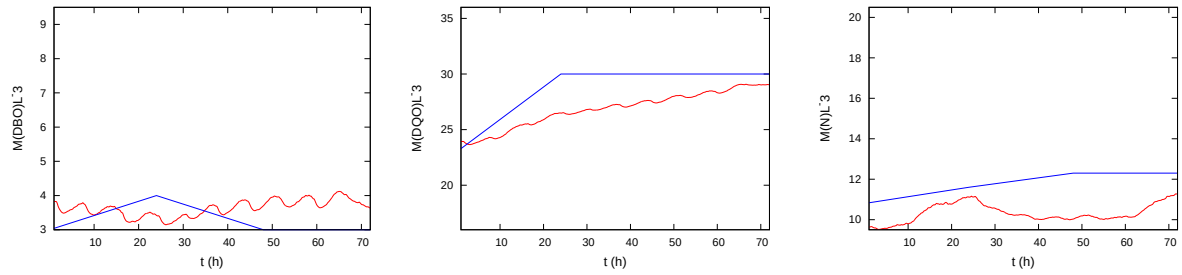

Figura 4.8: Resultados del Modelo 2 (—) y concentraciones reales en el efluente (—).

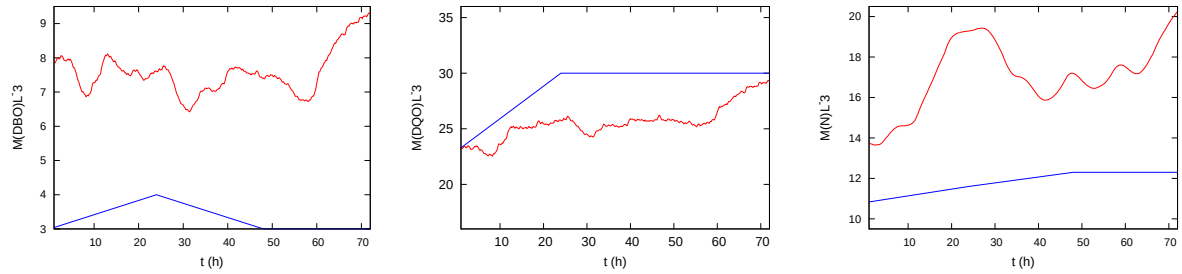

Figura 4.9: Resultados del Modelo 3 (Takacs) (—) y concentraciones reales en el efluente (—).

g/m^3. En cuanto a la concentración de DQO, ambas tendencias son ascendentes y los valores alcanzados son similares. Por último, la concentración de nitrógeno total del Modelo 3 (Takacs) es muy superior en todo momento a la real.

La evolución en el tiempo de las 3 especies antes mencionadas del Modelo 3, empleando la definición de Vesilind para la velocidad de sedimentación, es representada en la Figura 4.10

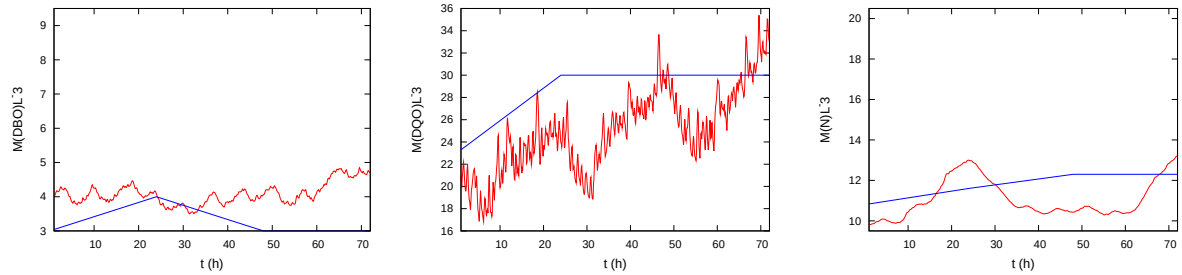

Figura 4.10: Resultados del Modelo 3 (Vesilind) (—) y concentraciones reales en el efluente (—).

En este caso los valores de las concentraciones alcanzados en la simulación son similares a los reales. La concentración de DBO de la simulación oscila entre 3 y 5 g/m^3, mientras que la real entre 3 y 4 g/m^3. La concentración de DQO alcanza valores en la simulación similares a la realidad. Por último, los valores de concentración de nitrógeno total de la simulación oscilan entre 10 y 13 g/m^3, mientras que la real entre 11 y 12 g/m^3.

Como conclusión, la evolución en el tiempo de las concentraciones de las simulaciones es diferente a la realidad. Esto es debido fundamentalmente a las simplificaciones detalladas en la Sección C.5. Por otra parte, pese a que el control de la purga de las simulaciones y la realidad es el mismo, el caudal de purga de las simulaciones difiere con respecto al real debido a que la calidad del fango de recirculación no es la misma. Los resultados proporcionados por las simulaciones permiten afirmar que

- Incluyendo los procesos del ASM1 en el interior del decantador se obtienen mejores resultados que si no se tienen en cuenta (Modelo 2 frente a 1).

- Simulando la operación del decantador con un rendimiento se obtienen aproximaciones razonables del funcionamiento de la planta de tratamiento de aguas residuales (Modelo 2).
- Si se incluye el modelo 1D del decantador en la simulación de la planta deben conocerse o calibrarse de forma correcta los parámetros del mismo, tratando de utilizar parámetros experimentales de la planta (Modelo 3 con Vesilind).

Capítulo 5

Conclusiones

El trabajo desarrollado ha generado una herramienta de simulación numérica del tratamiento secundario de las plantas de tratamiento de aguas residuales en condiciones reales, incluyendo porcesos transitorios. Partiendo de un modelo biológico sofisticado y con el mínimo número de incógnitas, ASM1, se han alcanzado los siguientes objetivos:

- Acoplar cada uno de los elementos del tratamiento secundario y entender correctamente su funcionamiento (3.1.1).
- Modelar/calibrar las relaciones entre las diferentes especies del modelo (3.1.1 y 4.1).
- Comparar la herramienta matemática de simulación de una planta de tratamiento de aguas residuales con el programa comercial Linx ASM1 (3.2) para validar la calidad de los resultados.
- Conocer, implementar y crear nuevos de control empleados en los sistemas de depuración de aguas (4.1), ajustando mejor los niveles de amonio a la salida de planta.
- Adaptar los procesos químicos y etapas hidráulica a la planta EDAR Río Huerva (4.3).

Los modelos matemáticos desarrollados en este trabajo pueden servir como herramienta de simulación para los coordinadores de las plantas de aguas residuales, permitiendo predecir el comportamiento de la planta frente a situaciones extremas de vertido, rotura de equipos, etc.

A pesar del extenso trabajo realizado todavía son posibles nuevas mejoras que podrían aplicarse a estos modelos. Las mejoras a realizar en la próxima etapa del proyecto de investigación son:

- Introducción de modelos biológicos más sofisticados que tienen en cuenta un amplio rango de concentraciones y procesos típicamente presentes en este tipo de sistemas, como ASM2. Sería interesante sustituir el Modelo ASM1 por el Modelo ASM2 para tratar de comprender las directrices del proceso de eliminación biológica del fósforo, ya que el Modelo ASM1 no lo contempla.
- El modelo matemático de los reactores podría mejorarse sustancialmente aplicando una discretización espacial 2D, utilizando un modelo de aguas poco profundas promediado en la vertical, permitiendo simular los gradientes de concentración debido a la operación de los Orbal. Un modelo 3D permitiría tener en cuenta la distribución de concentraciones en la coordenada vertical, aunque supondría un coste computacional de cálculo muy elevada que no permitiría hacer cálculos transitorios de largo tiempo.
- En el decantador, existen modelos matemáticos por calibrar más sofisticados que el modelo 1D empleado en este trabajo, los cuales tienen en cuenta consideraciones como la altura del manto de fango, la sedimentación de los flóculos, etc.

Este trabajo ha sido desarrollado en un contexto académico y empresarial. Durante su elaboración, el autor ha podido conocer el ámbito de la investigación. Sin duda es la actividad que aporta un mayor enriquecimiento personal y profesional del Grado de Ingeniería Mecánica.

Bibliografía

[1] Nelson M.I., Sidhu H.S., Analysis of the activated sludge model (number 1). Applied Mathematics Letters Volume 22, Issue 5, May 2009, Pages 629-635. Introduction.

[2] Sánchez O. Environmental engineering and Activated Sludge Processes: models, methodologies and applications. 2016. Introduction.

[3] Jeppsson U., MSc, PhD, A general description of the IAWQ Activated Sludge Model No. 1. Modelling aspects of wastewater treatment processes. Lund Institute of Technology, 1996, ISBN 91-88934-00-4. Introduction, p. 1.

[4] Henze M., Gujer W., Mino T., van Loosdrecht M. Activated sludge models ASM1, ASM2, ASM2d and ASM3 reprint ed. London : IWA Publishing, 2000. Preface.

[5] Makinia J., Wells S.A. A general model of the activated sludge reactor with dispersive flow-I. Model development and parameter estimation. Introduction, p. 3988. PII: S0043-1354(00)00150-032, 2000.

[6] Sun W. Modeling flocculation in sedimentation tank with depth-averaged method. 2014. Background: Sedimentation tanks, p. 3.

[7] Asensi Dasi E.J. Estudio y modelización de la velocidad de sedimentación zonal y de la aceleración de los fangos activados. 2015. Resumen.

[8] van Haandel A., van der Lubbe J. Handbook biological waste water treatment. Design and optimisation af activated sludge systems. Sludge treatment and disposal, p. 370. Published by: Quist Publishing, Leidschendam, The Netherlands, 2012.

[9] Molina Gil R., Rodríguez Hernández I., Pariente Castillo M.I., Martínez Castillejo R., Vasiliadou I., Melero Hernández J.A. A friendly-Biological Reactor Simulator (BioReSIM) for studying biologial processes in wastewater treatment processes. 2014. @*tic*, revista d'innovació educativa. Examples of application, p. 112.

[10] Grady L., Daigger G., Love G., Filipe C. Biological wastewater treatment, Third Edition. 2011. Preface, xxv.

[11] Henze M., Gujer W., Mino T., van Loosdrecht M. Activated sludge models ASM1, ASM2, ASM2d and ASM3. Activated sludge model no. 1, p. 6-8 reprint ed. London : IWA Publishing, 2000.

[12] Petersen B., Gernaey K., Henze M., Vanrolleghem P.A. Evaluation of an ASM1 model calibration procedure on a municipal and industrial wastewater treatment plant. Introduction, p. 15. IWA Publishing, 2000.

[13] Henze M., Gujer W., Mino T., van Loosdrecht M. Activated sludge models ASM1, ASM2, ASM2d and ASM3. Activated sludge model no. 1, p. 12-15 reprint ed. London : IWA Publishing, 2000.

[14] Herbert H. P. Fang. Environmental anaerobic technology: applications and new developments. 2010. chp. 11, p. 244, 2010.

[15] Henze M., Gujer W., Mino T., van Loosdrecht M. Activated sludge models ASM1, ASM2, ASM2d and ASM3. Activated sludge model no. 1, p. 10-12 reprint ed. London : IWA Publishing, 2000.

[16] Henze M., Gujer W., Mino T., van Loosdrecht M. Activated sludge models ASM1, ASM2, ASM2d and ASM3. Activated sludge model no. 1, p. 11 reprint ed. London : IWA Publishing, 2000.

[17] Henze M., Gujer W., Mino T., van Loosdrecht M. Activated sludge models ASM1, ASM2, ASM2d and ASM3. Activated sludge model no. 1, p. 7 reprint ed. London : IWA Publishing, 2000.

[18] Henze M., Gujer W., Mino T., van Loosdrecht M. Activated sludge models ASM1, ASM2, ASM2d and ASM3. Activated sludge model no. 1, p. 24 reprint ed. London : IWA Publishing, 2000.

[19] Henze M., Gujer W., Mino T., van Loosdrecht M. Activated sludge models ASM1, ASM2, ASM2d and ASM3. Activated sludge model no. 1, p. 25 reprint ed. London : IWA Publishing, 2000.

[20] Suárez J., Jacome A. Espesamiento de fangos de estaciones depuradoras de aguas residuales. 2007. Espesado por centrifugación, p. 21.

[21] Henry J., Heinke G. Ingeniería ambiental. 1999. Aguas residuales, p. 425.

[22] Bishop P., Toxicity Reduction: Evaluation and Control, Volumen 3. Toxicity control evaluation case study, p. 257.

[23] Chudoba J., Tucek F. Production, degradation, and composition of activated sludge in aeration systems without primary sedimentation. Journal (Water Pollution Control Federation). Vol. 57, No. 3, Part I (Mar., 1985), pp. 201-206

[24] Gavrila C., Gruia I. Simulated Suspended Solids Concentrations of Secondary Clarifiers in the Activated Sludge Process Using Comsol Multiphysics Program. Excerpt from the Proceedings of the COMSOL Users Conference 2007 Grenoble. Modelling of secondary clarifiers, p. 2.

[25] Holenda B., Pasztor I., Karpati A. and Redey A. Comparison of one-dimensional secondary settling tank models. 2006. European Water Association (EWA). Model of Hamilton, p. 9.

[26] Asensi Dasi E.J. Estudio y modelización de la velocidad de sedimentación zonal y de la aceleración de los fangos activados. 2015. Velocidad de sedimentación zonal, p. 83.

[27] Asensi Dasi E.J. Estudio y modelización de la velocidad de sedimentación zonal y de la aceleración de los fangos activados. 2015. Velocidad de sedimentación zonal, p. 85.

[28] Asensi Dasi E.J. Estudio y modelización de la velocidad de sedimentación zonal y de la aceleración de los fangos activados. 2015. Índice volumétrico de fango, p. 64.

[29] Spanjers H., Vanrolleghem P., Olsson G. and Doldt P. Respirometry in control of the activated sludge process: benchmarking control strategies. 2002. Settling process model, p. 13-14.

[30] Asensi Dasi E.J. Estudio y modelización de la velocidad de sedimentación zonal y de la aceleración de los fangos activados. 2015. La teoría de flujo de sólidos, p. 97-98.

[31] De Clercq J., Devisscher M., Boonen I., Vanrolleghem P. and Defrancq J. A new one-dimensional clarifier model verification using full scale experimental data. Water Science and Technology, Vol. 47, No. 12, IWA Publishing 2003. Numerical integration, p. 109.

[32] Murillo J. and García Navarro P. Weak solutions for partial differential equations with source terms: Application to the shallow water equations. Journal of Computational Physics 229 (2010). Numerical integration, p. 4329.

[33] Cadet C., Dos Santos Martins V. and Dochain D. Dynamic modeling of clarifier-thickeners for the control of wastewater treatment plants: a critical analysis. Published by IEEE, 2015. Application to settling tanks, p. 4.

[34] Karantonis A. Numerical Solution of Reaction-Diffusion Equations by the Finite Difference Method. 2001. http://users.ntua.gr/antkar/. Thomas algorithm, p. 9-10.

Índice de figuras

3.1. Primera configuración de la planta de aguas residuales. 17
3.2. Quinta configuración de la planta de aguas residuales. 18
3.3. Concentración de la materia orgánica presente en el efluente del Modelo 1 (—), Modelo 2 (—), Modelo 3 (—), Modelo 4 (—), Modelo 5 (—). 20
3.4. Concentración de biomasa heterótrofa en los reactores [0] (—), reactor[1] (—), reactor[2] (—) y efluente (—) del Modelo 1 (izquierda) y 3 (derecha). 21
3.5. Concentración del amonio y amoníaco presente en el efluente del Modelo 1 (—), Modelo 2 (—), Modelo 3 (—), Modelo 4 (—), Modelo 5 (—). 21
3.6. Concentración de biomasa autótrofa en los reactores [0] (—), reactor[1] (—), reactor[2] (—) y efluente (—) del Modelo 1 (izquierda) y 3 (derecha). 21
3.7. Concentración de productos inertes presentes en el efluente del Modelo 1 (—), Modelo 2 (—), Modelo 3 (—), Modelo 4 (—), Modelo 5 (—). 22
3.8. Esquema de la planta. 23

4.1. Esquema de la planta 27
4.2. Velocidad de rotación del rotor A (—), D (—), B (—) y C (—) durante el ciclo de subida-bajada 27
4.3. Secuencia de decisión cuando la concentración de amonio-amoníaco aumenta (izquierda) o disminuye (derecha) en el tercer reactor. 28
4.4. Concentración de nitrógeno total en el tercer reactor empleando el método de control manual (izquierda) y el método de control alternativo (derecha). 29
4.5. Configuración de la planta. 29
4.6. Discretización del clarificador 31
4.7. Resultados del Modelo 1 (—) y concentraciones reales en el efluente (—). 32
4.8. Resultados del Modelo 2 (—) y concentraciones reales en el efluente (—). 33
4.9. Resultados del Modelo 3 (Takacs) (—) y concentraciones reales en el efluente (—). 33
4.10. Resultados del Modelo 3 (Vesilind) (—) y concentraciones reales en el efluente (—). 33

A.1. Plot of the growth rate provided by Equation (A.3) (red line) and Equation (A.4) (blue line) 46
A.2. Scheme of processes carried out in ASM1. 50

B.1. Plant layout and nomenclature of the relevant points. 52
B.2. Plant layout and nomenclature of the relevant points. 53
B.3. Plant layout and nomenclature of the relevant points. 54
B.4. Control Volumes. 55
B.5. Plant layout and nomenclature of the relevant points. 56

B.6. Control Volume. 58
B.7. Control Volumes. 59
B.8. Plant layout and nomenclature of the relevant points. 60
B.9. Control Volume. 61
B.10. Control Volume. 62
B.11. Control Volumes. 63
B.12. Section B.6.1. Influent volumetric flow. 65
B.13. Section B.6.1. Concentration of the 13 species in the influent. 66
B.14. Section B.6.2. Volumetric flow of the effluent. 67
B.15. Section B.6.2. Concentration of the 13 species in the reactor[0] (—), reactor[1] (—), reactor[2] (—), effluent (—). 68
B.16. Volumetric flow of the effluent (—), recirculation (—). 69
B.17. Concentration of the 13 species in the reactor[0] (—), reactor[1] (—), reactor[2] (—), effluent (—). 70
B.18. Concentration of the 13 species in the recirculation. 71
B.19. Volumetric flow of the effluent (—), recirculation (—), purge (—). 72
B.20. Concentration of the 13 species in the reactor[0] (—), reactor[1] (—), reactor[2] (—), effluent (—). 73
B.21. Concentration of the 13 species in the recirculation and purge. 74
B.22. Volumetric flow of the effluent (—), recirculation (—), purge (—). 75
B.23. Concentration of the 13 species in the reactor[0] (—), reactor[1] (—), reactor[2] (—), effluent (—). 76
B.24. Concentration of the 13 species in the total recirculation (—), purge (—). 77
B.25. Volumetric flow of the effluent (—), recirculation (—), purge (—), dehydrated sludge (—). 78
B.26. Concentration of the 13 species in the reactor[0] (—), reactor[1] (—), reactor[2] (—), effluent (—). 79
B.27. Concentration of the 13 species in the total recirculation (—), purge (—). 80
B.28. Concentration of the 13 species in the dehydrated sludge. 81
B.29. Concentration of the 13 species in the effluent from Model 1 (—), Model 2 (—), Model 3 (—), Model 4 (—), Model 5 (—). 82
B.30. η_{DBO} and η_{NH} from Model 1 (—), Model 2 (—), Model 3 (—), Model 4 (—), Model 5 (—). 83
B.31. Plant layout and nomenclature of the relevant points. 86
B.32. Volumetric flow of the influent (—), effluent (—), recirculation (—), purge (—), dehydrated sludge (—). 87
B.33. Concentration of the 13 species in the influent. 88
B.34. Concentration of the 13 species in the reactor. 89
B.35. Concentration of the 13 species in the effluent. 90
B.36. Concentration of the 13 species in the total recirculation (—), purge (—). 91
B.37. Concentration of the 13 species in the dehydrated sludge. 92

C.1. Concentration of ammonium (—), nitrite (—) and oxygen dissolved (—) in the third reactor. 98
C.2. Concentration of ammonium (—), nitrite (—) and oxygen dissolved (—) in the third reactor. 98
C.3. Influent (—) and effluent (—). 99
C.4. Purge flow. 100
C.5. Influent (—), effluent (—) and recirculation (—). 101

C.6. Plant scheme . . . 103
C.7. Rotational speed in rotor A (—), D (—), B (—) and C (—) during an up-down cycle, considering the above-mentioned regulation parameters . . . 105
C.8. Ammonium-ammonia concentration increase case. . . . 106
C.9. Ammonium-ammonia concentration decrease case. . . . 107
C.10. Concentration of total nitrogen in third reactor using manual control (left) and automatic control (right). . . . 108
C.11. Plant layout and nomenclature of the relevant points. . . . 109
C.12. Control Volumes. . . . 110
C.13. Plant layout and nomenclature of the relevant points. . . . 112
C.14. Control Volumes. . . . 113
C.15. Plant layout and nomenclature of the relevant points. . . . 115
C.16. Clarifier zones . . . 118
C.17. Clarifier discretization . . . 119
C.18. Solid flux . . . 120
C.19. Distribution of the concentration throughout the clarifier from 1400 to 2300 seconds. . . . 121
C.20. Distribution of the concentration throughout the clarifier taking into account the diffusion term, from 1400 to 2300 seconds. . . . 124
C.21. Influent (—) and recirculation ratio (—). . . . 125
C.22. Concentration of the 13 species in effluent. . . . 126
C.23. Volumetric flow of the effluent (—) and purge (—) using the Model described in Subsection C.4.1. . . . 128
C.24. Volumetric flow of the effluent (—) and purge (—) using the Model described in Subsection C.4.2. . . . 128
C.25. Volumetric flow of the effluent (—) and purge (—) using the Model described in Subsection C.4.3 (Takacs). . . . 129
C.26. Volumetric flow of the effluent (—) and purge (—) using the Model described in Subsection C.4.3 (Vesilind). . . . 129
C.27. Concentration of the 13 species in the effluent using the Model described in Subsection C.4.1. . . . 130
C.28. Concentration of the 13 species in effluent using the Model described in Subsection C.4.2. 131
C.29. Concentration of the 13 species in effluent using the Model described in Subsection C.4.3 (Takacs). . . . 132
C.30. Concentration of the 13 species in effluent using the Model described in Subsection C.4.3 (Vesilind). . . . 133
C.31. Concentration of DBO (—), DQO (—) and total nitrogen (—) in the effluent using the Model described in Subsection C.4.1. . . . 134
C.32. Concentration of DBO (—), DQO (—) and total nitrogen (—) in the effluent using the Model described in Subsection C.4.2. . . . 134
C.33. Concentration of DBO (—), DQO (—) and total nitrogen (—) in the effluent using the Model described in Subsection C.4.3 (Takacs). . . . 134
C.34. Concentration of DBO (—), DQO (—) and total nitrogen (—) in the effluent using the Model described in Subsection C.4.3 (Vesilind). . . . 134
C.35. Results of the simulation described in Subsection C.4.1 (—) and real concentrations in the effluent (—). . . . 135
C.36. Results of the simulation described in Subsection C.4.2 (—) and real concentrations in the effluent (—). . . . 135

C.37. Results of the simulation described in Subsection C.4.3 (—), using Takacs' definition of settling velocity, and real concentrations in the effluent (—). 136
C.38. Results of the simulation described in Subsection C.4.3 (—), using Vedilind's definition of settling velocity, and real concentrations in the effluent (—). 137

Índice de cuadros

2.1. Componentes solubles, $S_{(\cdot)}$. . . . 14
2.2. Componentes particulados, $X_{(\cdot)}$. . . . 14
2.3. Porcesos cinéticos y estequiométricos de la oxidación del carbono, nitrificación y desnitrificación en ASM1. . . . 16

3.1. Variables de los modelos 18
3.2. Parámetros de caudales de la planta 19
3.3. Parámetros de equipos centrífugos de la planta 20
3.4. Parámetros de la planta 23
3.5. Resumen de resultados 23

4.1. Variables de los modelos 30

A.1. Summary of soluble components, $S_{(\cdot)}$. . . . 47
A.2. Summary of particulated components, $X_{(\cdot)}$. . . . 47
A.3. Summary of the main variables in the ASM1. . . . 47
A.4. Table of stoichiometric and kinetic parameters. . . . 48
A.5. Process kinetics and stoichometry for carbon oxidation, nitrification and denitrification in ASM1. . . . 49

B.1. Table of variables in the model 52
B.2. Table of variables in the model 53
B.3. Table of variables in the model 54
B.4. Table of variables in the model 56
B.5. Table of variables in the model 60
B.6. Table of variables in the model 86
B.7. Summary of soluble components, $S_{(\cdot)}$. . . . 93
B.8. Study on the sensitivity of the concentration of dissolved oxygen in the reactors. . . . 94
B.9. Study on the sensitivity of the concentration of purge flow. . . . 94

C.1. Orbal parameters. . . . 104
C.2. Table of variables in the model 109
C.3. Table of variables in the model 112
C.4. Table of variables in the model 115
C.5. Correlations of sedimentation parameters. . . . 117
C.6. Initial concentration of the 13 species in the reactors. . . . 127

C.7. Initial concentration of the 13 species in the reactors and in the clarifier. 127

Apéndice A

Biological modelling

A.1. Kinetics of the microbial-growth processes

Let us consider the concentration of an arbitrary component i (either soluble or particulated), denoted by ϕ_i, and suppose that its variation in time due to a chemical process is given by a function r_i, as follows

$$\frac{d\phi_i}{dt} = r_i \tag{A.1}$$

Consider also that r_i depends upon three parameters as

$$r_i = r_i(r_{i,max}, K_j, \phi_j)\,, \tag{A.2}$$

where $r_{i,max}$ is the maximum rate of variation, K_j is the half-velocity constant (value of ϕ_j when $r_i/r_{i,max} = 0{,}5$) and ϕ_j the concentration of the limiting substance. Then, two types of microbial-growth processes can be defined:

- If the microbial-growth for substance i is only possible when substance j is present, then the growth rate is given by the so-called *Monod equation* [11]

$$r_i = r_{i,max}\frac{\phi_j}{K_j + \phi_j}\,. \tag{A.3}$$

  This was particularly necessary for processes that depend upon the type of electron acceptor present.

- If the microbial-growth for substance i only occurs when substance j is absent, then the growth rate is given by

$$r_i = r_{i,max}\frac{K_j}{K_j + \phi_j}\,. \tag{A.4}$$

  Processes which occur only when dissolved oxygen is absent may be turned on by Equation A.4.

The two types of microbial growth rate are depicted in Figure A.1, where the growth rate provided by Equation (A.3) is represented by red line and while that in Equation (A.4) by blue line.

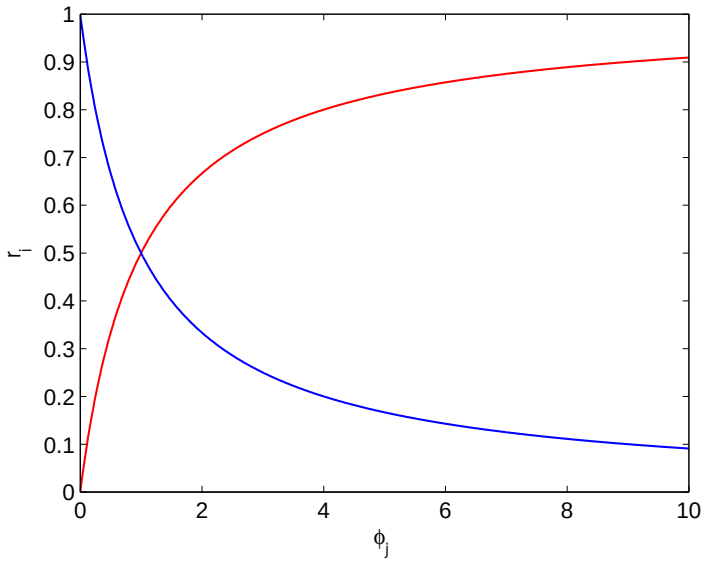

Figura A.1: Plot of the growth rate provided by Equation (A.3) (red line) and Equation (A.4) (blue line)

A.2. The Activated Sludge Model No. 1 (ASM1) model

The ASM1 model includes eight processes that are fundamental to the activated sludge process. These are: aerobic and anoxic growth of heterotrophic biomass, death of heterotrophic biomass, aerobic growth of autotrophic biomass, decay of autotrophic biomass, ammonification of soluble organic nitrogen and hydrolysis of both entrapped particulate organic matter and entrapped organic nitrogen [13].

A.2.1. Type of components in the model

Two kind of components can be found within the flow inside biological reactors in waste water processes:

- Soluble components, $S_{(.)}$: Are those components transported with the water. May carry ionic charge.
- Particulate components, $X_{(.)}$: Are those components which are floculated onto the activated sludge.

A.2.2. Measurement of the components

Three measures have gained acceptance and are nowadays widely used in activated sludge models:

- Biochemical oxygen demand (BOD)
- Total organic carbon (TOC)
- Chemical oxygen demand (COD)

the latter being, the COD, the most superior among them because it provides a link between electron equivalents in the organic substrate, the biomass and the oxygen utilized [14].

A.2.3. Definition of the components

The complete relation of soluble components, $S_{(.)}$, are defined in Table A.1 and that of particulate components, $X_{(.)}$, in Table A.2 [15].

Symbol	Component name	Dimensions
S_S	Readily biodegradable substrate	$M(COD)L^{-3}$
S_I	Soluble inert organic matter	$M(COD)L^{-3}$
S_O	Dissolved oxygen	$M(O_2)L^{-3}$
S_{NO}	Nitrate and nitrite nitrogen	$M(N)L^{-3}$
S_{NH}	$NH_4^+ + NH_3$ nitrogen	$M(N)L^{-3}$
S_{ND}	Soluble biodegradable organic nitrogen	$M(N)L^{-3}$
S_{ALK}	Alkalinity of wastewater	$mol(HCO_3^-)L^{-3}$

Cuadro A.1: Summary of soluble components, $S_{(\cdot)}$.

Symbol	Component name	Dimensions
X_I	Particulate inert organic matter	$M(COD)L^{-3}$
X_S	Slowly biodegradable substrate	$M(COD)L^{-3}$
$X_{B,H}$	Active heterotrophic biomass	$M(COD)L^{-3}$
$X_{B,A}$	Active autotrophic biomass	$M(COD)L^{-3}$
X_P	Particulate products arising from biomass decay	$M(COD)L^{-3}$
X_{ND}	Particulate biodegradable organic nitrogen	$M(N)L^{-3}$

Cuadro A.2: Summary of particulated components, $X_{(\cdot)}$.

A.2.4. Equations of the ASM1 model

Preliminaries and notation

Matrix notation will be hereafter used for the description of the ASM1 model. Components in Tables A.1 and A.2 are denoted by subscript i and stored in the vector ϕ_i, with $i = 1, ..., N_{comp}$, where N_{comp} the total number of components, while the processes (chemical reactions) are characterized by subscript j, with $j = 1, ..., N_{proc}$, where N_{proc} is the total number of processes. In the ASM1 we have

$$N_{comp} = 13\,, \qquad N_{proc} = 8\,. \tag{A.5}$$

The stoichiometric coefficients are expressed in the form of a stoichiometric matrix, ν_{ji}, presented in Table A.5 and the process rate equations in the form of a vector, ρ_j, also presented in Table A.5. The rate of production of component i is expressed in the form of another vector, r_i, which will be detailed later. A complete relation of the ASM1 variables is presented in Table A.3 [16].

Variable	Variable name	index	Dimension	Dimension (num.)
ϕ_i	Components	i	N_{comp}	13
	Processes	j	N_{proc}	8
ν_{ji}	Stoichiometric matrix		$N_{proc} \times N_{comp}$	8×13
ρ_j	Process rate equations		N_{proc}	8
r_i	Growth rate		N_{comp}	13

Cuadro A.3: Summary of the main variables in the ASM1.

Growth equation

The growth rate for each component i is computed as a matrix-vector product of ν_{ji} with ρ_j [17], as follows

$$r_i = \sum_{j=1}^{N_{proc}} \nu_{ji} \cdot \rho_j\,, \tag{A.6}$$

with the summation accounts for the contribution of each process in the growth of ϕ_i. The growth rate for each equation can be computed straightforward from Table A.5.

Parameter values

The parameter values used in this report are listed in Table A.4 for $20°C$ [18]. These values are considered to be habitual for neutral pH and domestic wastewater.

Symbol	Units	Value	θ
Stoichiometric param.			
Y_A	(g cell COD formed) / (g N oxidixed)	0.24	
Y_H	(g cell COD formed) / (g COD oxidixed)	0.6	
f_P	dimensionless	0.08	
i_{XB}	(g N in biomass)/(g COD) in biomass	0.086	
i_{XE}	(g N in endogenous mass)/(g COD) in endogenous mass	0.06	
Kinetic param.			
μ_H	day^{-1}	2.95	1.072
K_S	g COD/m^3	20	
$K_{O,H}$	g O2/m^3	0.2	
K_{NO}	g NO3-N/m^3	0.5	
b_H	day^{-1}	0.06	1.072
η_g	dimensionless	0.8	
η_h	dimensionless	0.4	
k_h	(g slowly biodegradable COD)/(g cell COD)/(day)	3.0	1.116
K_X	(g slowly biodegradable COD)/(g cell COD)	0.03	1.116
μ_A	day^{-1}	0.8	1.103
K_{NH}	gNH3-N /(m^3)	1.0	
$K_{O,A}$	g O2/(m^3)	0.4	
k_a	m^3 COD /(g $\cdot$ day)	0.08	1.072
b_A	day^{-1}	0.36	1.120

Cuadro A.4: Table of stoichiometric and kinetic parameters.

It should be noted that, within a narrow temperature range, a temperature increase generally results in a coefficient value increase, like μ, b or k_h, in a manner that can be described by a modified Arrhenius equation [19], as follows

$$P(T) = P(20°C)\theta_p^{T-20}, \tag{A.7}$$

where P is the temperature-dependent parameter under consideration, $P(20°C)$ the nominal value for P at $20°C$ and θ_p the corresponding temperature correction factor in Table A.4.

The above-mentioned parameters and processes which are included in ASM1 Model are depicted in Table A.5

Cuadro A.5: Process kinetics and stoichometry for carbon oxidation, nitrification and denitrification in ASM1.

Process $j \rightarrow$ Component i $\downarrow$	*Aerobic growth of heterotrophs*	*Anoxic growth of heterotrophs*	*Aerobic growth of autotrophs*	*Decay of heterotrophs*	*Decay of autotrophs*	*Ammonification of soluble organic nitrogen*	*Hidrolysis of entrapped organics*	*Hidrolysis of entrapped organic nitrogen*
S_I	0	0	0	0	0	0	0	0
S_S	$-\frac{1}{Y_H}$	$-\frac{1}{Y_H}$	0	0	0	0	1	0
X_I	0	0	0	0	0	0	0	0
X_S	0	0	0	1-f_P	1-f_P	0	-1	0
$X_{B,H}$	1	1	0	-1	0	0	0	0
$X_{B,A}$	0	0	1	0	-1	0	0	0
X_P	0	0	0	f_P	f_P	0	0	0
S_O	$-\frac{1-Y_H}{Y_H}$	0	$-\frac{4,57-Y_A}{Y_A}$	0	0	0	0	0
S_{NO}	0	$-\frac{1-Y_H}{2,86Y_H}$	$\frac{1}{Y_A}$	0	0	0	0	0
S_{NH}	$-i_{XB}$	$-i_{XB}$	$-i_{XB}-\frac{1}{Y_A}$	0	0	1	0	0
S_{ND}	0	0	0	0	0	-1	0	1
X_{ND}	0	0	0	$-i_{XB}-f_P i_{XP}$	$-i_{XB}-f_P i_{XP}$	0	0	-1
S_{ALK}	$-\frac{i_{XB}}{14}$	$\frac{1-Y_H}{14\cdot 2,86Y_H}-\frac{i_{XB}}{14}$	$\frac{i_{XB}}{14}-\frac{1}{7Y_A}$	0	0	$\frac{1}{14}$	0	0
Process rate $\rho_j\left[ML^{-3}T^{-1}\right]$	$\hat{u}_H\left(\frac{S_S}{K_S+S_S}\right)\left(\frac{S_O}{K_{O,H}+S_O}\right)X_{B,H}$	$\hat{u}_H\left(\frac{S_S}{K_S+S_S}\right)\left(\frac{K_{O,H}}{K_{O,H}+S_O}\right)\left(\frac{S_{NO}}{K_{NO}+S_{NO}}\right)\eta_g X_{B,H}$	$\hat{u}_A\left(\frac{S_{NH}}{K_{NH}+S_{NH}}\right)\left(\frac{S_O}{K_{O,A}+S_O}\right)X_{B,A}$	$b_H X_{B,H}$	$b_A X_{B,A}$	$k_a S_{N,D} X_{B,H}$	$k_h\frac{X_S/X_{B,H}}{K_X+(X_S/X_{B,H})}[\left(\frac{S_O}{K_{O,H}+S_O}\right)+$ $+\eta_b\left(\frac{K_{O,H}}{K_{O,H}+S_O}\right)\left(\frac{S_{NO}}{K_{NO}+S_{NO}}\right)]X_{B,H}$	$\rho_7\left(\frac{X_{ND}}{X_S}\right)$

In order to understand what parameters intervene in each reaction, the following scheme is presented

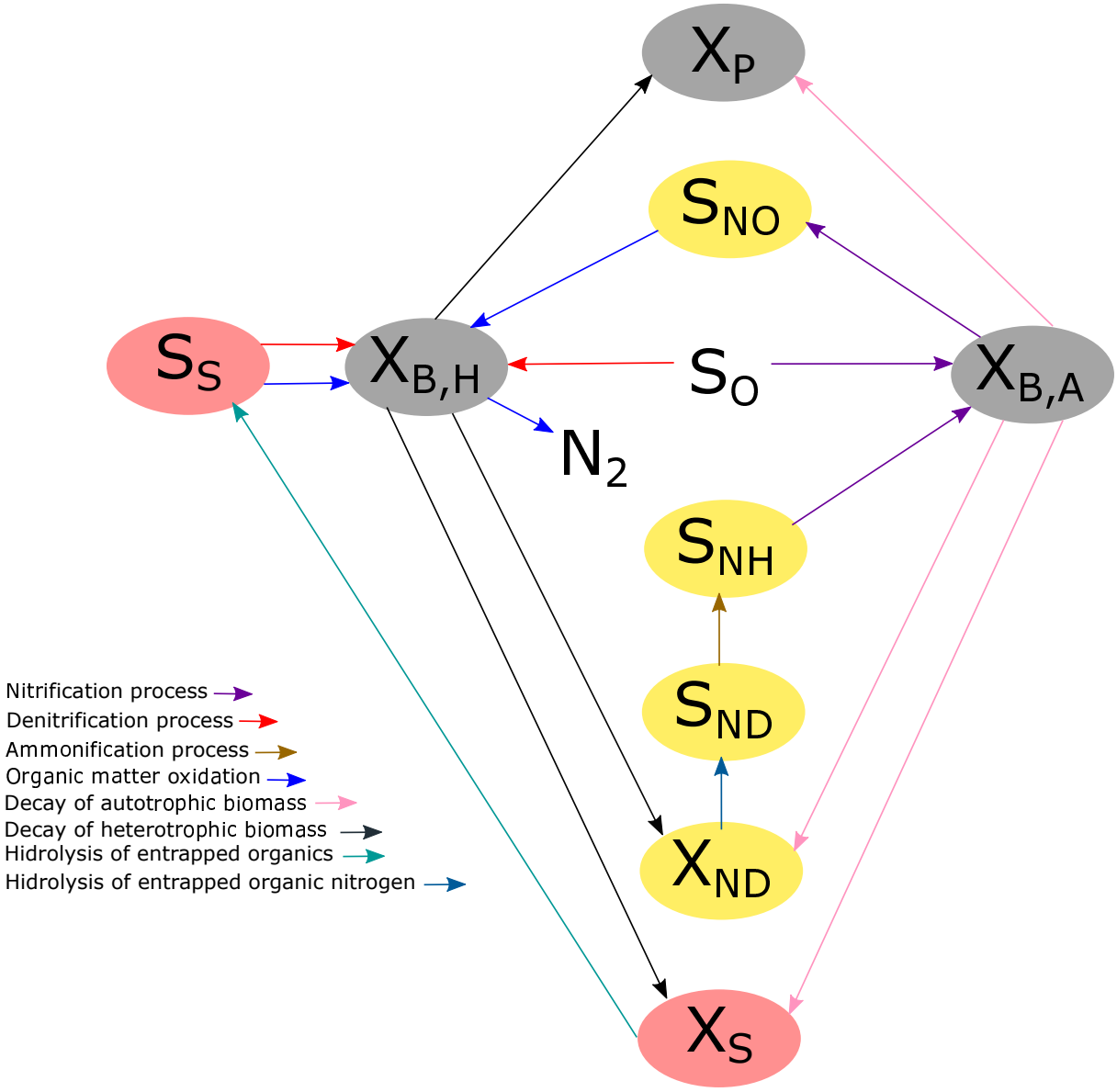

Figura A.2: Scheme of processes carried out in ASM1.

As can be observed, there are some process which are not named as in ASM1 Model. These processes are organic matter oxidation, nitrification and denitrification. This is because the aforementioned processes take part of others. For example, the nitrification process take part of aerobic growth of autotrophs, the denitrification process take part of anoxic growth of heterotrophs and the organic matter oxidation takes part of aerobic growth of heterotrophs.

Apéndice B

Modelling of the water treatment plant vs. Linx ASM1

In this Chapter, five wastewater plant models which has been simulated are presented. The aforementioned simulations are carried out in zero-dimensional space, which means the concentrations of the 13 species in each reactors are the same in all the volume. On the one hand, the first and second reactor are connected by a side gate, as well as the second and third reactor. The side gates are located at the bottom of the reactors. The flow discharge between reactors is calculated as follows

$$Q_{br} = 0{,}611 b_g h_g \sqrt{2g|l_2 - l_1|}, \tag{B.1}$$

where l_2 and l_1 are the reactor levels, b_g is the width of the gate, h_g is the gate opening and g is the gravity acceleration.

On the other hand, the third reactor has two side spillways in order to evacuate the extra volume of the reactor. The flow discharge, which leaves from the third reactor and is carried to the clarifier, is calculated as follows

$$Q_{sp} = F_r \sqrt{g H_w} H_w L_{sp}, \tag{B.2}$$

where F_r is the Froude number and takes a value of 1, L_{sp} is the spillway length, H_w is the height of the water layer and g is the gravity acceleration.

Finally, the clarifier has one spillway in order to evacuate the extra volume of it. The flow discharge, which leaves from the clarifier, is defined as the effluent discharge and is calculated likewise Equation B.2.

B.1. Model 1

The layout of the first simulated wastewater plant is depicted in Figure B.1. As can be observed, this model recreates a wastewater plant without sludge recirculation. It consists of three reactors and one clarifier. The main variables included in the model are summarized in Table B.1. Note that from the concentration and volumetric discharge, the massflow can be defined as $\dot{m}_{(\cdot)} = X_{(\cdot)} \cdot q_{(\cdot)}$.

In the model designed here, it is necessary to make the following assumptions:

- In the reactors, the first of them operates under anoxic conditions ([0]) and the remainder of them, under aerobic conditions ([1] and [2]). In order to represent both situations, the oxygen dissolved

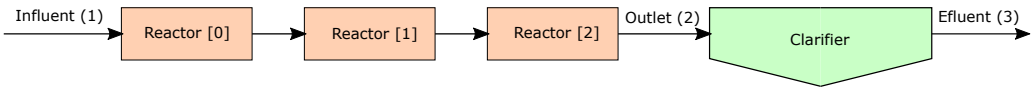

Figura B.1: Plant layout and nomenclature of the relevant points.

Concentration	Discharge	Description
X_1, S_1	q_1	Influent of the plant
X_2, S_2	q_2	Outlet of the reactor (spillway)
X_3, S_3	q_3	Effluent of the plant

Cuadro B.1: Table of variables in the model

concentration is fixed at 0 and 1 ($M(-COD)L^{-3}$), respectively. Furthermore, the ASM1 processes are only carried out within them.

- In the clarifier, the soluble components are considered to be homogeneously distributed within the volume. It is modelled in order to separate particulate components and soluble components. The concentration of the soluble components in the effluent is considered to be the concentration of those components at the outlet of the reactor, $S_3 = S_2$.
- In the clarifier, the particulate components are considered to be partially deposited by sedimentation, that means most of solids come out of the plant. However, a small fraction of these solids come out of the plant through the effluent. The concentration of the particulate components in the effluent are calculated, as follows

$$X_3 = X_2(1 - \eta_c), \tag{B.3}$$

where η_c is the clarifier yield.

B.2. Model 2

The layout of the second simulated wastewater plant is depicted in Figure B.2. As can be observed, this model recreates a wastewater plant with sludge recirculation. It consists of three reactors, one clarifier and a recirculation line. The main variables included in the model are also summarized in Table B.2, as shown in Model 1. Note that from the concentration and volumetric discharge, the massflow can be defined as $\dot{m}_{(\cdot)} = X_{(\cdot)} \cdot q_{(\cdot)}$.

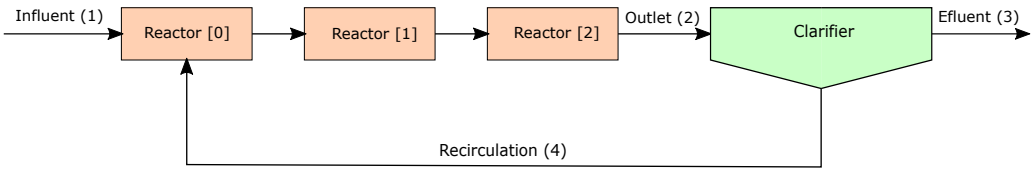

Figura B.2: Plant layout and nomenclature of the relevant points.

Concentration	Discharge	Description
X_1, S_1	q_1	Influent of the plant
X_2, S_2	q_2	Outlet of the reactor (spillway)
X_3, S_3	q_3	effluent of the plant
X_4, S_4	q_4	Recirculation

Cuadro B.2: Table of variables in the model

In the model designed here, it is necessary to make the following assumptions:

- The recirculation discharge is defined as $q_4 = rq_1$, where r is the recirculation factor.
- The effluent discharge is defined as $q_3 = q_1$.
- In the reactors, the first of them operates under anoxic conditions ([0]) and the remainder of them, under aerobic conditions ([1] and [2]). In order to represent both situations, the oxygen dissolved concentration is fixed at 0 and 1 ($M(COD)L^{-3}$), respectively. Furthermore, the ASm1 processes are only carried out within them.
- In the clarifier, the soluble components are considered to be homogeneously distributed within the volume. It is modelled in order to separate particulate components and soluble components. The concentration of the soluble components in both the effluent and the recirculation are considered to be the concentration of those components at the outlet of the reactor, $S_2 = S_3 = S_4$.
- In the clarifier, the particulate components are considered to be partially deposited by sedimentation, that means most of solids come out of the plant through the recirculation and they come back to the first reactor. However, a small fraction of these solids come out of the plant through the effluent. The concentration of the particulate components in the effluent are calculated, as follows

$$X_3 = X_2(1 - \eta_c), \tag{B.4}$$

where η_c is the clarifier yield.

Once the assumptions have been made, it is necessary to determine the transfer function between the concentration of the particulate components in the recirculation and in the outlet of the reactor ($X_4 = f(X_2)$). For this purpose, a mass balance for water and particulate components in the clarifier is made. The mass balance for water is represented as

$$q_2 = q_3 + q_4. \tag{B.5}$$

Considering that $q_4 = rq_1$ and $q_3 = q_1$, it results

$$q_2 = q_1(1 + r). \tag{B.6}$$

The second mass balance is represented as

$$\dot{m}_2 = \dot{m}_4 + \dot{m}_3, \tag{B.7}$$

that can be written as

$$X_2 q_2 = X_4 q_4 + X_3 q_3. \tag{B.8}$$

Considering equation (B.6), $q_4 = r q_1$, equation (B.4) and $q_3 = q_1$, it results

$$X_2 q_1 (1 + r) = X_4 r q_1 + X_2 (1 - \eta_c) q_1. \tag{B.9}$$

Finally, the concentration of the particulate components in the recirculation are

$$X_4 = \frac{X_2 (r + \eta_c)}{r}. \tag{B.10}$$

B.3. Model 3

The layout of the third simulated wastewater plant is depicted in Figure B.3. As can be observed, this model recreates a wastewater plant with sludge recirculation and purge. It consists of three reactors, one clarifier, a recirculation line and purge discharge. The main variables included in the model are also summarized in Table B.3, as shown in Model 1 and 2. Note that from the concentration and volumetric discharge, the massflow can be defined as $\dot{m}_{(\cdot)} = X_{(\cdot)} \cdot q_{(\cdot)}$.

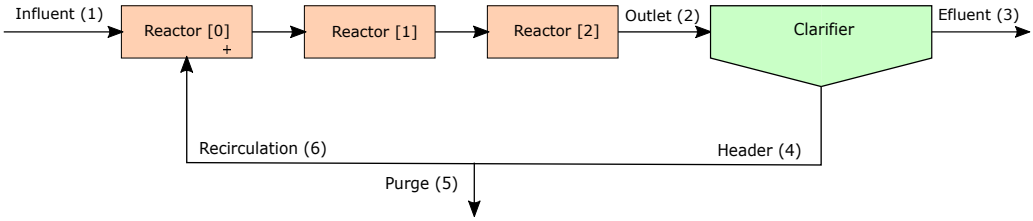

Figura B.3: Plant layout and nomenclature of the relevant points.

Concentration	Discharge	Description
X_1, S_1	q_1	Influent of the plant
X_2, S_2	q_2	Outlet of the reactor (spillway)
X_3, S_3	q_3	effluent of the plant
X_4, S_4	q_4	Header
X_5, S_5	q_5	Purge
X_6, S_6	q_6	Recirculation

Cuadro B.3: Table of variables in the model

In the model designed here, it is necessary to make the following assumptions:

- The header discharge is defined as $q_4 = r q_1$, where r is the recirculation factor.
- The recirculation discharge is defined as $q_6 = q_4 (1 - p)$, where p is the fraction of header discharge purged.
- In the reactors, the first of them operates under anoxic conditions ([0]) and the remainder of them, under aerobic conditions ([1] and [2]). In order to represent both situations, the oxygen dissolved concentration is fixed at 0 and 1 ($M(-COD)L^{-3}$), respectively. Furthermore, the ASm1 processes are only carried out within them.

- In the clarifier, the soluble components are considered to be homogeneously distributed within the volume. It is modelled in order to separate particulate components and soluble components. The concentration of the soluble components in both the effluent and the recirculation are considered to be the concentration of those components at the outlet of the reactor, $S_2 = S_3 = S_4$. It should be noted that the concentration of all the components in the header, purge and recirculation do coincide.
- In the clarifier, the particulate components are considered to be partially deposited by sedimentation, that means most of solids come out of the plant through the header. However, a small fraction of these solids come out of the plant through the effluent. The concentration of the particulate components in the effluent are calculated, as follows

$$X_3 = X_2(1 - \eta_c), \tag{B.11}$$

where η_c is the clarifier yield.

Once the assumptions have been made, it is necessary to determine the transfer function between the concentration of the particulate components in the recirculation and in the outlet of the reactor ($X_4 = f(X_2)$). For this purpose, two control volumes are defined and a mass balance for water and particulate components in the clarifier is made. It should be noted that the concentrations of the particulate components in both the purge and the recirculation are considered to be the concentration of those components in the header. The first control volume is depicted on the left side and the other is depicted on the right side of Figure B.4.

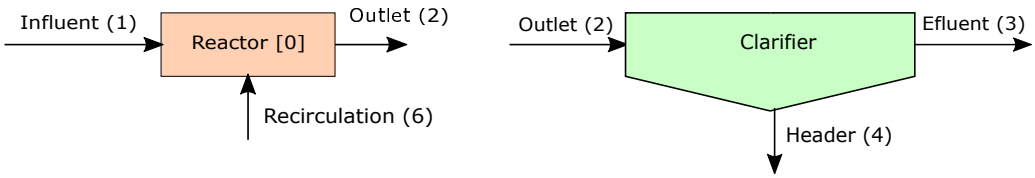

Figura B.4: Control Volumes.

Writing a water mass balance for the first control volume,

$$q_2 = q_1 + q_6, \tag{B.12}$$

and knowing that $q_4 = rq_1$ and $q_6 = q_4(1 - p)$, it results

$$q_2 = q_1(1 + r - rp). \tag{B.13}$$

Writing a water mass balance for the second control volume,

$$q_2 = q_3 + q_4, \tag{B.14}$$

and knowing that $q_4 = rq_1$, it results

$$q_2 = q_3 + q_1 r. \tag{B.15}$$

Combining both equations, (B.13) and (B.15), q_e results

$$q_3 = q_1(1 - rp). \tag{B.16}$$

Writing a particulate components mass balance for the second control volume, it results

$$\dot{m}_2 = \dot{m}_4 + \dot{m}_3, \tag{B.17}$$

that can be written as

$$X_2 q_2 = X_4 q_4 + X_3 q_3. \tag{B.18}$$

Considering equation (B.13), $q_4 = r q_1$, equation (B.11) and (B.16), it results

$$X_2 q_1 (1 + r - rp) = X_4 r q_1 + X_2 (1 - \eta_c) q_1 (1 - rp). \tag{B.19}$$

Finally, the concentrations of the particulate components in the header are

$$X_4 = \frac{X_2 (r + \eta_c - r\eta_c p)}{r}. \tag{B.20}$$

B.4. Model 4

The layout of the fourth simulated wastewater plant is depicted in Figure B.5. As can be observed, this model recreates a wastewater plant with sludge recirculation, purge and sludge thickener. It also consists of three reactors, one clarifier and two recirculation lines. The first of them comes from the clarifier and the other comes from the sludge thickener. The main variables included in the model are also summarized in Table B.4, as shown in Model 1, 2 and 3. Note that from the concentration and volumetric discharge, the massflow can be defined as $\dot{m}_{(\cdot)} = X_{(\cdot)} \cdot q_{(\cdot)}$.

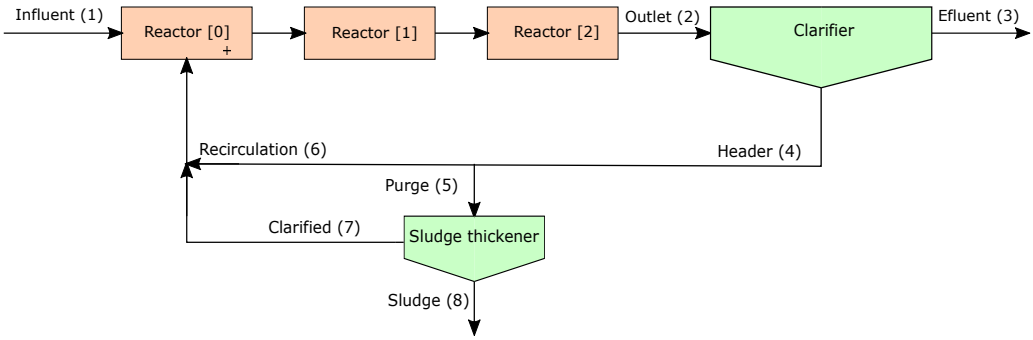

Figura B.5: Plant layout and nomenclature of the relevant points.

Concentration	Discharge	Description
X_1, S_1	q_1	Influent of the plant
X_2, S_2	q_2	Outlet of the reactor (spillway)
X_3, S_3	q_3	effluent of the plant
X_4, S_4	q_4	Header
X_5, S_5	q_5	Purge
X_6, S_6	q_6	Recirculation
X_7, S_7	q_7	Clarified
X_8, S_8	q_8	Sludge

Cuadro B.4: Table of variables in the model

In the model designed here, it is necessary to make the following assumptions:

- The header discharge is defined as $q_4 = r q_1$, where r is the recirculation factor.
- The recirculation discharge is defined as $q_6 = q_4(1 - p)$, where p is the fraction of header discharge purged.

- The clarified discharge is defined as $q_7 = q_5 f_{cl}$, where f_{cl} is the fraction of purged discharge thickened.
- In the reactors, the first of them operates under anoxic conditions ([0]) and the remainder of them, under aerobic conditions ([1] and [2]). In order to represent both situations, the oxygen dissolved concentration is fixed at 0 and 1 ($M(-COD)L^{-3}$), respectively. Furthermore, the ASm1 processes are only carried out within them.
- In the clarifier, the soluble components are considered to be homogeneously distributed within the volume. It is modelled in order to separate particulate components and soluble components. The concentration of the soluble components in both the effluent and the recirculation are considered to be the concentration of those components at the outlet of the reactor, $S_2 = S_3 = S_4$. It should be noted that the concentration of all the components in the header, purge and recirculation do coincide.
- In the clarifier, the particulate components are considered to be partially deposited by sedimentation, that means most of solids come out of the plant through the header. However, a small fraction of these solids come out of the plant through the effluent. The concentration of the particulate components in the effluent are calculated, as follows

$$X_3 = X_2(1 - \eta_c), \tag{B.21}$$

  where η_c is the clarifier yield.
- In the sludge thickener, the soluble components are considered to be homogeneously distributed within the volume and the purged discharge is fed to the unit continuously. It is also modelled in order to separate particulate components and soluble components, even though it operates differently form the clarifier, as will be detailed later. The concentration of the soluble components in both the clarified and the sludge are considered to be the concentration of those components in the purge, $S_5 = S_7 = S_8$.
- Considering that the sludge thickener is centrifugal, most of solids are concentrated in the periphery and they come out of the plant through the sludge. However, a small fraction of these solids comes out of the plant through the clarified and comes back to the first reactor. The concentration of the particulate components in the clarified are calculated as of the sludge thickener yield [20], assuming that the sludge thickener yield corresponds to the capture percentage, it results

$$\eta_s = 1 - \frac{X_7(X_8 - X_5)}{X_5(X_8 - X_7)}, \tag{B.22}$$

  that can be written as

$$X_7 = \frac{X_5 X_8 K}{X_8 - X_5 + X_5 K}, \tag{B.23}$$

  where $K = 1 - \eta_s$.

  It should be noted that X_7 also depends upon X_8. Hence, it is necessary to make a mass balance for particulate components, in order to express X_7 in function of parameters which will be determined subsequently, for the control volume pictured in Figure B.6.

  Hence,

$$\dot{m}_5 = \dot{m}_7 + \dot{m}_8, \tag{B.24}$$

  that can be written as

$$X_5 q_5 = X_7 q_7 + X_8 q_8. \tag{B.25}$$

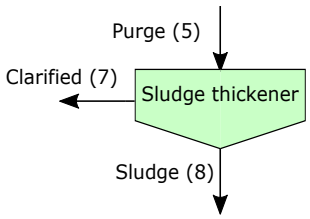

Figura B.6: Control Volume.

Considering equation (B.23), $q_7 = q_5 f_{cl}$ and $q_8 = q_5(1 - f_{cl})$, it results

$$X_8^2(1 - f_{cl}) + X_8(X_5 K - X_5 + X_5 f_{cl} - f_{cl} X_5 K) + X_5^2(1 - K) = 0. \tag{B.26}$$

The above equation has a solution whether $(\eta_s - 1)X_5 f_{cl} \eta_s \neq 0$. The solution is depicted, as follows

$$X_8 = \frac{\eta_s X_5}{1 - f_{cl}}. \tag{B.27}$$

Once the assumptions have been made, it is necessary to determine the transfer function between the concentration of the particulate components in the header and in the outlet of the reactor ($X_4 = f(X_2)$). For this purpose, two control volumes are defined and a mass balance for water and particulate components in the clarifier is made. It should be noted that the concentrations of the particulate components in both the purge and the recirculation are considered to be the concentration of those components in the header. The first control volume is depicted on the left side and the other is depicted on the right side of Figure B.7.

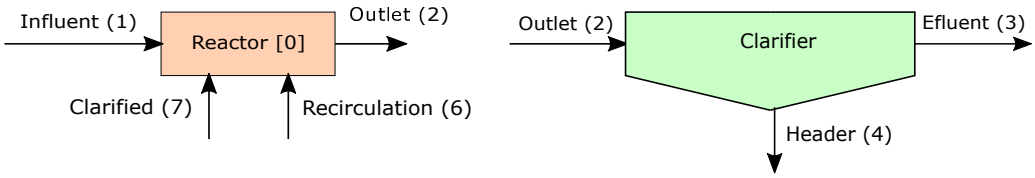

Figura B.7: Control Volumes.

Writing a water mass balance for the first control volume,

$$q_2 = q_1 + q_6 + q_7, \tag{B.28}$$

and knowing that $q_4 = rq_1$, $q_6 = q_4(1-p)$, $q_7 = q_5 f_{cl}$ and $q_5 = q_1 rp$, it results

$$q_2 = q_1(f_{cl}rp + r - rp + 1). \tag{B.29}$$

Writing a water mass balance for the second control volume,

$$q_2 = q_3 + q_4, \tag{B.30}$$

and knowing that $q_4 = rq_1$, it results

$$q_2 = q_3 + q_1 r. \tag{B.31}$$

Combining both equations, (B.29) and (B.31), q_3 results

$$q_e = q_i(f_{cl}rp - rp + 1). \tag{B.32}$$

Writing a particulate components mass balance for the second control volume, it results

$$\dot{m}_2 = \dot{m}_4 + \dot{m}_3, \tag{B.33}$$

that can be written as

$$X_2 q_2 = X_4 q_4 + X_3 q_3. \tag{B.34}$$

Considering equation (B.29), $q_4 = rq_1$, equation (B.21) and (B.32), it results

$$X_2 q_1(f_{cl}rp + 1 + r - rp) = X_4 rq_1 + X_2(1-\eta_c)q_1(f_{cl}rp + 1 - rp). \tag{B.35}$$

Finally, the concentrations of the particulate components in the header are

$$X_4 = \frac{X_2(r + \eta_c - r\eta_c p + \eta_c f_{cl} rp)}{r}. \tag{B.36}$$

B.5. Model 5

The layout of the fifth simulated wastewater plant is depicted in Figure B.8. As can be observed, this model recreates a wastewater plant with sludge recirculation, purge, sludge thickener and dehydrator. It consists of three reactors, one clarifier and three recirculation lines. The first of them comes from the clarifier, the second of them comes from the sludge thickener and the last of them comes from the dehydrator. The main variables included in the model are also summarized in Table B.5, as shown in the previous models. Note that from the concentration and volumetric discharge, the massflow can be defined as $\dot{m}_{(\cdot)} = X_{(\cdot)} \cdot q_{(\cdot)}$.

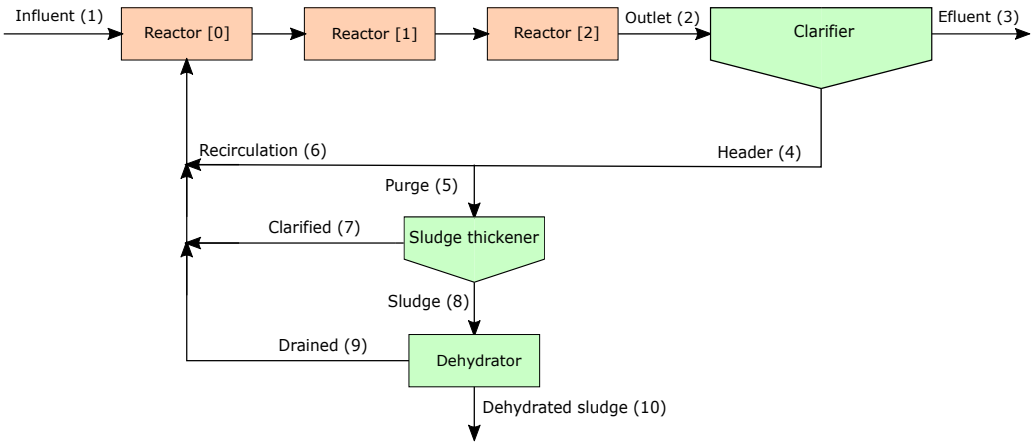

Figura B.8: Plant layout and nomenclature of the relevant points.

Concentration	Discharge	Description
X_1, S_1	q_1	Influent of the plant
X_2, S_2	q_2	Outlet of the reactor (spillway)
X_3, S_3	q_3	Effluent of the plant
X_4, S_4	q_4	Header
X_5, S_5	q_5	Purge
X_6, S_6	q_6	Recirculation
X_7, S_7	q_7	Clarified
X_8, S_8	q_8	Sludge
X_9, S_d	q_9	Drained
X_{10}, S_{10}	q_{10}	Dehydrated sludge

Cuadro B.5: Table of variables in the model

In the model designed here, it is necessary to make the following assumptions:

- The header discharge is defined as $q_4 = rq_1$, where r is the recirculation factor.
- The recirculation discharge is defined as $q_6 = q_4(1-p)$, where p is the fraction of header discharge purged.
- The clarified discharge is defined as $q_7 = q_5 f_{cl}$, where f_{cl} is the fraction of purged discharge thickened.
- The drained discharge is defined as $q_9 = q_8 f_d$, where f_d is the fraction of drained discharge dehydrated.
- In the reactors, the first of them operates under anoxic conditions ([0]) and the remainder of them, under aerobic conditions ([1] and [2]). In order to represent both situations, the oxygen dissolved concentration is fixed at 0 and 1 ($M(-COD)L^{-3}$), respectively. Furthermore, the ASm1 processes are only carried out within them.
- In the clarifier, the soluble components are considered to be homogeneously distributed within the volume. It is modelled in order to separate particulate components and soluble components. The concentration of the soluble components in both the effluent and the recirculation are considered to be the concentration of those components at the outlet of the reactor, $S_2 = S_3 = S_4$. It should be noted that the concentration of all the components in the header, purge and recirculation do coincide.

- In the clarifier, the particulate components are considered to be partially deposited by sedimentation, that means most of solids come out of the plant through the header. However, a small fraction of these solids come out of the plant through the effluent. The concentration of the particulate components in the effluent are calculated, as follows

$$X_3 = X_2(1 - \eta_c), \tag{B.37}$$

where η_c is the clarifier yield.

- In the sludge thickener, the soluble components are considered to be homogeneously distributed within the volume and the purged discharge is fed to the unit continuously. It is also modelled in order to separate particulate components and soluble components, even though it operates differently form the clarifier, as will be detailed later. The concentration of the soluble components in both the clarified and the sludge are considered to be the concentration of those components in the purge, $S_5 = S_7 = S_8$.

- Considering that the sludge thickener is centrifugal, most of solids are concentrated in the periphery and they come out of the plant through the sludge. However, a small fraction of these solids comes out of the plant through the clarified and comes back to the first reactor. The concentration of the particulate components in the clarified are calculated as of the sludge thickener yield, assuming that the sludge thickener yield corresponds to the capture percentage, it results

$$\eta_s = 1 - \frac{X_7(X_8 - X_5)}{X_5(X_8 - X_7)}, \tag{B.38}$$

that can be written as

$$X_7 = \frac{X_5 X_8 K}{X_8 - X_5 + X_5 K}, \tag{B.39}$$

where $K = 1 - \eta_s$.

It should be noted that X_7 also depends upon X_8. Hence, it is necessary to make a mass balance for particulate components, in order to express X_7 in function of parameters which will be determined subsequently, for the control volume pictured in Figure B.9.

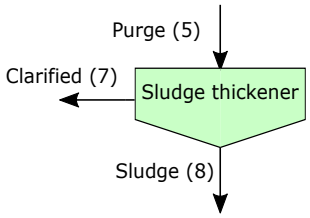

Figura B.9: Control Volume.

Hence,

$$\dot{m}_5 = \dot{m}_7 + \dot{m}_8, \tag{B.40}$$

that can be written as

$$X_5 q_5 = X_7 q_7 + X_8 q_8. \tag{B.41}$$

Considering equation (B.39), $q_7 = q_5 f_{cl}$ and $q_8 = q_5(1 - f_{cl})$, it results

$$X_8^2(1-f_{cl}) + X_8(X_5K - X_5 + X_5f_{cl} - f_{cl}X_5K) + X_5^2(1-K) = 0. \tag{B.42}$$

The above equation has a solution whether $(\eta_s - 1)X_5 f_{cl}\eta_s \neq 0$. The solution is depicted, as follows

$$X_8 = \frac{\eta_s X_5}{1 - f_{cl}}. \tag{B.43}$$

- In the sludge dehydrator, the soluble components are considered to be homogeneously distributed within the volume and the sludge is fed to the unit continuously. It is also modelled in order to separate particulate components and soluble components, even though it operates differently from the clarifier, as will be detailed later. The concentration of the soluble components in both the drained and the dehydrated sludge are considered to be the concentration of those components in the sludge, $S_8 = S_9 = S_{10}$.
- The dehydration process is carried out with the external heating of the dehydration chamber provided by steam, gas or electric power. Considering that the dehydrator is centrifugal, most of solids are concentrated in the periphery and they come out of the plant through the dehydrated sludge, in the same way that it occurs within the sludge thickener. However, a small fraction of these solids comes out of the plant through the drained and comes back to the first reactor. The concentration of the particulate components in the drained are calculated as of the dehydrator yield, assuming that the dehydrator yield corresponds to the capture percentage, it results

$$\eta_d = 1 - \frac{X_9(X_{10} - X_8)}{X_8(X_{10} - X_9)}, \tag{B.44}$$

that can be written as

$$X_9 = \frac{X_8 X_{10} K_2}{(X_{10} - X_8 + X_8 K_2)}. \tag{B.45}$$

where $K_2 = 1 - \eta_d$.

It should be noted that X_9 also depends on X_{10}. Hence, it is necessary to make a mass balance for particulate components, in order to express X_9 in function of parameters which will be determined subsequently, for the control volume depicted in Figure B.10.

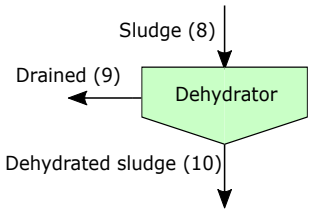

Figura B.10: Control Volume.

Hence,

$$\dot{m}_8 = \dot{m}_9 + \dot{m}_{10}, \tag{B.46}$$

that can be written as

$$X_8 q_8 = X_9 q_9 + X_{10} q_{10}. \tag{B.47}$$

Considering equation (B.45), $q_9 = q_8 f_d$ and $q_{10} = q_8(1 - f_d)$, it results

$$X_{10}^2(1-f_d) + X_{10}(X_8K_2 - X_8 + X_8f_d - f_dX_{.8}K_2) + X_8^2(1-K_2) = 0 \tag{B.48}$$

The above equation has a solution whether $(\eta_d - 1)X_8 f_d \eta_d \neq 0$. The solution is depicted, as follows

$$X_{10} = \frac{\eta_{ds} X_8}{1 - f_d}. \tag{B.49}$$

Once the assumptions have been made, it is necessary to determine the transfer function between the concentration of the particulate components in the header and in the outlet of the reactor ($X_4 = f(X_2)$). For this purpose, two control volumes are defined and a mass balance for water and particulate components in the clarifier is made. It should be noted that the concentrations of the particulate components in both the purge and the recirculation are considered to be the concentration of those components in the header. The first control volume is depicted on the left side and the other is depicted on the right side of Figure B.11.

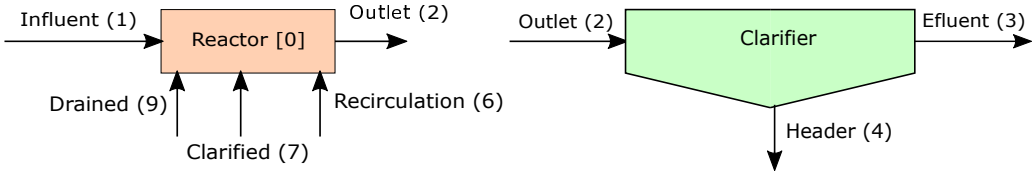

Figura B.11: Control Volumes.

Writing a water mass balance for the first control volume,

$$q_2 = q_1 + q_6 + q_7 + q_9, \tag{B.50}$$

and knowing that $q_4 = rq_1$, $q_6 = q_4(1-p)$, $q_7 = q_5 f_{cl}$, $q_5 = q_1 rp$, $q_9 = q_s f_d$ and $q_8 = q_1 rp f_d(1-f_{cl})$, it results

$$q_2 = q_1(1 + rpf_d(1-f_{cl}) + rpf_{cl} + r(1-p)). \tag{B.51}$$

Writing a water mass balance for the second control volume,

$$q_2 = q_3 + q_4, \tag{B.52}$$

and knowing that $q_4 = rq_1$, it results

$$q_2 = q_3 + q_1 r. \tag{B.53}$$

Combining both equations, (B.51) and (B.53), q_3 results

$$q_3 = q_1(1 + rpf_d(1-f_{cl}) + rpf_{cl} - rp). \tag{B.54}$$

Writing a particulate components mass balance for the second control volume, it results

$$\dot{m}_2 = \dot{m}_4 + \dot{m}_3, \tag{B.55}$$

that can be written as

$$X_2 q_2 = X_4 q_4 + X_3 q_3. \tag{B.56}$$

Considering equation (B.51), $q_4 = rq_1$, equation (B.37) and (B.54), it results

$$X_2 q_1(1 + rpf_d(1 - f_{cl}) + rpf_{cl} + r(1 - p)) = X_4 rq_1 + X_2(1 - \eta_c)q_i(1 + rpf_d(1 - f_{cl}) + rpf_{cl} - rp). \quad \text{(B.57)}$$

Finally, the concentrations of the particulate components in the header are

$$X_4 = \frac{X_2(r + \eta_c + r\eta_c p(f_{cl} + f_d(1 - f_{cl}) - 1))}{r}. \quad \text{(B.58)}$$

B.6. ASM1 results

In this Section, the numerical results for the 5 different layouts previously detailed are presented. The characterization of the influent is first presented in Subsection B.6.1, where the evolution over time of the concentration and volumetric flow is displayed. The numerical results for the 5 different test cases are presented from Subsection B.6.2 to B.6.6. For each case, the evolution over time of the volumetric flow and the concentration are displayed at different locations of the plant.

B.6.1. Influent analysis

In this Subsection, the characterization of the influent is provided. The volumetric flow and the concentration of the 13 species in the influent are presented in Figures B.12 and B.13, respectively. The aforementioned variables have been chosen to be constant throughout the simulation, as observed in the plots.

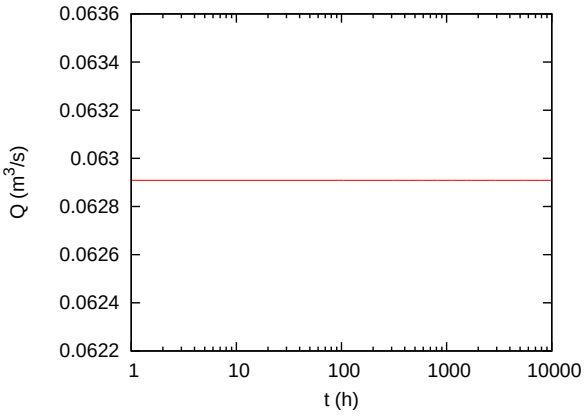

Figura B.12: Section B.6.1. Influent volumetric flow.

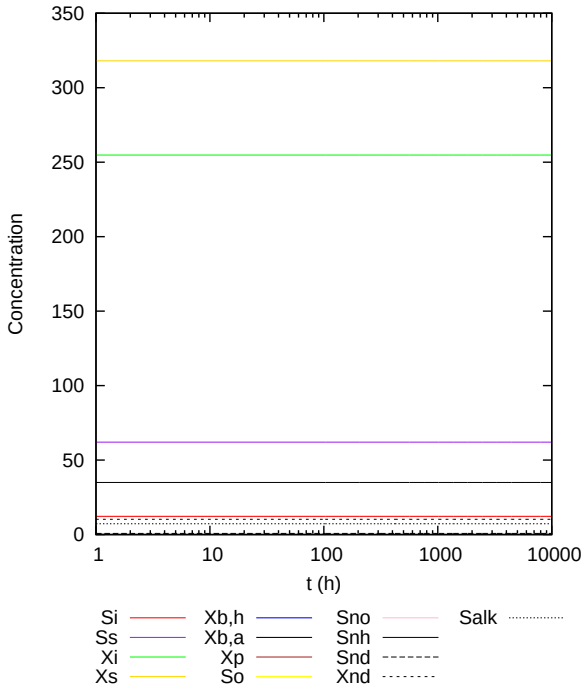

Figura B.13: Section B.6.1. Concentration of the 13 species in the influent.

B.6.2. Test case 1: Model 1 ($r = 0$)

In this Subsection, the numerical results for the Model 1 are presented. The evolution over time of the effluent volumetric flow is displayed in Figure B.14 and the concentration of the 13 species in the effluent and reactors are depicted in Figure B.15.

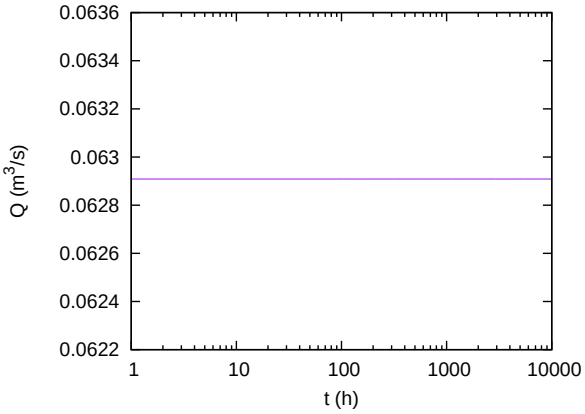

Figura B.14: Section B.6.2. Volumetric flow of the effluent.

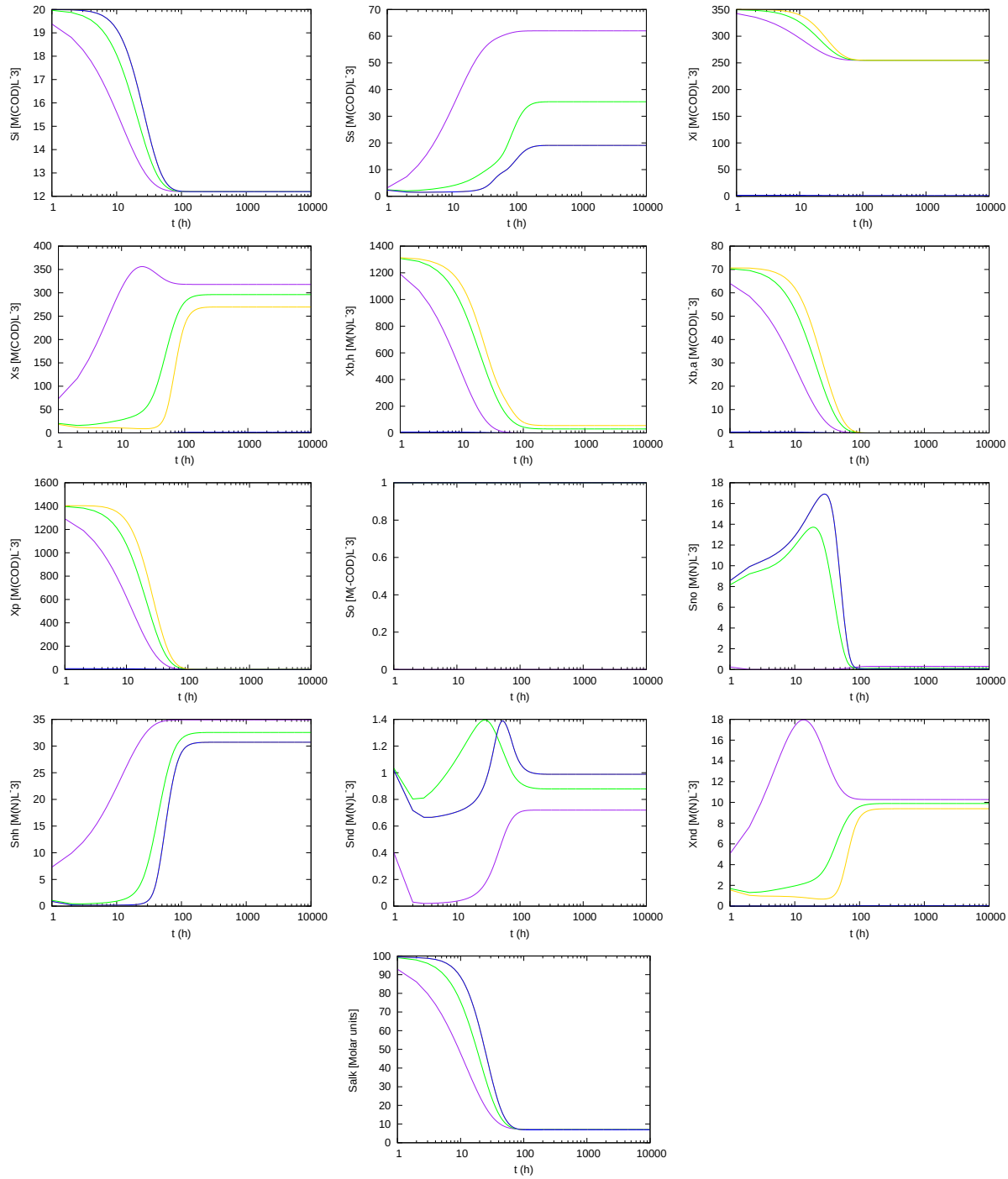

Figura B.15: Section B.6.2. Concentration of the 13 species in the reactor[0] (—), reactor[1] (—), reactor[2] (—), effluent (—).

B.6.3. Test case 2: Model 2 ($r = 1$)

In this Subsection, the numerical results for the Model 2 are presented. The evolution over time of the effluent volumetric flow is displayed in Figure B.16. The evolution over time of the concentration of the 13 species in the effluent and reactors and in the recirculation line are depicted in Figures B.17 and B.18, respectively.

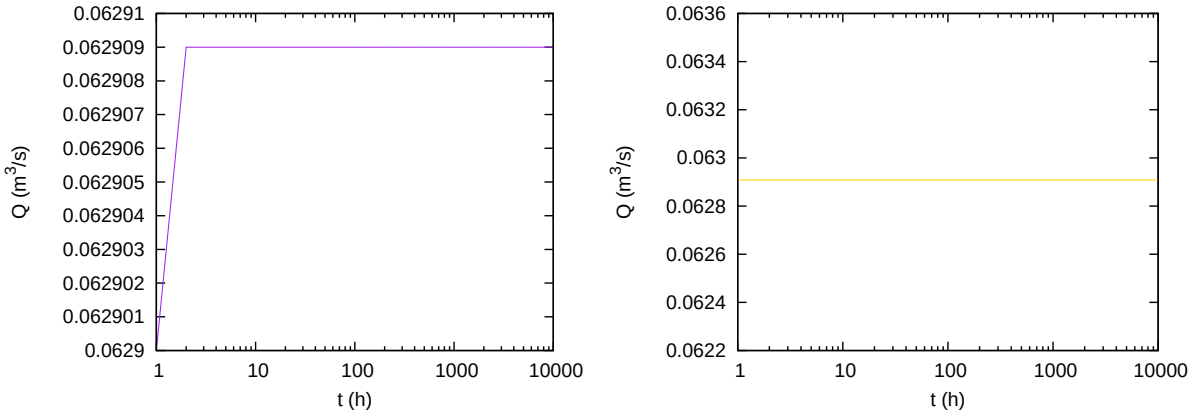

Figura B.16: Volumetric flow of the effluent (—), recirculation (—).

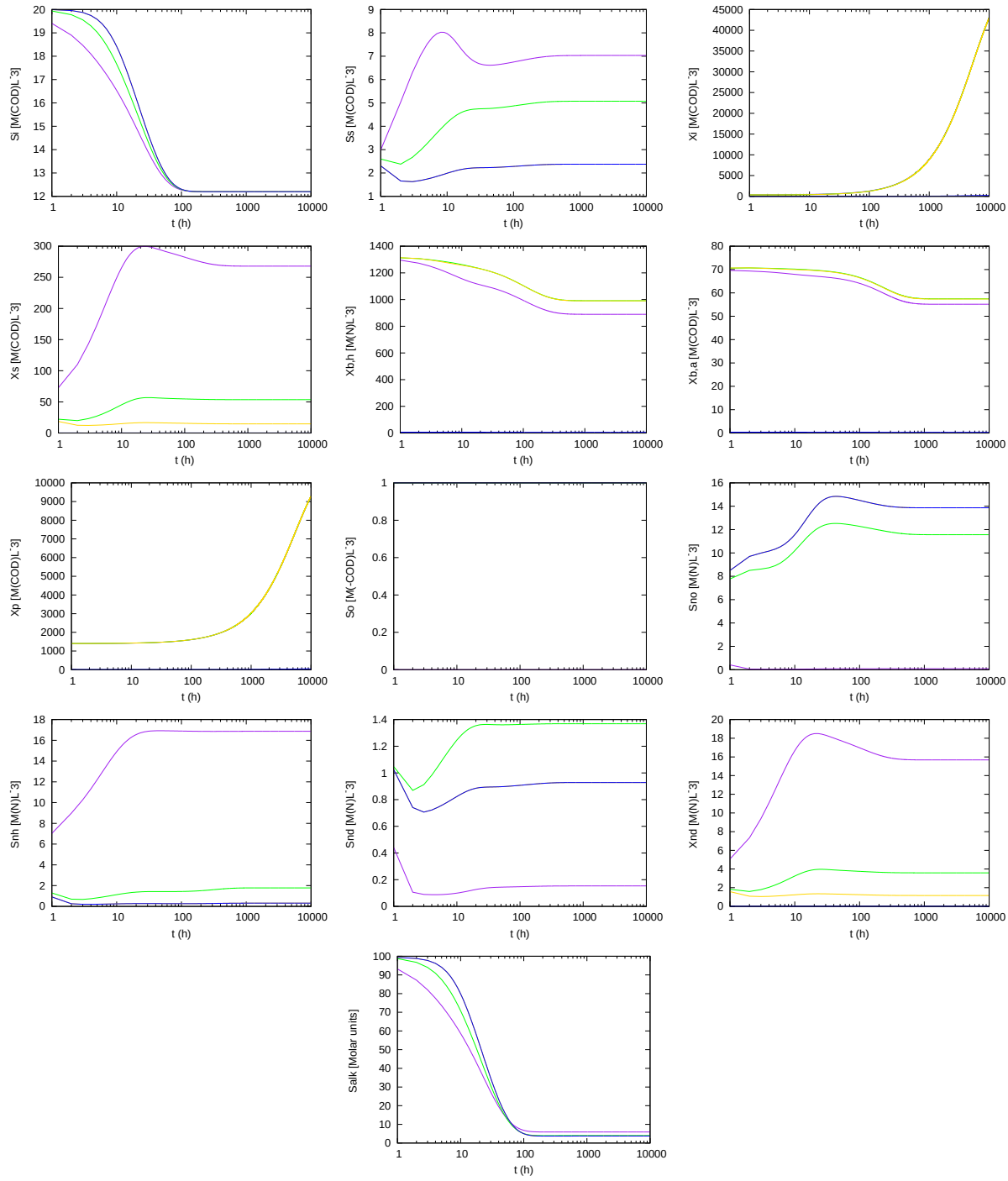

Figura B.17: Concentration of the 13 species in the reactor[0] (—), reactor[1] (—), reactor[2] (—), effluent (—).

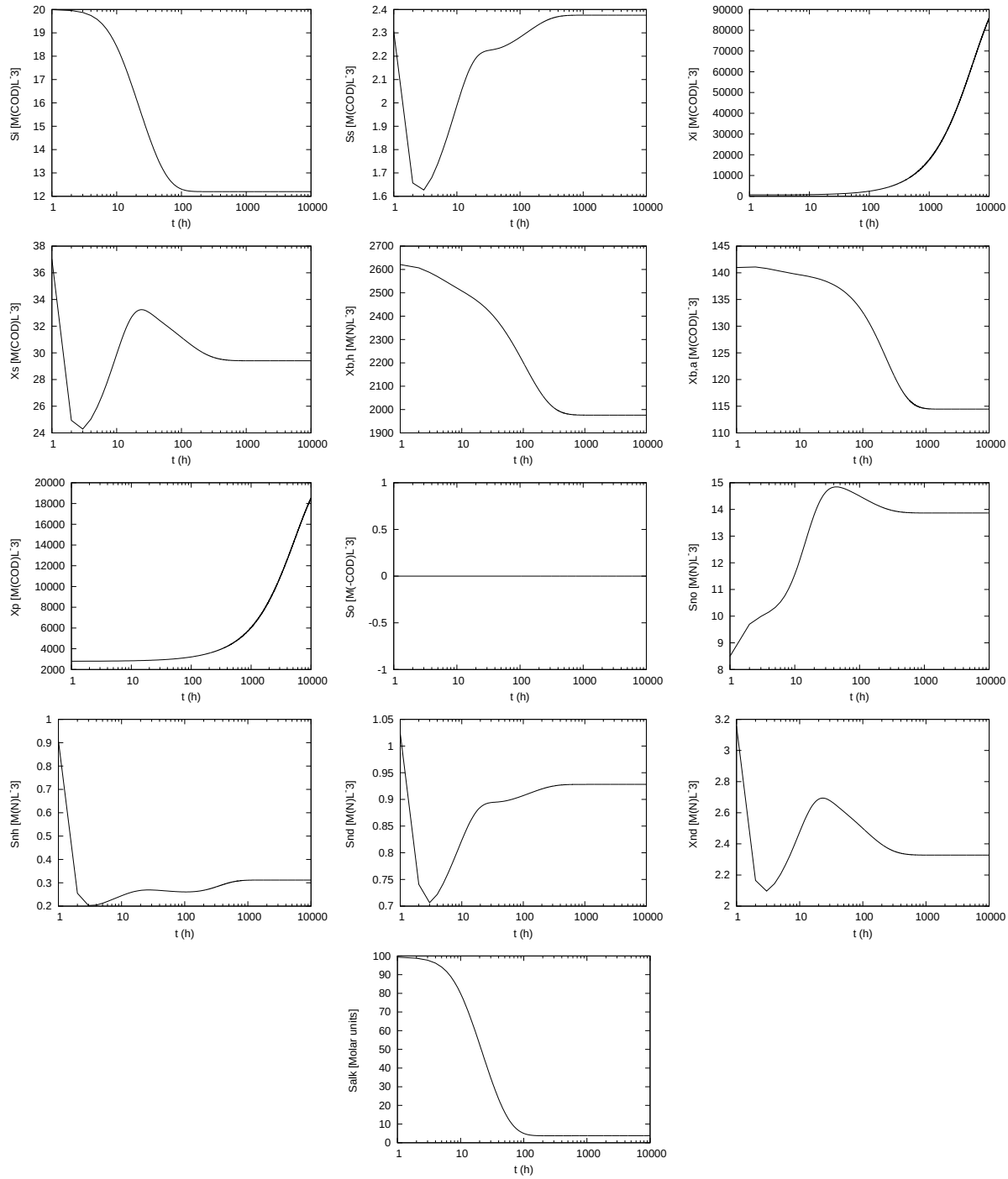

Figura B.18: Concentration of the 13 species in the recirculation.

B.6.4. Test case 3: Model 3 ($r = 1$, $p = 0{,}02$)

In this Subsection, the numerical results for the Model 3 are presented. The evolution over time of the effluent volumetric flow is displayed in Figure B.19. The evolution over time of the concentration of the 13 species in the effluent and reactors and in the recirculation and purgue line are depicted in Figures B.20 and B.21, respectively.

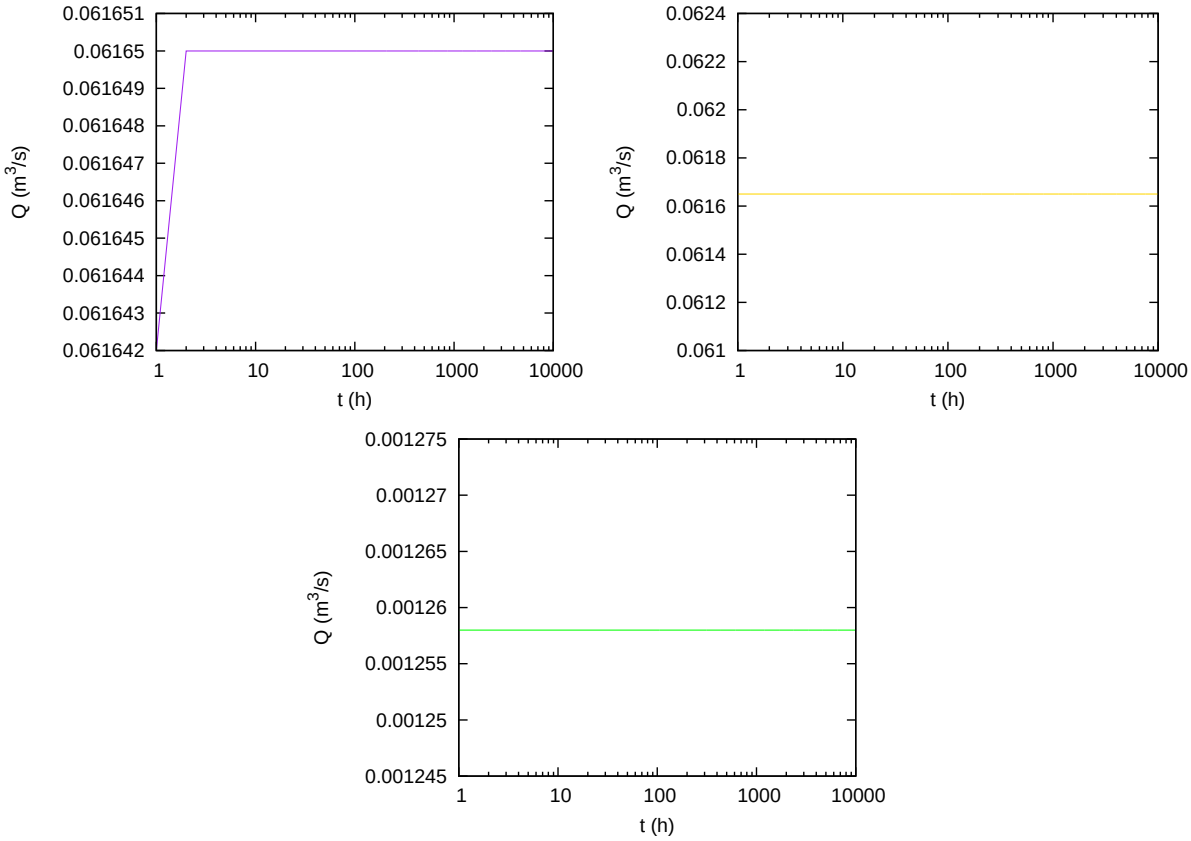

Figura B.19: Volumetric flow of the effluent (—), recirculation (—), purge (—).

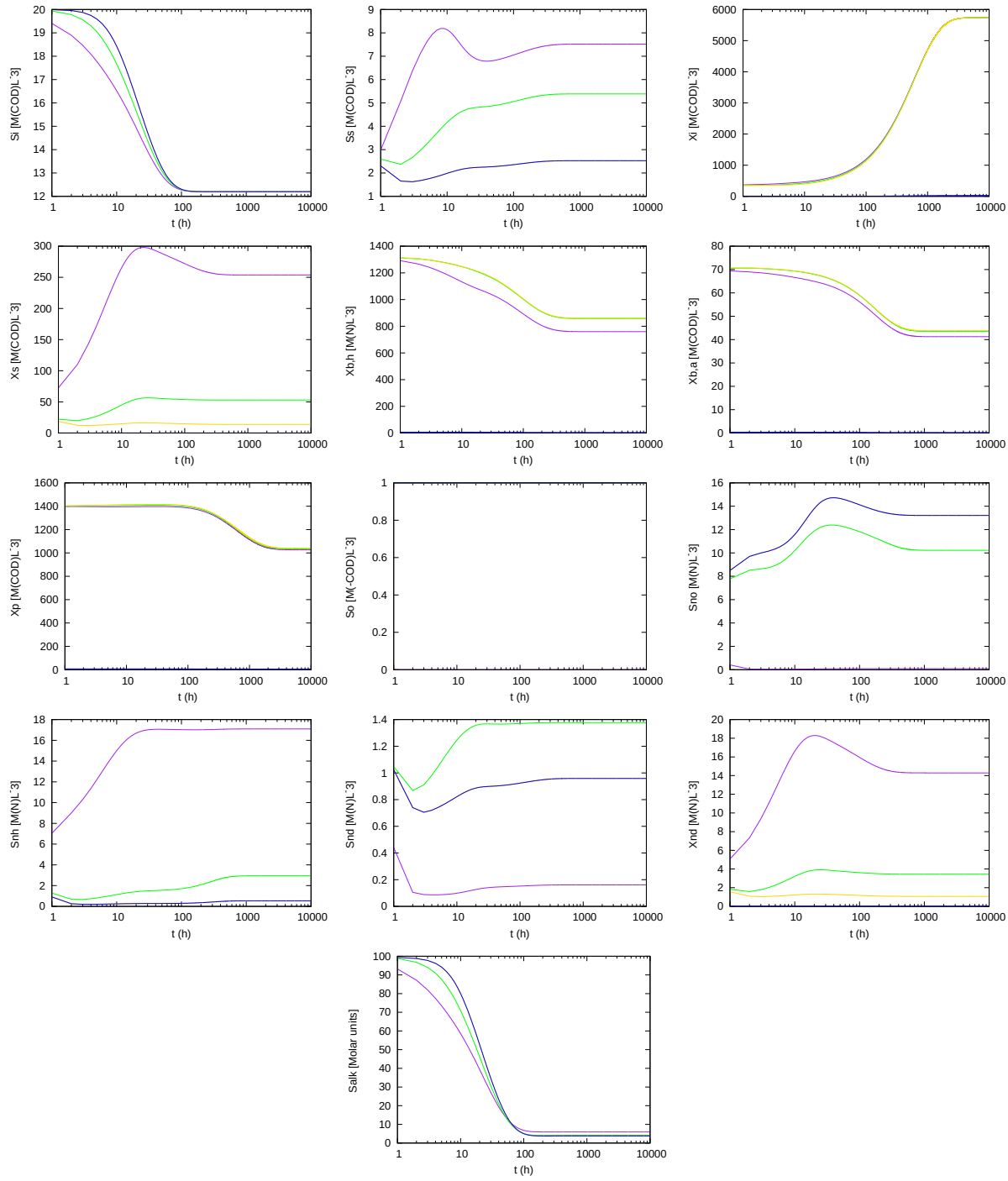

Figura B.20: Concentration of the 13 species in the reactor[0] (—), reactor[1] (—), reactor[2] (—), effluent (—).

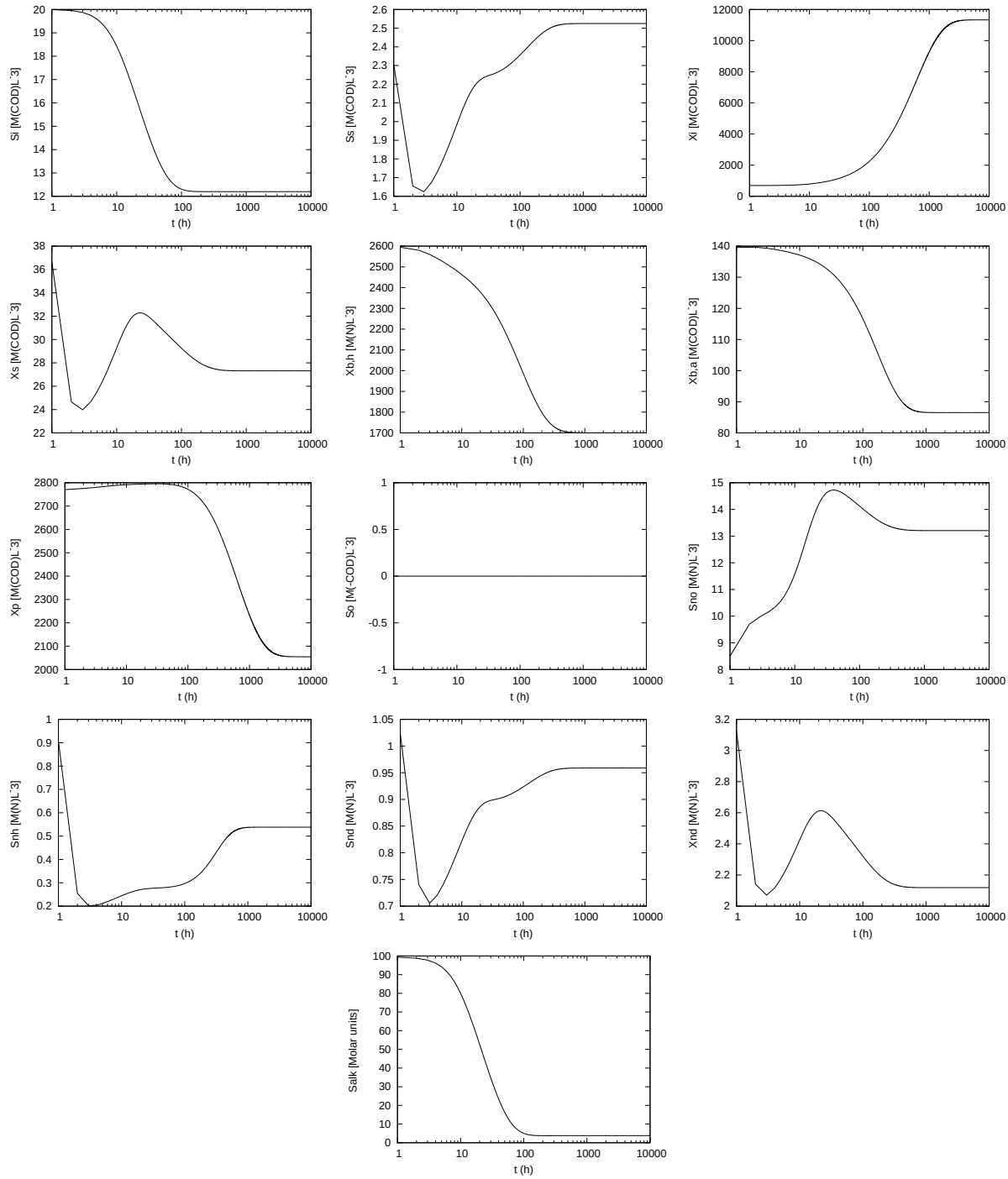

Figura B.21: Concentration of the 13 species in the recirculation and purge.

B.6.5. Test case 4: Model 4 ($r = 1$, $p = 0{,}02$, $\eta_s = 0{,}96$, $f_{cl} = 0{,}8$)

In this Subsection, the numerical results for the Model 4 are presented. The evolution over time of the effluent volumetric flow is displayed in Figure B.22. The evolution over time of the concentration of the 13 species in the effluent and reactors and in the total recirculation and purge line are depicted in Figures B.23 and B.24, respectively.

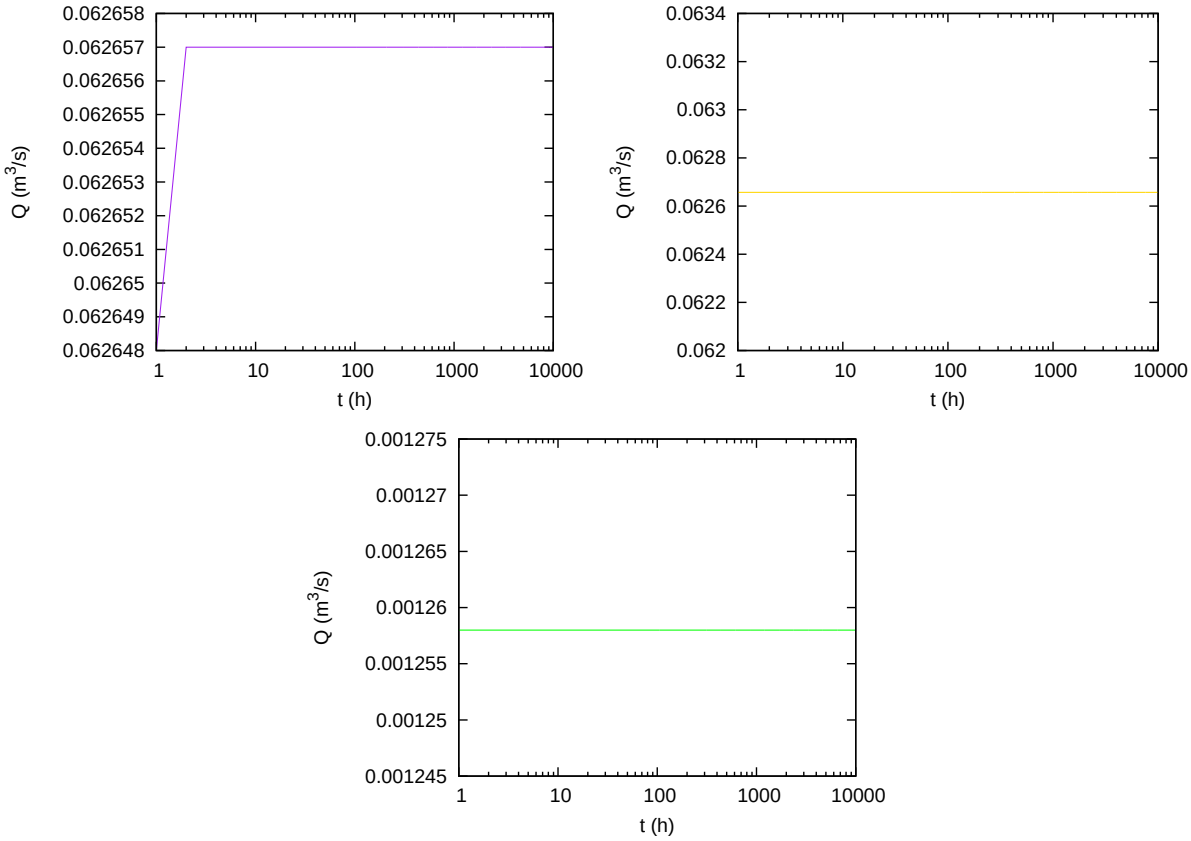

Figura B.22: Volumetric flow of the effluent (—), recirculation (—), purge (—).

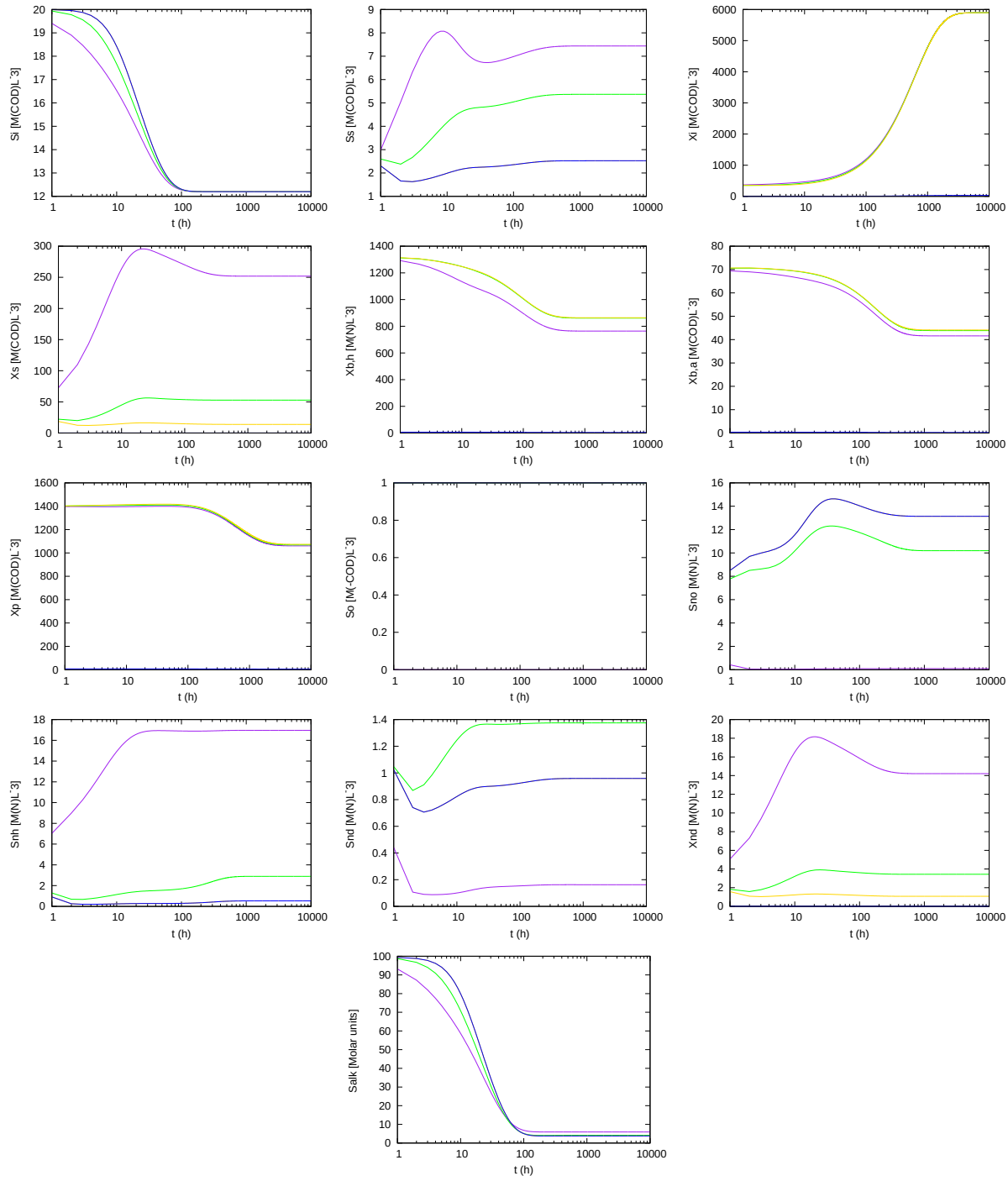

Figura B.23: Concentration of the 13 species in the reactor[0] (—), reactor[1] (—), reactor[2] (—), effluent (—).

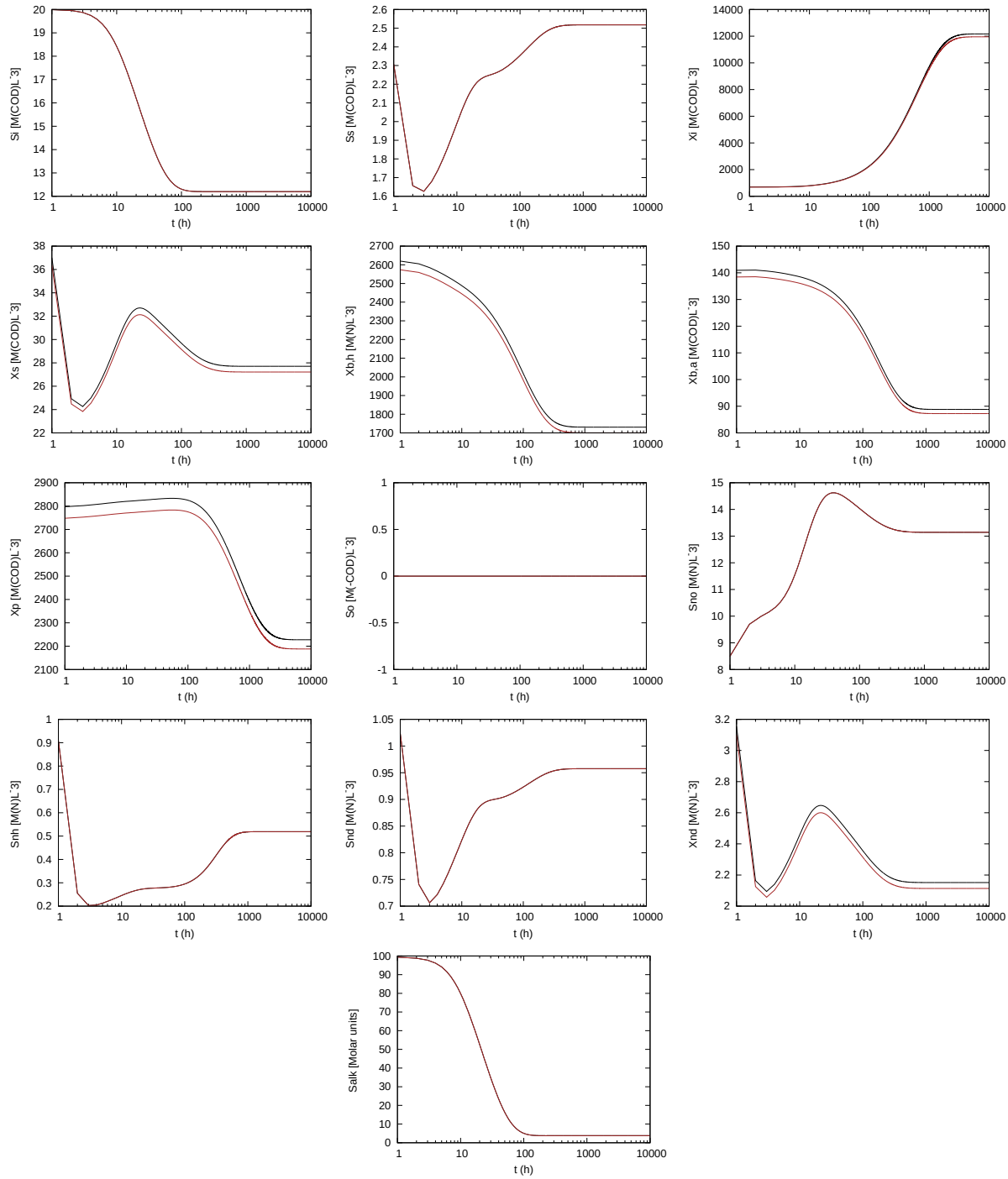

Figura B.24: Concentration of the 13 species in the total recirculation (—), purge (—).

B.6.6. Test case 5: Model 5 ($r = 1$, $p = 0{,}02$, $\eta_s = 0{,}96$, $f_{cl} = 0{,}8$, $\eta_d = 0{,}96$, $f_d = 0{,}8$)

In this Subsection, the numerical results for the Model 5 are presented. The evolution over time of the effluent volumetric flow is displayed in Figure B.25. The evolution over time of the concentration of the 13 species in the effluent and reactors, in the total recirculation and purge line and in the dehydrated sludge are depicted in Figures B.26, B.27 and B.28, respectively.

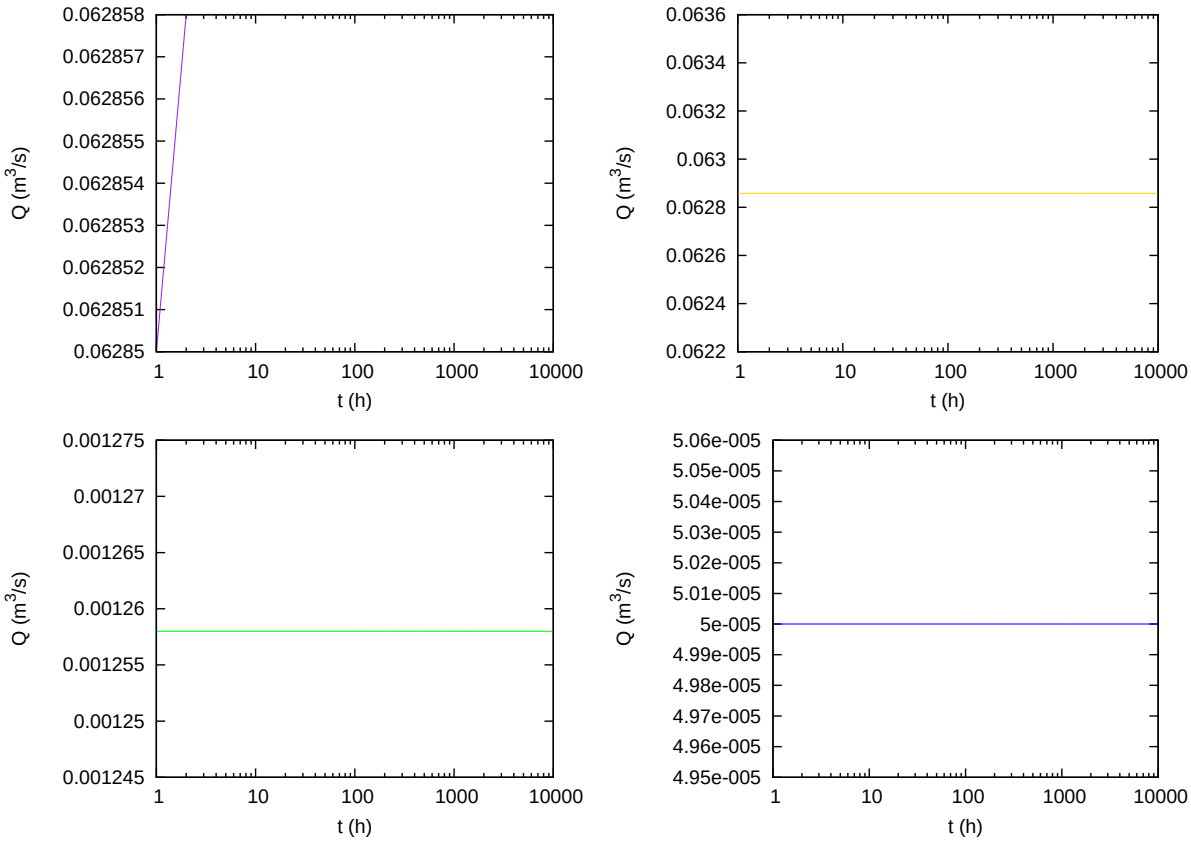

Figura B.25: Volumetric flow of the effluent (—), recirculation (—), purge (—), dehydrated sludge (—).

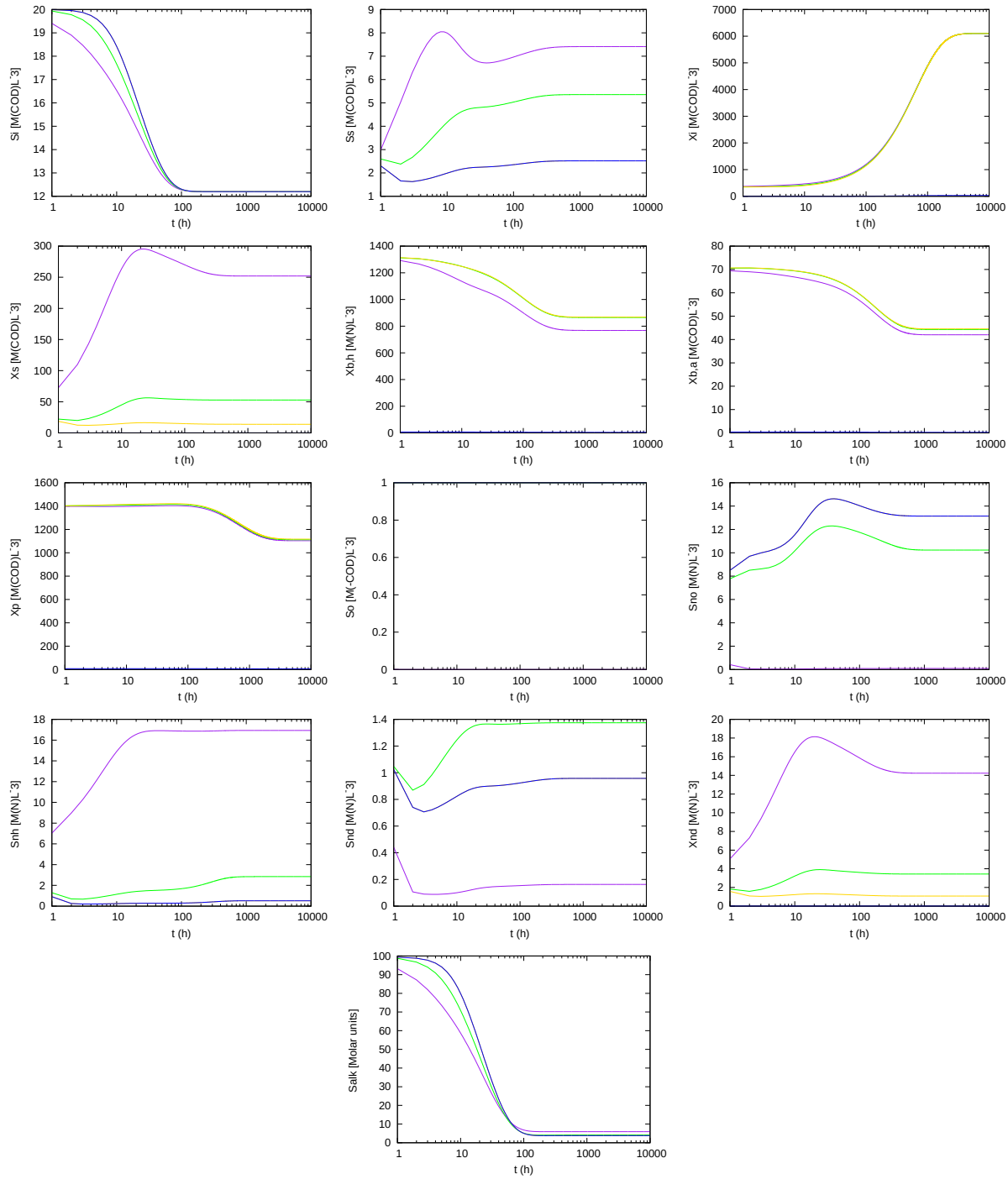

Figura B.26: Concentration of the 13 species in the reactor[0] (—), reactor[1] (—), reactor[2] (—), effluent (—).

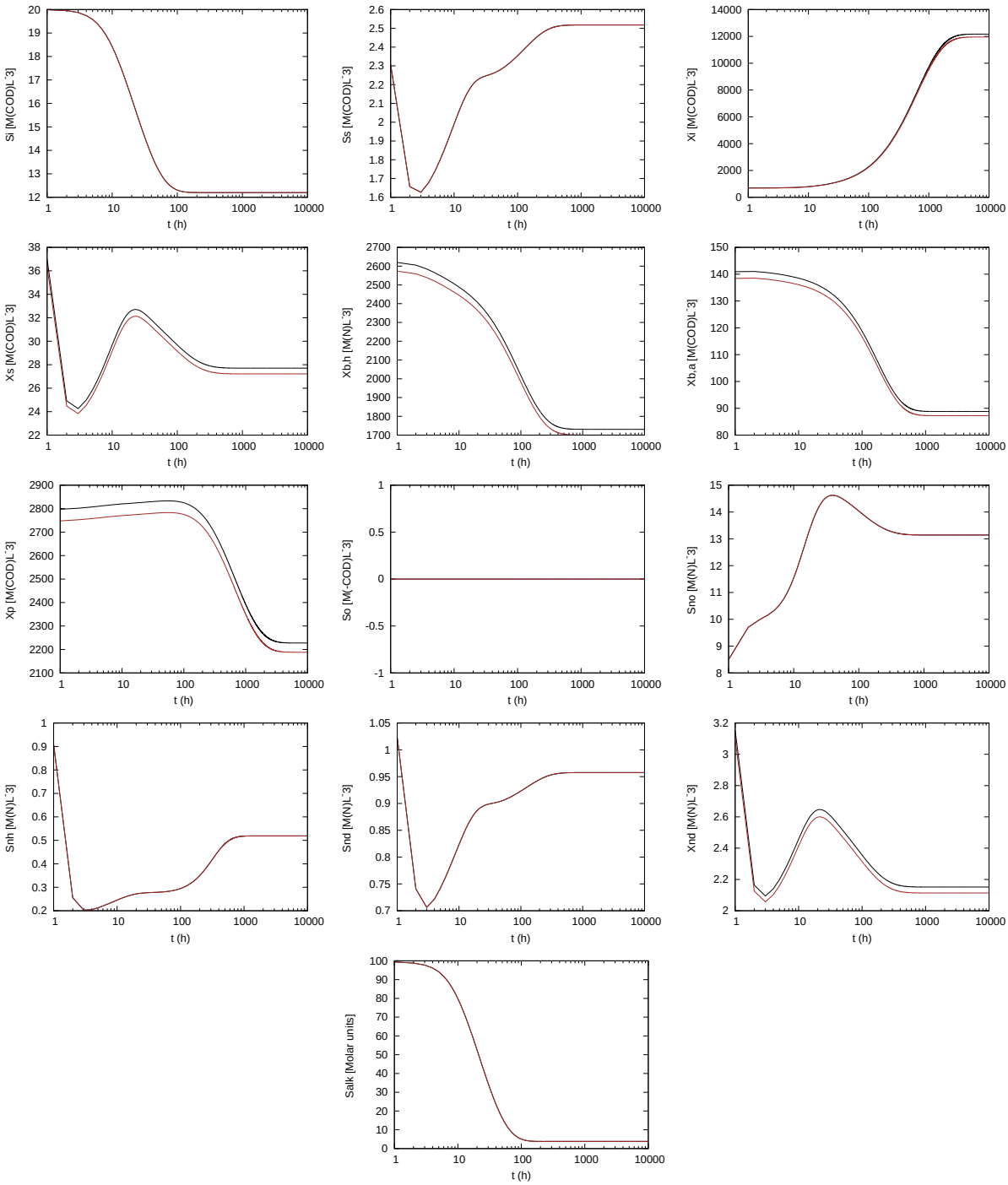

Figura B.27: Concentration of the 13 species in the total recirculation (—), purge (—).

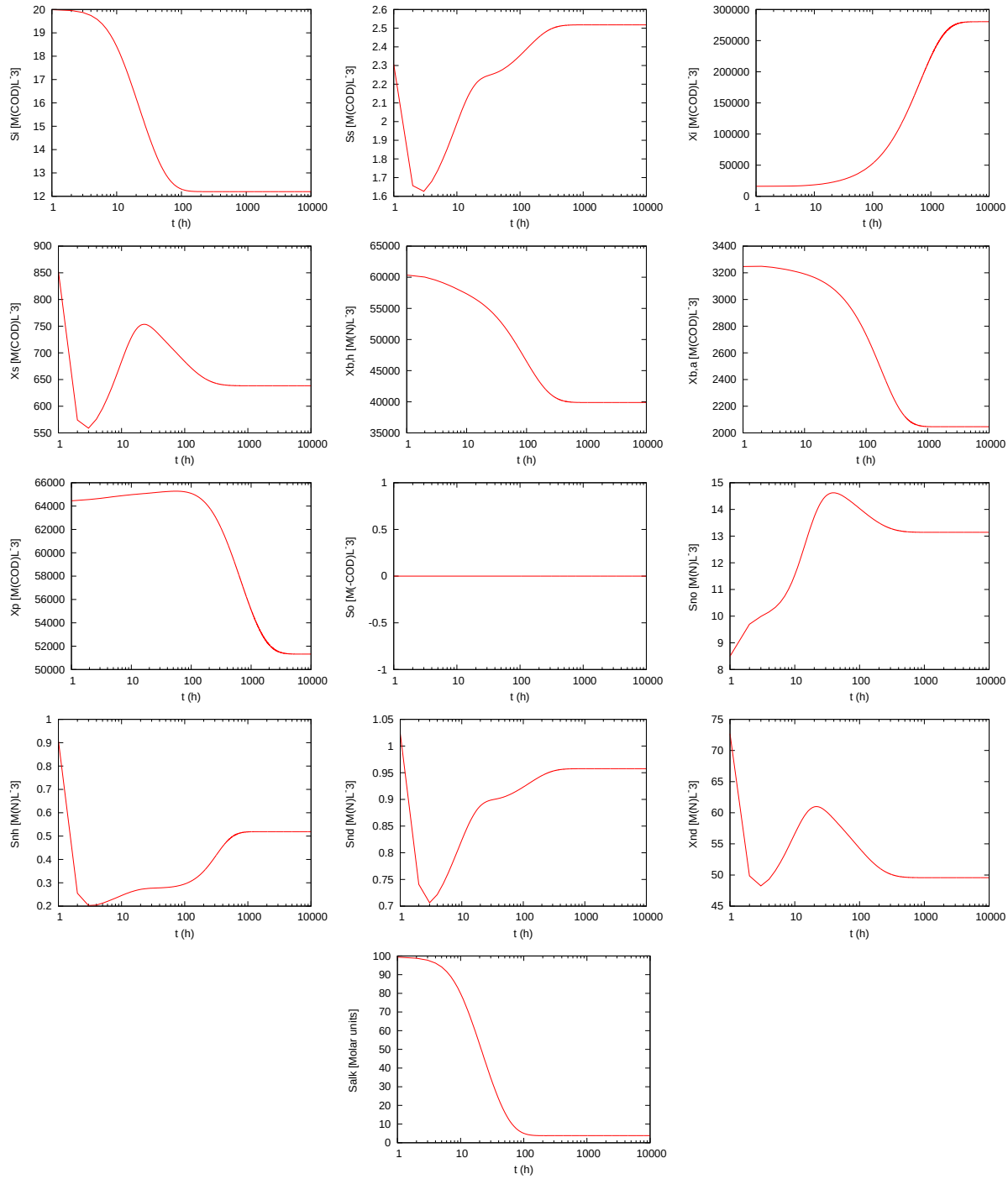

Figura B.28: Concentration of the 13 species in the dehydrated sludge.

B.6.7. Effluent analysis

In this Subsection, the evolution over time of the concentration of the components in the effluent for all the models are presented in Figure B.29.

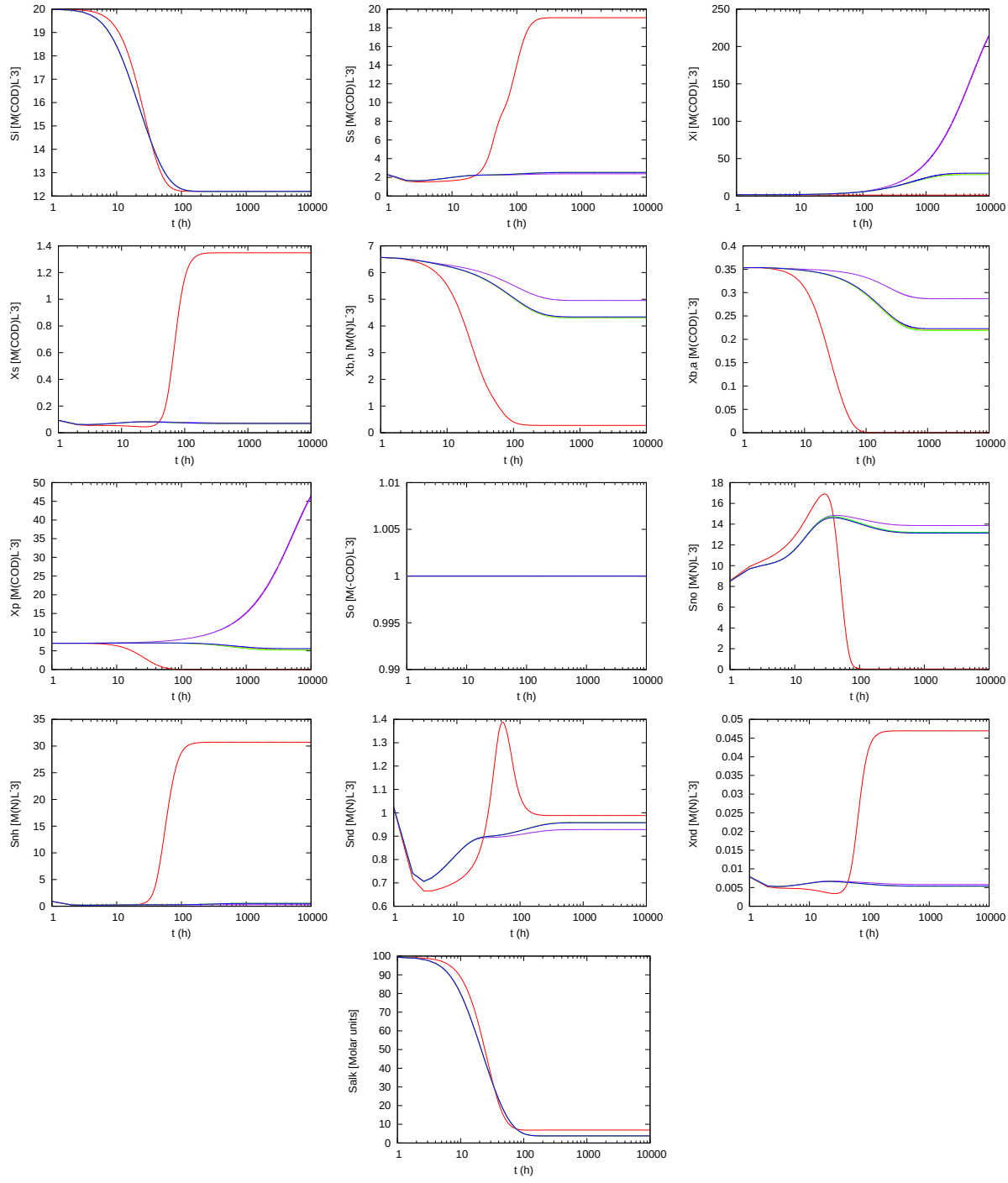

Figura B.29: Concentration of the 13 species in the effluent from Model 1 (—), Model 2 (—), Model 3 (—), Model 4 (—), Model 5 (—).

In order to emphasize the operational improvement that can be achieved adding a recirculation line in the plant, explained in Subsection B.7.2, it is necessary to define two plant yields. The first of them measures the reduction of soluble and insoluble biodegradable organic matter concentration and is defined as

$$\eta_{DBO} = 1 - \left(\frac{\dot{m}_e}{\dot{m}_i}\right)_b, \tag{B.59}$$

where $\dot{m}_{e_b}$ is the biodegradable organic matter mass flow in the effluent and $\dot{m}_{i_b}$ in the influent. Equation B.59 can be written as

$$\eta_{DBO} = 1 - \frac{q_e \left(X_s + S_s\right)_e}{q_i \left(X_s + S_s\right)_i}, \tag{B.60}$$

where q_e and q_i are the volumetric flow in the effluent and influent, respectively, X_{s_e} and S_{s_e} are the concentration of insoluble and soluble biodegradable organic matter and in the effluent, respectively, and X_{s_i} and S_{s_i} are the concentration of insoluble and soluble biodegradable organic matter and in the influent, respectively.

The other plant yield measures the reduction of ammonia and ammonium ion concentration, as follows

$$\eta_{NH} = 1 - \left(\frac{\dot{m}_e}{\dot{m}_i}\right)_{nh}, \tag{B.61}$$

where $\dot{m}_{e_{nh}}$ is the ammonia and ammonium ion mass flow in the effluent and $\dot{m}_{i_{nh}}$ in the influent. Equation B.61 can be written as

$$\eta_{NH} = 1 - \left(\frac{q_e S_e}{q_i S_i}\right)_{nh}, \tag{B.62}$$

where S_{nh_e} and S_{nh_i} are the concentration of insoluble and soluble biodegradable organic matter in the effluent and influent, respectively. The evolution over time of the aforementioned yields are depicted in Figure B.30.

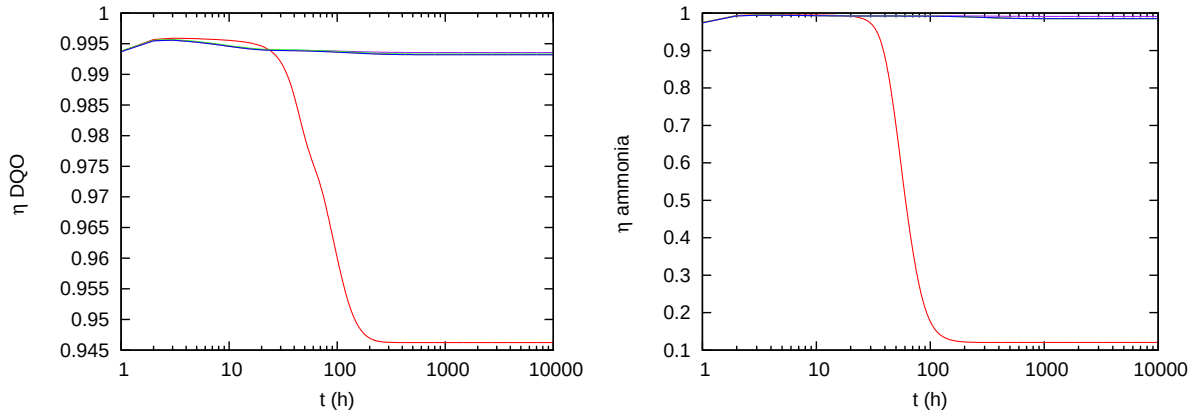

Figura B.30: η_{DBO} and η_{NH} from Model 1 (—), Model 2 (—), Model 3 (—), Model 4 (—), Model 5 (—).

B.7. Analysis of the results

In this Section, a deep analysis of the results is included and some conclusions are extracted. In Section B.7.1, the analysis of the results submitted in Sections B.6.2, B.6.3, B.6.4, B.6.5 and B.6.6 are presented. In Section B.7.2, the general conclusions of the modeling simulations (Model 1, 2, 3, 4 and 5) are presented.

B.7.1. Analysis of models

- In Model 1, the concentration of the components reaches an steady state in all the reactors, as shown in Figure B.15. However, the steady state of the active heterotrophic and autotrophic biomass concentration are not adequate for a proper performance of the plant as they become nil and almost nil, respectively. As can be observed in Figures A.5 and A.2, such components are products of the readily biodegradable substrate, nitrate and nitrite nitrogen (heterotrophic) and ammonia-ammonium nitrogen (autotrophic) are necessary to trigger the reactions. In order to retain a sufficient amount of these components, a recirculation line is needed.

- In Model 2, a recirculation line is added and the concentration of the components reaches an steady state in all the reactors, except the concentration of particulate products arising from biomass decay (X_p) and particulate inert organic matter (X_i), as shown in Figure B.17. The aforementioned particulate products increase over time because they do not undergo any reaction and they accumulate progressively due to the recirculation. Hence, a purge line is needed in order to limit their accumulation. For the particulate components, the concentration in the recirculation line are well above than in the effluent, while the concentration of the soluble components in the recirculation line and effluent do coincide, as shown in Figure B.18.

- In Model 3, a purge line is added and the concentration of the components reaches an steady state in all the reactors, as shown in Figure B.20. In this case, proper values of concentrations are achieved for all the components. The component concentrations in the purge and recirculation are the same, as shown in Figure B.21.

- In Model 4, a sludge thickener is added and the evolution over time of the component concentrations in the reactors is virtually similar to that Model 3, as shown in Figure B.23. This is because the sludge thickener is mainly used to reduce the sludge volume so that the sludge can be easily transported. It is worth pointing out that the particulate component concentrations in the purge and total recirculation do not coincide due to the sludge thickener yield, as shown in Figure B.24.

- In Model 5, a dehydrator is added and the evolution over time of the component concentrations in the reactors is virtually similar to that Model 3 and 4, as shown in Figure B.26. This is because the dehydrator is used in the same way as the sludge thickener. The particulate component concentrations in the purge and total recirculation do not coincide due to the sludge thickener and the dehydrator yield, as shown in Figure B.26. The particulate component concentrations in the sludge are well above the other models, as shown in Figure B.27.

B.7.2. General conclusions

- In Figure B.29, a reduction of the soluble and insoluble biodegradable organic matter concentration (readily biodegradable substrate and slowly biodegradable substrate, S_s and X_s, respectively) in the effluent is achieved by recirculating a fraction of the influent from the clarifier to the first reactor. The reduction of the aforementioned concentration is also display in Figure B.30, where an increase of the yield defined in Equation B.59 (η_{DBO}) is observed. This is because the recirculation increases the concentration of active heterotrophic, as shown in Figures A.5 and A.2.

- In Figure B.29, the concentration of the ammonia and ammonium ion concentration ($NH_4^+ + NH_3$ nitrogen, S_{nh}) computed in those models with a recirculation line (Model 2, 3, 4 and 5) is lower than

that in Model 1 (without recirculation line) in the effluent. The reduction of the aforementioned concentration is also display in Figure B.30, where an increase of the yield defined in Equation B.61 (η_{nh}) is observed. This is because the recirculation increases the concentration of active autotrophic biomass, as shown in Figures A.5 and A.2.

- In Figure B.29, the particulate products arising from biomass decay (X_p) and particulate inert organic matter (X_i) in Model 2 (with recirculation line, but without purge) increase over time due to the absence of purge, as the aforementioned particulate products do not undergo any reaction and they accumulate progressively.

- In Model 3, 4 and 5, virtually similar component concentrations are observed, as shown in Figure B.29. This is because Models 4 and 5 only include an sludge thickener or a sludge thickener and a dehydrator, respectively, compared to Model 3. These elements are mainly used to reduce the sludge volume so that the sludge can be easily transported. However, the concentration of particulate components in the effluent of Model 5 is slightly higher than that of Model 4 and the latter also is slightly higher than that of Model 3. This is because the yield of the sludge thickener and the dehydrator, η_s and η_d, are lower than 1 and there is a mass flow of particulate components that comes back to the recirculation line.

B.8. Comparison with Linx ASM1 example Model

In this Section, a example model is characterized in Section B.8.1. A comparison between the numerical results for the example model using a free software called Linx ASM1 and a develop software are presented in Section B.8.3.

B.8.1. Characterization of the example model

The layout of wastewater plant simulated with Linx ASM1 is depicted in Figure B.31. As can be observed, this model recreates a wastewater plant with sludge recirculation, purge, sludge thickener and dehydrator. It consists of one reactor, one clarifier and three recirculation lines. The first of them comes from the clarifier, the second of them comes from the sludge thickener and the last of them comes from the dehydrator. The main variables included in the model are also summarized in Table B.6, as shown in the previous models. Note that from the concentration and volumetric discharge, the massflow can be defined as $\dot{m}_{(\cdot)} = X_{(\cdot)} \cdot q_{(\cdot)}$.

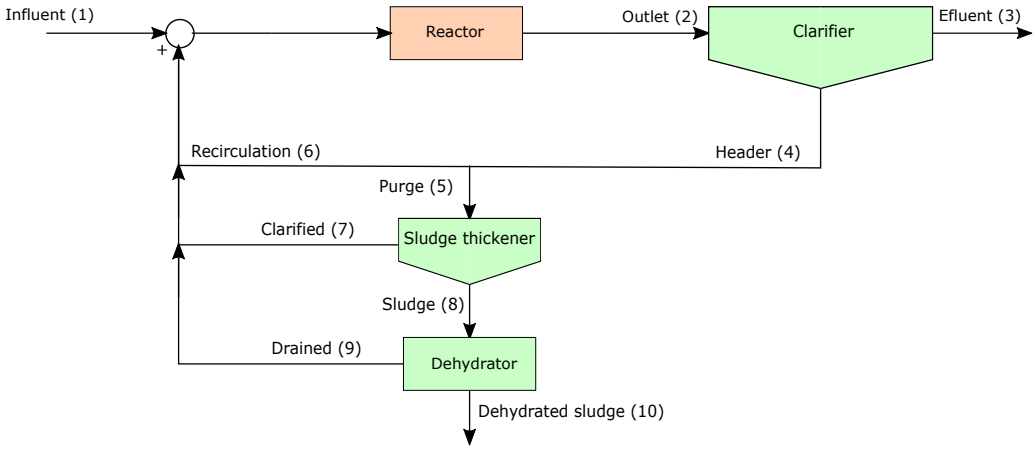

Figura B.31: Plant layout and nomenclature of the relevant points.

Concentration	Discharge	Description
X_1, S_1	q_1	Influent of the plant
X_2, S_2	q_2	Outlet of the reactor (spillway)
X_3, S_3	q_3	effluent of the plant
X_4, S_4	q_4	Header
X_5, S_5	q_5	Purge
X_6, S_6	q_6	Recirculation
X_7, S_7	q_7	Clarified
X_8, S_8	q_8	Sludge
X_9, S_d	q_9	Drained
X_{10}, S_{10}	q_{10}	Dehydrated sludge

Cuadro B.6: Table of variables in the model

In the model designed here, it is necessary to make the same assumptions performed in Model 5. However, the plant consists of one aerobic reactor instead of three reactors. In order to represent such situation, the oxygen dissolved concentration in the reactor is fixed at 1.5 $(M(-COD)L^{-3})$.

B.8.2. Results of the example Model

In this Subsection, the numerical results for the example Model previously detailed in Subsection B.8.1 are presented. The evolution over time of the volumetric flow of the influent, effluent, total recirculation, purge and dehydrated sludge are presented in Figure B.32. The evolution over time of the concentration of the components in the influent, in the reactor, in the effluent, in the total recirculation and purge and in the dehydrated sludge are depicted in Figures B.33, B.34, B.35, B.36 and B.37, respectively

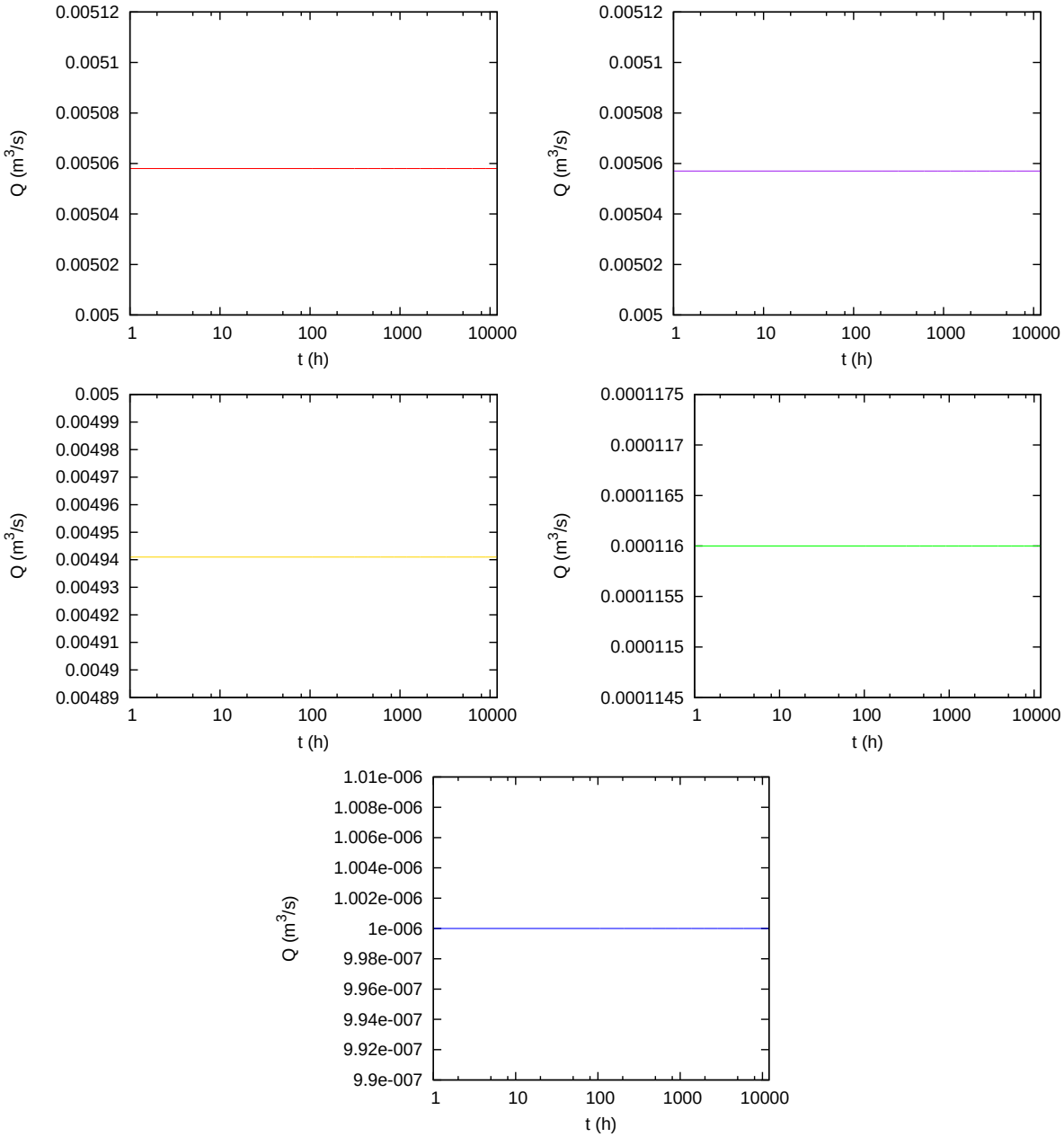

Figura B.32: Volumetric flow of the influent (—), effluent (—), recirculation (—), purge (—), dehydrated sludge (—).

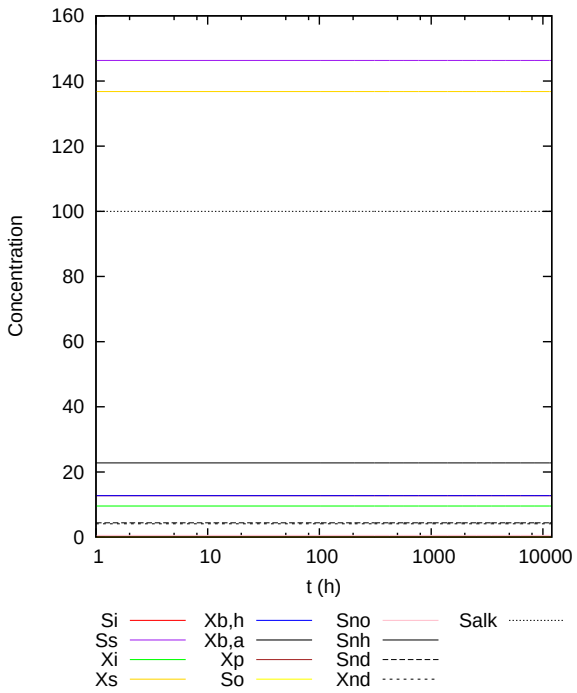

Figura B.33: Concentration of the 13 species in the influent.

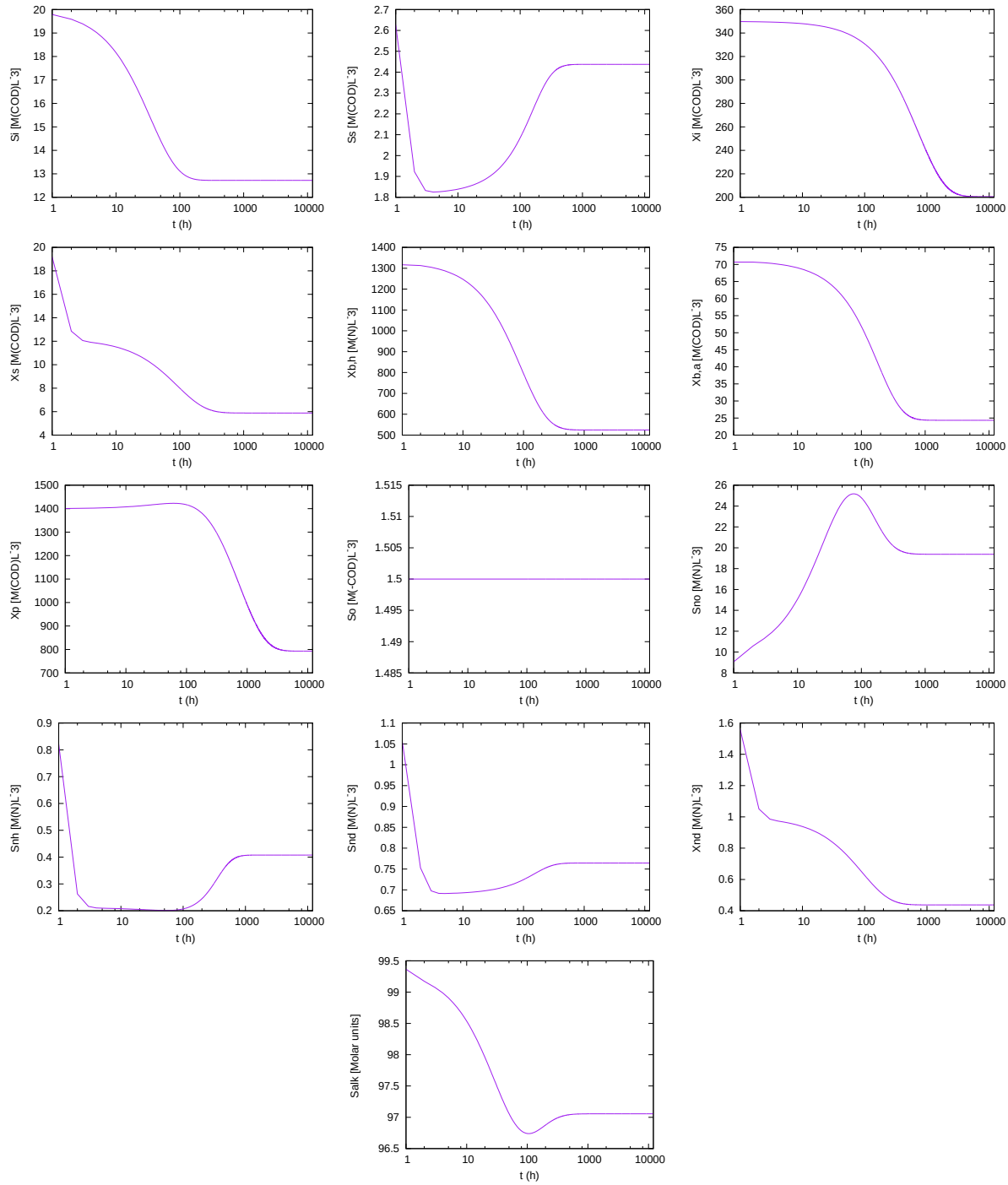

Figura B.34: Concentration of the 13 species in the reactor.

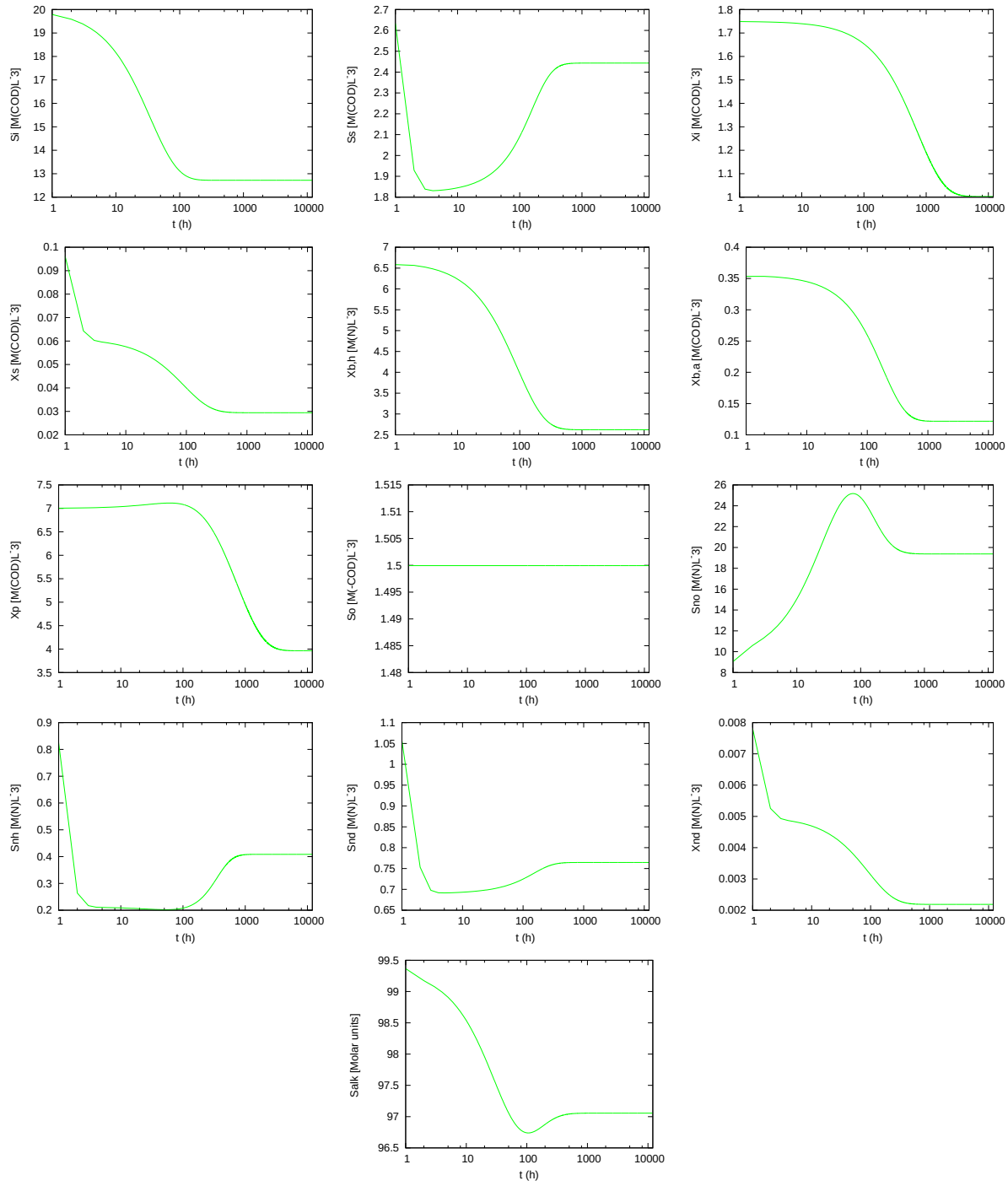

Figura B.35: Concentration of the 13 species in the effluent.

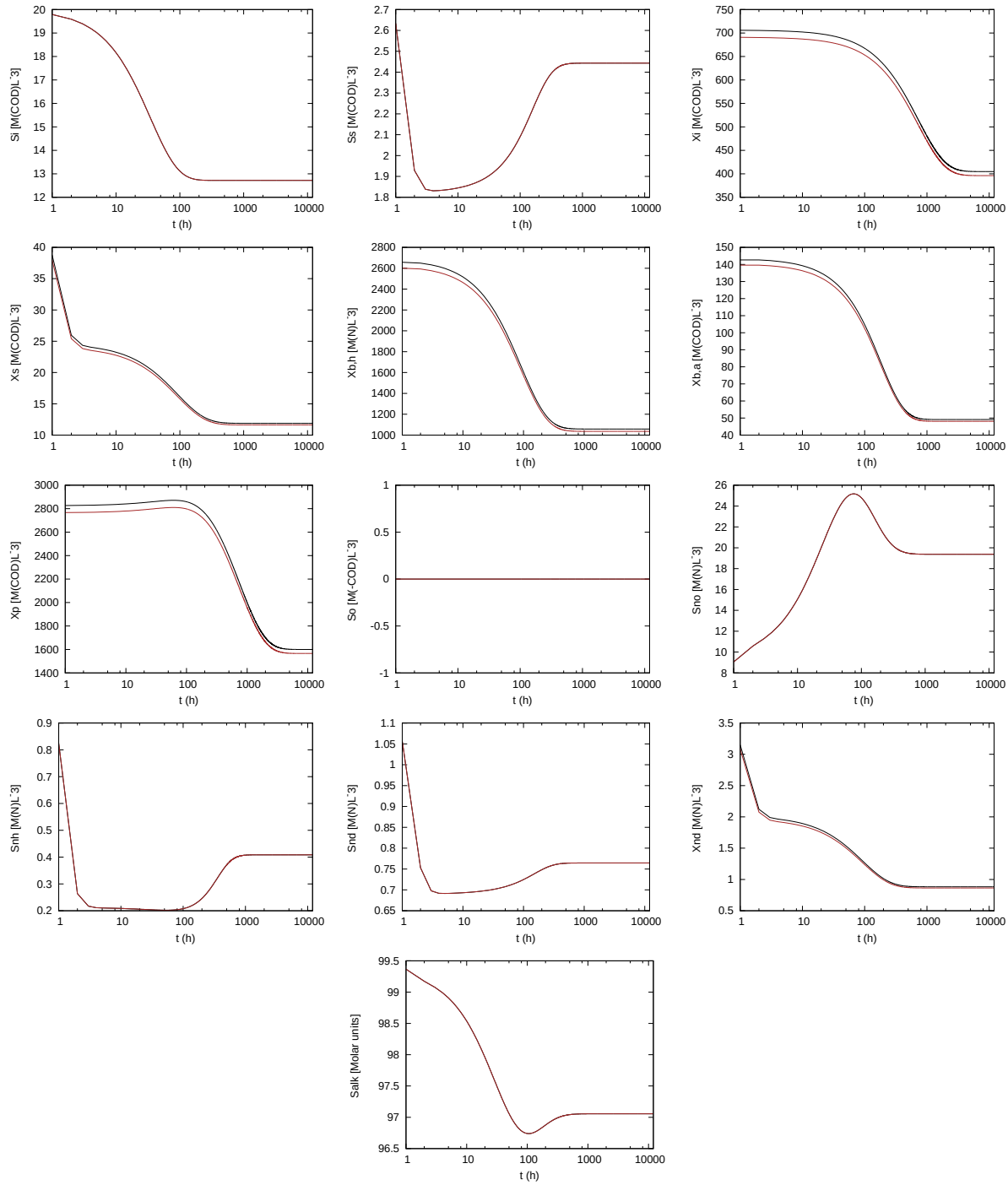

Figura B.36: Concentration of the 13 species in the total recirculation (—), purge (—).

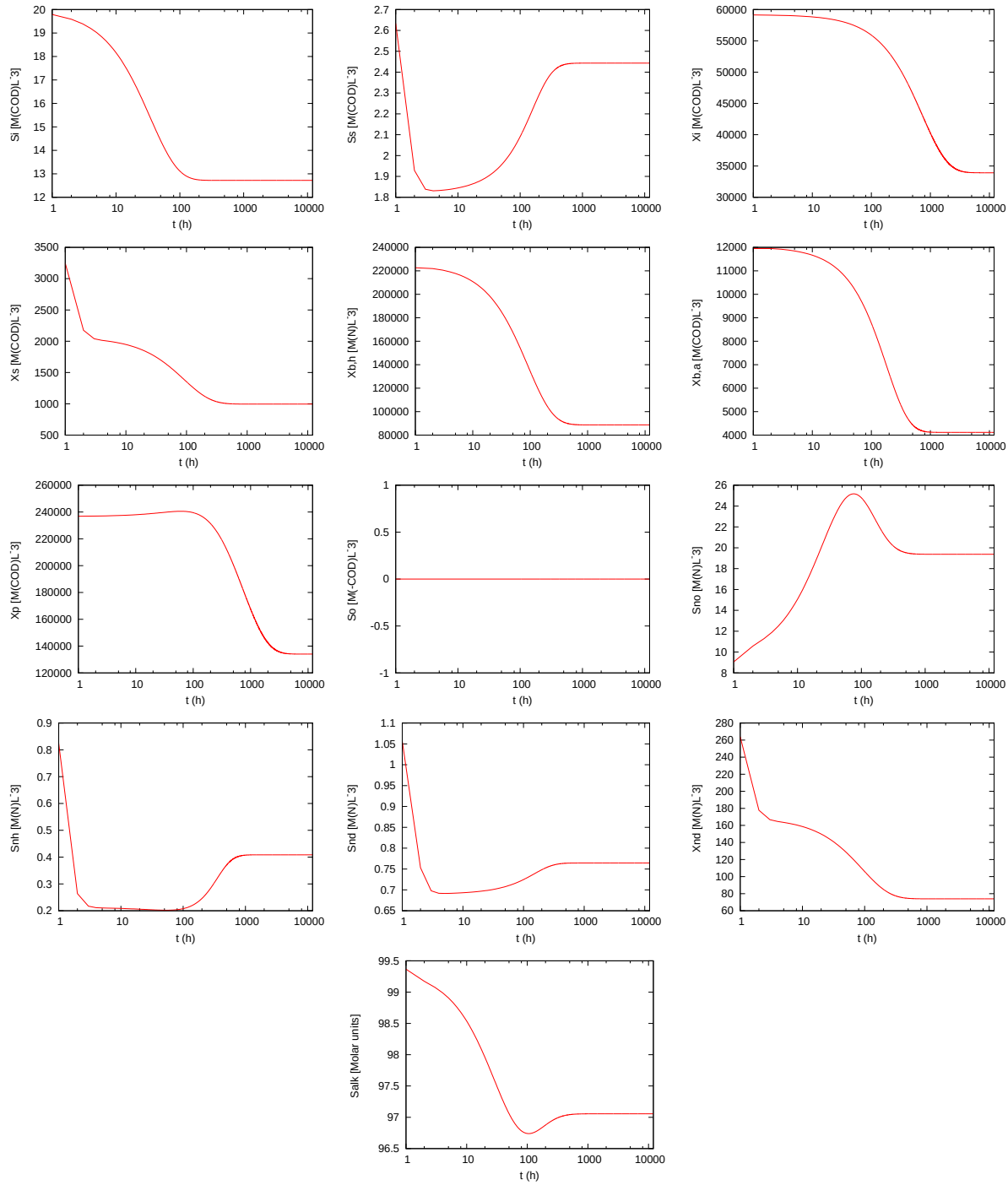

Figura B.37: Concentration of the 13 species in the dehydrated sludge.

B.8.3. Numerical comparison

In this Subsection, a numerical comparison of the component concentrations in the effluent between the simulation carried out with the Linx $ASM1$ software and the software developed are presented. In order to be compared, it is necessary to assume that the parameter K_{NH_H} is fixed to 0 in the Linx $ASM1$ simulation because is not used in $ASM1$. The aforementioned results after simulating 12000 hours are depicted in Table B.7.

Component	Linx ASM1 simulation	Software developed simulation	Dimensions
S_S	2.443	2.443	$M(COD)L^{-3}$
S_I	12.720	12.720	$M(COD)L^{-3}$
S_O	1.500	1.500	$M(O_2)L^{-3}$
S_{NO}	19.373	19.377	$M(N)L^{-3}$
S_{NH}	0.408	0.408	$M(N)L^{-3}$
S_{ND}	0.764	0.764	$M(N)L^{-3}$
S_{ALK}	97.065	97.055	$mol(HCO_3^-)L^{-3}$
X_I	1.003	1.003	$M(COD)L^{-3}$
X_S	0.029	0.029	$M(COD)L^{-3}$
$X_{B,H}$	2.617	2.622	$M(COD)L^{-3}$
$X_{B,A}$	0.122	0.122	$M(COD)L^{-3}$
X_P	3.966	3.964	$M(COD)L^{-3}$
X_{ND}	0.002	0.002	$M(N)L^{-3}$

Cuadro B.7: Summary of soluble components, $S_{(\cdot)}$.

As can be observed in Table B.7, the component concentrations in the effluent of both simulations are virtually equal.

B.9. Study on the sensitivity of the concentration of dissolved oxygen in the reactors and purge flow

In this Section, a numerical comparison of the component concentrations in the effluent between different situations are presented in order to assess the impact of the variability of the purge flow and the concentration of the dissolved oxygen in the reactors. For that purpose, a simulation using the parameters of the simulation detailed in Section B.8 is carried out. The aforementioned results after simulating 10000 hours are depicted in Table B.8 and B.9. Table B.8 represents the component concentrations in the effluent with a different concentration of the dissolved oxygen in the reactors and 0.05 of purge factor.

Component	S_O 1 $M(O_2)L^{-3}$ model	S_O 2 $M(O_2)L^{-3}$ model	S_O 3 $M(O_2)L^{-3}$ model	Dimensions
S_S	2.906	2.592	2.497	$M(COD)L^{-3}$
S_I	12.2	12.2	12.2	$M(COD)L^{-3}$
S_O	1.0	2.0	3.0	$M(O_2)L^{-3}$
S_{NO}	12.622	15.99	17.105	$M(N)L^{-3}$
S_{NH}	1.692	0.771	0.611	$M(N)L^{-3}$
S_{ND}	1.033	0.978	0.96	$M(N)L^{-3}$
S_{ALK}	3.947	3.64	3.55	$mol(HCO_3^-)L^{-3}$
X_I	13.176	13.176	13.176	$M(COD)L^{-3}$
X_S	0.077	0.062	0.0578	$M(COD)L^{-3}$
$X_{B,H}$	3.957	3.945	3.941	$M(COD)L^{-3}$
$X_{B,A}$	0.168	0.173	0.174	$M(COD)L^{-3}$
X_P	1.941	1.95	1.95	$M(COD)L^{-3}$
X_{ND}	0.0057	0.0047	0.0044	$M(N)L^{-3}$

Cuadro B.8: Study on the sensitivity of the concentration of dissolved oxygen in the reactors.

As dissolved oxygen increases, the concentration of ammonia nitrogen decreases due to the nitrification process. The ammonia nitrogen reacts with the dissolved oxygen to form nitrate, water and energy. Besides, a dissolved oxygen increase causes an increase of heterotrophic and autotrophic biomass, which are necessary to trigger both denitrification and nitrification porcesses, respectively.

The component concentrations in the effluent with a different purged percentage are depicted in Table B.9.

Component	7,27 % Purge	5,5 % Purge	3,5 % Purge	2 % Purge
S_S	6.758	5.133	3.523	3.2622
S_I	10.04	10.04	10.04	10.04
S_O	0.65	0.65	0.65	0.65
S_{NO}	0.000362	0.847	10.3306	10.917
S_{NH}	24.547	20.27	2.476	1.0784
S_{ND}	1.643	1.578	1.312	1.245
S_{ALK}	7.566	6.018	5.25	5.11
X_I	7.729	10.1	15.455	25.657
X_S	0.717	0.229	0.0985	0.0963
$X_{B,H}$	2.808	3.374	3.979	4.551
$X_{B,A}$	0.0	0.038	0.2066	0.2818
X_P	0.622	0.99	1.853	3.5478
X_{ND}	0.0548	0.018	0.008	0.0079

Cuadro B.9: Study on the sensitivity of the concentration of purge flow.

As purge percentage increases, the concentration of active biomass in the reactors increases due to the increase of biomass mass entering into the reactors. As has been commented previously, the active

biomass is essential to trigger both denitrification and nitrification porcesses. Hence, a purge flow increase implies a concentration of ammonia-ammonium decrease. However the purge factor is also related to the solids accumulation, as has been detailed in Subsection B.7.2, so that it must be a critical parameter of a wastewater treatment plant.

Apéndice C

Wastewater treatment plant simulation with automatic control

In this Chapter, the wastewater plant performance is simulated. The numerical results provided by the company are outlined in Section C.1. The purge regulation carried out by the plant coordinator is presented in Section C.2. The oxygen-ammonium controller performance are adressed in Section C.3. The characterization of the simulation models, which have been carried out in order to simulate the performance of the real waste water plant, are presented in Section C.4. The boundary conditions, which has been used in order to simulate the wastewater plant performance, are presented in Section C.5. The results of the aforementioned simulations are outlined in Section C.6. Finally, the comparison between the experimental information and the results of the simulations is adressed in Section C.7.

C.1. Experimental data

In this Section, the experimental data is presented in order to review the available information. The aforementioned data has been provided by the wastewater treatment plant and consist of

- Ammonium and nitrate concentration in the third reactor. This information has been extracted every five minute and has been measured by an ammonium and nitrate probe.
- Oxygen concentration in the third reactor. This information has been extracted every minute.
- Influent, effluent, recirculation and purge flow. This information has been extracted every minute.
- DBO, DQO, suspended solids, ammonium, nitrate and total nitrogen in the influent as well as the effluent. This information has been extracted every five days and has been measured from an average samples.

The following graphic represents the evolution over time during the days between 10th March and 8 April for the above-mentioned concentrations in the third reactor. The ammonium, nitrate and oxygen concentration in the third reactor are depicted in Figure C.1.

In most cases, an ammonium concentration increase causes an oxygen concentration increase, as can be observed between the 100 and 200 hours. This is to the nitrification-denitrification process to be carried out. As can be observed in Figures A.5 and A.2, an increase of oxygen concentration produces an increase of biomass concentration, essential for the aforementioned process. The autotrophic biomass and the dissolved oxygen are needed so that the nitrification process to be carried out, while the heterotrophic biomass is needed so that the denitrification process to be carried out.

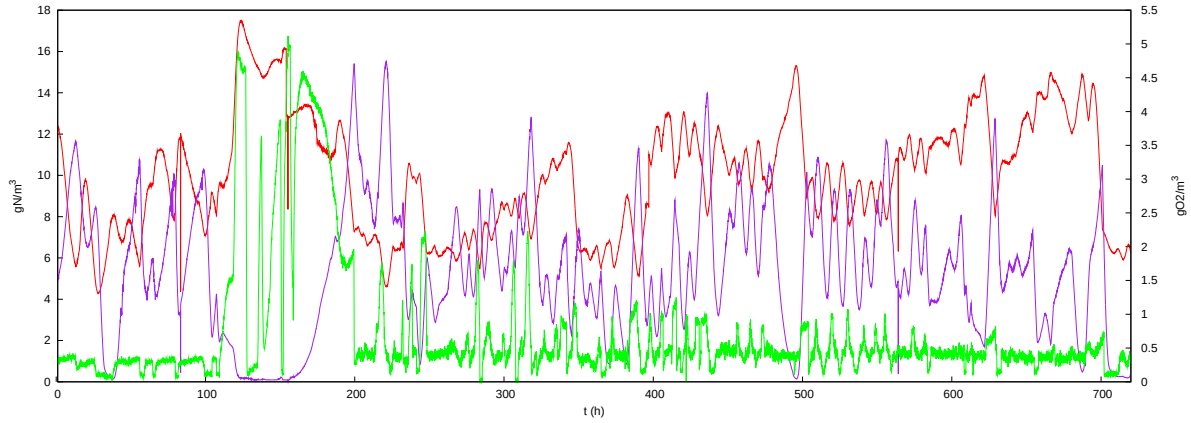

Figura C.1: Concentration of ammonium (—), nitrite (—) and oxygen dissolved (—) in the third reactor.

Nevertheless, around the 500 hour, 620 hour and 680 hour, the oxygen concentration remains constant even though the ammonium concentration is high. This is because the legislation does not allow that the total nitrogen concentration exceeds a threshold value ($15g/m^3$). When the aforementioned value is reached due to the nitrate-nitrate concentration increase, the plant coordinator usually reduces the Orbal power manually. This matter causes a decrease of the oxygen concentration, resulting in a nitrite-nitrate concentration decrease. The nitrate-nitrite concentration is more sensitive that the Ammonium nitrogen concentration. Hence, the ammonium-ammonia nitrogen concentration variation is less pronounced than the nitrite-nitrate concentration variation. Therefore, the plant coordinator is usually able to keep the total nitrogen concentration below the threshold value.

The following graphics represent the evolution in time during the days between 17th April and 19th April for the above-presented list information. The manual control previously described is not carried out during these days. This is because these type of control is just carried out when the influent load is not high. Due to the lack of the manual control information, the aforementioned control is not applied in the simulation. Again, the ammonium-ammonia, nitrate-nitrite nitrogen and oxygen concentration in the third reactor during these days are depicted in Figure C.2.

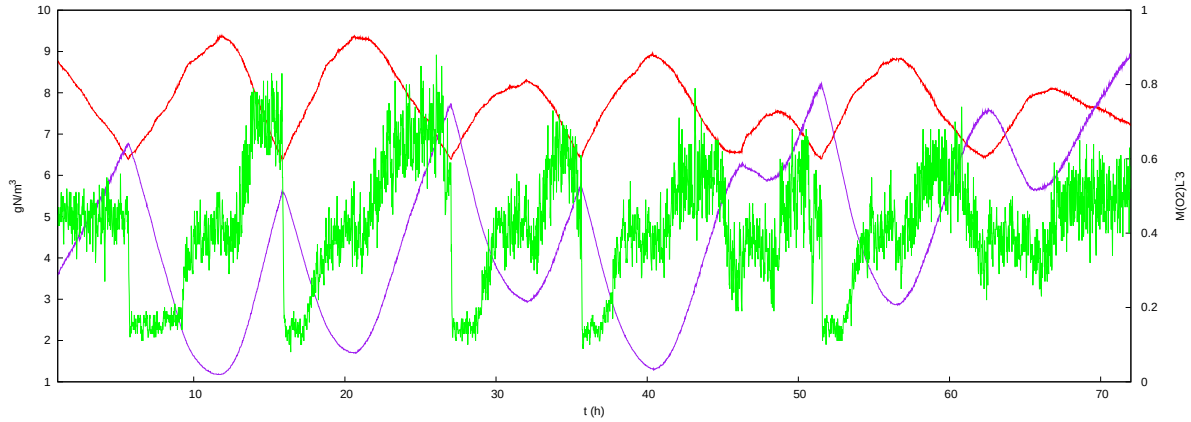

Figura C.2: Concentration of ammonium (—), nitrite (—) and oxygen dissolved (—) in the third reactor.

As can be observed, a time-lag exists between the oxygen concentration increase and the ammonia-ammonium concentration increase, being the ammonia-ammonium concentration ahead of the oxygen concentration. Besides, the oxygen fluctuation over time is greater than the ammonium fluctuation. The oxygen-ammonium automatic control is explained in Section C.3.

The evolution over time of the influent and effluent DBO, DQO, total nitrogen, ammonium, and nitrate are depicted in Figure C.3.

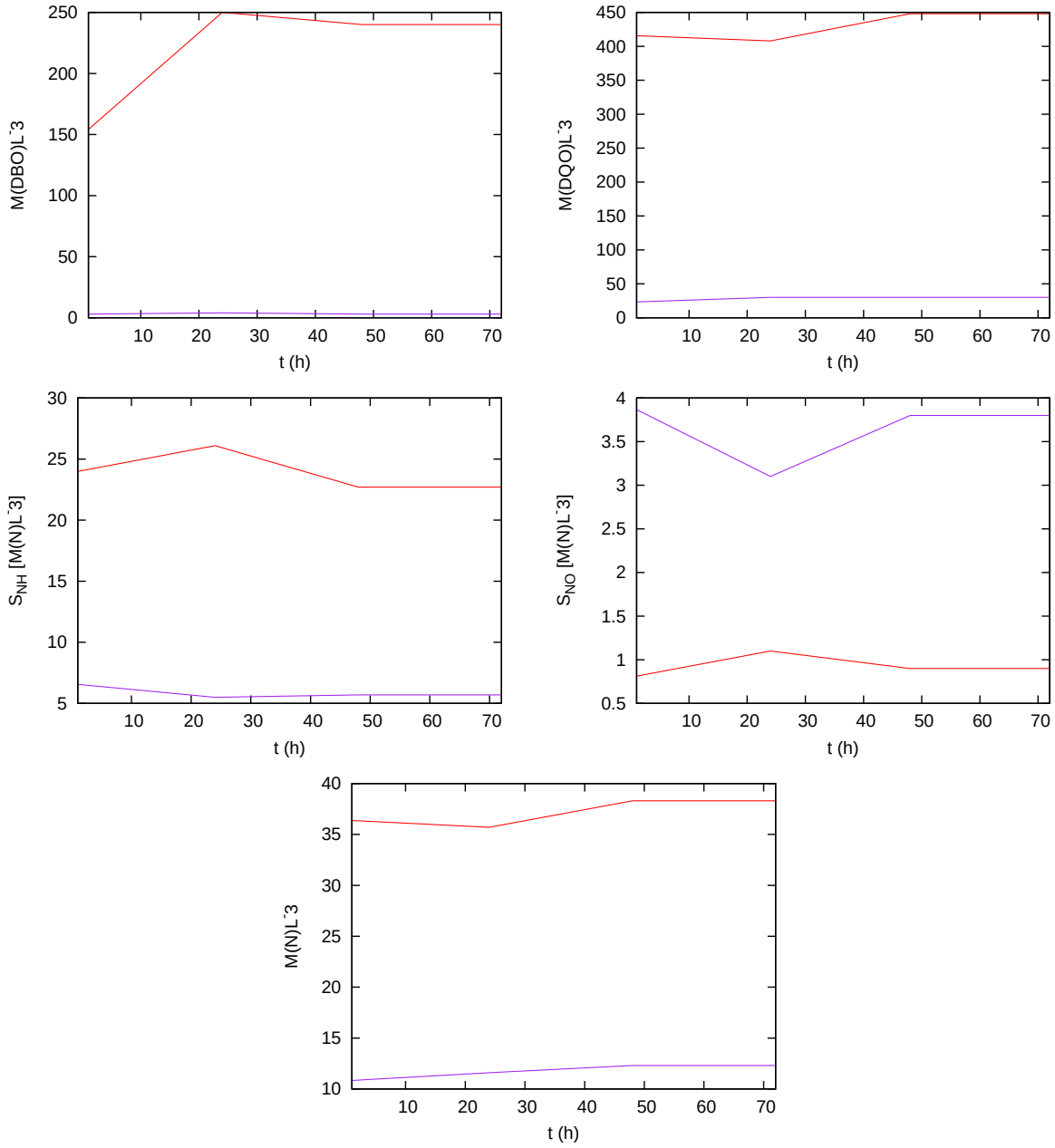

Figura C.3: Influent (—) and effluent (—).

An operator takes samples every hour of a day and mixes them in order to measure the aforementioned parameters. This process is carried out every five days. It should be noted that daily values have been interpolated in order to obtain better precision in the simulation.

The evolution over time of the purge flow is depicted in Figure C.4.

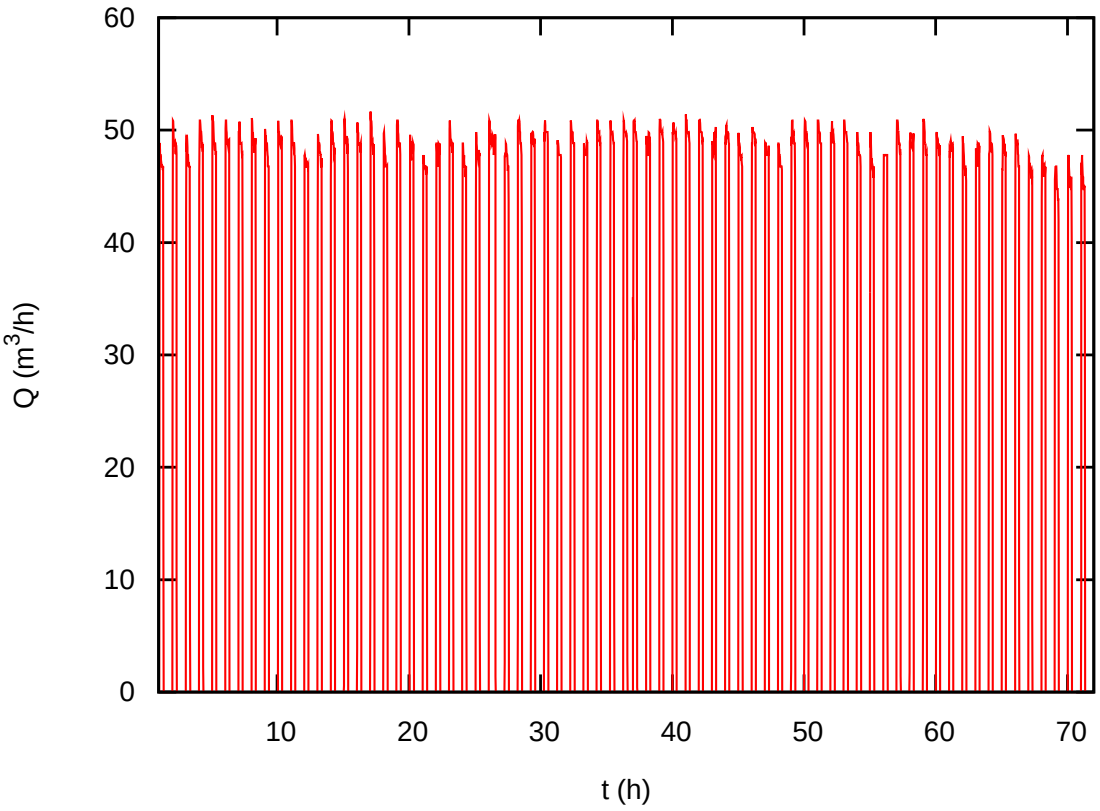

Figura C.4: Purge flow.

As can be observed, the purge flow is highly fluctuating. The plant coordinator regulates the purge flow as described in Section C.2.

The evolution over time of the influent and effluent flow and recirculation ratio are depicted in Figure C.4.

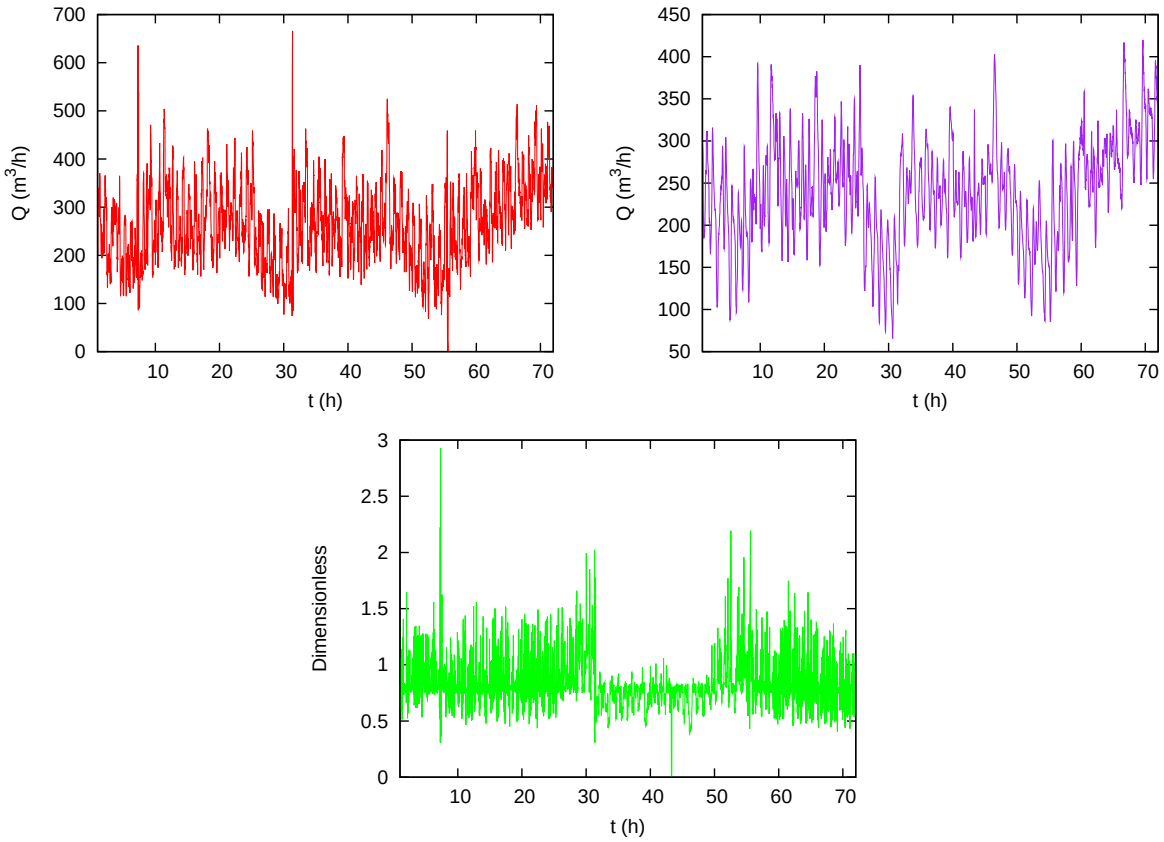

Figura C.5: Influent (—), effluent (—) and recirculation (—).

As can be observed above, the recirculation ratio during 18th April is lower than during 17th and 19h April. This difference is because the plant coordinator can regulate the recirculation ratio manually, which is defined as

$$r = \left(\frac{q_{recirculation}}{q_{influent}} \right). \tag{C.1}$$

C.2. Purge regulation

In this Section, the purge regulation details are presented. The purge flow is regulated using a pump which is controlled by an on/off system. The aforementioned pump regulates the purge flow considering the difference between the influent and effluent DBO. The plant coordinator calculates the operation time of the pump required during the next three days, each Monday and Thursday, in order to determine in which moment the pump must be operate. Considering that the maximum operation time of the pump is one hour, the aforementioned calculation is performed as follows

- First of all, it is necessary to determine the DBO eliminated mass per 3 day as

$$\frac{\Delta KgDBO}{3day} = \frac{(\frac{gDBO}{m^3})_e - (\frac{gDBO}{m^3})_s}{1000\frac{g}{Kg}} Q_{inlet}[\frac{m^3}{3day}], \tag{C.2}$$

- Moreover, it is necessary to estimate the ratio between the generated suspended solids and the DBO eliminated in order to calculate the biological sludge production. For that purpose, the plant coordinator carried out a calculation based on Chudoba's model which considers experimental parameters of the sludge [23]. The aforementioned ratio is estimated as follows

$$\frac{KgSS}{\Delta KgDBO} = 0{,}8. \tag{C.3}$$

  where $KgSS$ is the generated suspended solids mass and $\Delta KgDBO$ is the DBO eliminated mass.

- The generated suspended solids mass per 3 day is determined from the DBO eliminated mass per 3 day, using a ratio defined in Equation C.3 as follows

$$\frac{\Delta KgSS}{3day} = (\frac{\Delta KgDBO}{3day})(\frac{KgSS}{\Delta KgDBO}), \tag{C.4}$$

  where $\frac{KgSS}{\Delta KgDBO}$ is 0,8, as has been commented previously.

- The purged volume required during these three days in order to keep the suspended solids in the reactors constant is calculated from the eliminated suspended solid mass per 3 day and the concentration of suspended solids in the recirculation, as follows

$$Q_{purge}[\frac{m^3}{3day}] = \frac{\frac{\Delta SS}{3day}}{SS_{recirculation}[\frac{kg}{m^3}]}, \tag{C.5}$$

  where the suspended solids in the recirculation are estimated using an experimental ratio between the total COD and the suspended solids in the recirculation. The aforementioned ratio takes a value of 0.873.

- Finally, the operation time of the pump required during these three days is determined using the nominal pump flow ($48\frac{m^3}{h}$), as follows

$$t_{pump}[\frac{s}{3day}] = \frac{Q_{purge}[\frac{m^3}{day}]}{Q_{pump}[\frac{m^3}{s}]}, \tag{C.6}$$

Once the operation time of the pump during these three days has been calculated, the operation time of the pump within an hour is determined, considering that the maximum operation time of the pump is one hour. The calculation needed to determine the operation time of the pump within an hour, assuming that it remains constant during 3 days, is

$$t_o[\frac{s}{h}] = \frac{t_{pump}[\frac{s}{3day}]}{t_{bc}[\frac{s}{3day}]} t_{om}[\frac{s}{h}], \tag{C.7}$$

where t_{om} is the maximum operation time of the pump (1 hour) and t_{bc} is the time between calculations (3 days).

As has been mentioned, DQO an DBO are measured every five days. Hence, it is sometimes necessary to interpolate these parameters in order to make the estimation of the purge. This is because the purge calculation is performed every three days and the DBO and DQO samples are obtained every five days.

As can be observed, the lower the DBO eliminated mass per 3 day, the lower the operation time of the pump. If this occurs, the recirculation flow increases and the concentration of heterotrophic biomass in the reactors as well. As can be observed in Figures A.5 and A.2, an heterotrophic biomass concentration increase causes the denitrification process, in presence of soluble organic matter. The soluble organic matter consumption diminishes the DBO concentration in the effluent. Hence, the DBO eliminated mass per 3 day increases.

C.3. Oxygen-ammonium automatic control

In this Section, the details for the oxygen-ammonium automatic control are presented. Two stages are carried out during the nutrients elimination process: nitrification and denitrification.

The oxygen-ammonium regulation using an ammonium-nitrate probe is based on the optimization of nutrients elimination. The aforementioned regulation allows to set the sought ammonium-ammonia concentration in the third reactor. For this purpose, the automatic controller acts on frequency converter to adjust the rotational speed of the Orbal. This allows to increase or reduce the oxygen supply, as appropriate.

First of all, the provision of the Orbal in the wastewater treatment plant is presented in Figure C.6

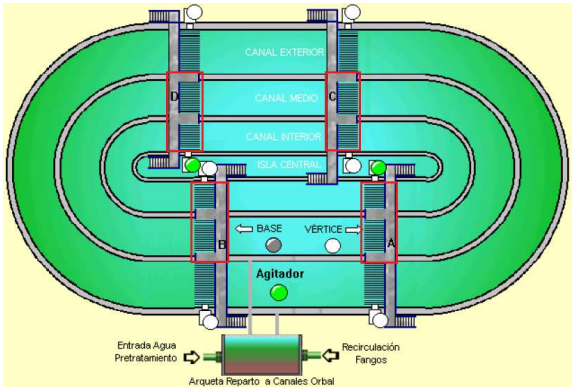

Figura C.6: Plant scheme

As can be observed, in the second and third reactor there are four disk sets in each of them. However, in the first reactor there is a vehiculator whose function is to mix the fluid in order to homogenize the concentrations. The aforementioned disk sets are combined in pairs. Each pair of Orbal is formed by a disk set of the second reactor and other of the third reactor (red color). The disk sets of the second reactor consist of 20 disks and the disk sets of the third reactor consist of 11 disks. Besides, each pair of Orbal is driven by the same rotor. Hence, the rotational speed of each Orbal pair is the same.

The oxygen supply of each disk set depends on the rotor immersion and rotational speed, as well as the disk number of the Orbal. Assuming that the Orbal operational mode is basis, the oxygen supply and the power consumed per unit of disk according to the rotor immersion and rotational speed is depicted in Table C.1

Rotor immersion (mm)	34,2 rpm		57 rpm	
	KgO_2/hr	W	KgO_2/hr	W
229	0.23543	79.43	0.61	330.74
305	0.294	81.59	0.75	441.8788
381	0.34628	126.0854	0.9	485.4286
457	0.4048	143.506	1.04	566.333
533	0.4671	163.49	1.2	654.59

Cuadro C.1: Orbal parameters.

The parameters which are involved in the above-mentioned regulation and can be modified by the plant coordinator are presented

- Regulation set point (S_{NH}^{ref}). This parameter is used as a reference and is usually set as 7 g/m3.
- Stop set point (S_{NH}^{stop}). If the ammonium concentration is below the aforementioned parameter, the minimum rotational speed of each Orbal is set. It is usually set as 6.4 g/m3.
- Dead-Band (S_{NH}^{band}). This parameter is used as a regulation range and is usually set as 0.2 g/m3. When the ammonium concentration is between the regulation set point minus or plus the dead-band, the regulation stops.
- Time between corrections. This parameter is the time required to increase or decrease the Orbal rotational speed to the correction. It is usually set as 300 s.
- Correction. This parameter is the percentage of the Orbal rotational speed which is increased or decreased within the time between corrections. It is usually set as 2 %.
- Maximum number of activated rotors. This parameter allows the maximum number of activated rotors to be set, simultaneously. Currently, it is set as 3.

The designation and the working rotational speed of each Orbal are described. For the shake of clarity, the pairs of Orbals will be referred to as A, B, C and D. The Orbal pairs have an assigned working sequence so that the rotational speed of each rotor increase or decrease in the following order.

- Appointed rotor as A is the first to operate. The minimum rotational speed of the aforementioned rotor is 34.2 revolutions per minute (60 %), while the maximum rotational speed is 57 revolutions per minute (100 %).
- Appointed rotor as D is the second to operate. The minimum rotational speed of the aforementioned rotor is 34.2 revolutions per minute (60 %), while the maximum rotational speed is 57 revolutions per minute (100 %).
- Appointed rotor as B is the third to operate. The minimum rotational speed of the aforementioned rotor is 0 revolutions per minute (0 %), while the maximum rotational speed is 57 revolutions per minute (100 %). It should be noted that the rotational speed of the rotor increases from 0 to 34.2 revolutions per minute without considering the above mentioned correction and vice versa.
- Appointed rotor as C is the last to operate. The minimum rotational speed of the aforementioned rotor is 0 revolutions per minute (0 %), while the maximum rotational speed is 57 revolutions per minute (100 %). It should be noted that the rotational speed of the rotor increases from 0 to 34.2 revolutions per minute without considering the above mentioned correction and vice versa.

The working order of the rotors described is depicted in Figure C.7

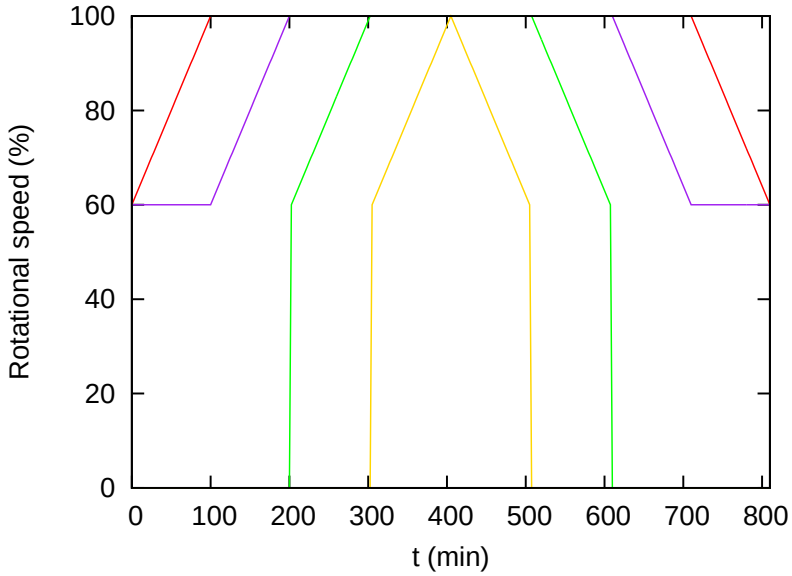

Figura C.7: Rotational speed in rotor A (—), D (—), B (—) and C (—) during an up-down cycle, considering the above-mentioned regulation parameters

Following the working order depicted in Figure C.7, the interaction between the ammonium concentration in the third reactor and the rotational speed of each Orbal pair is presented. For this purpose, it is necessary to define two operating states. The first of them is defined as increase in the concentration of ammonium-ammonia in the third reactor. In this case, the rotational speed performance is depicted in Figure C.8.

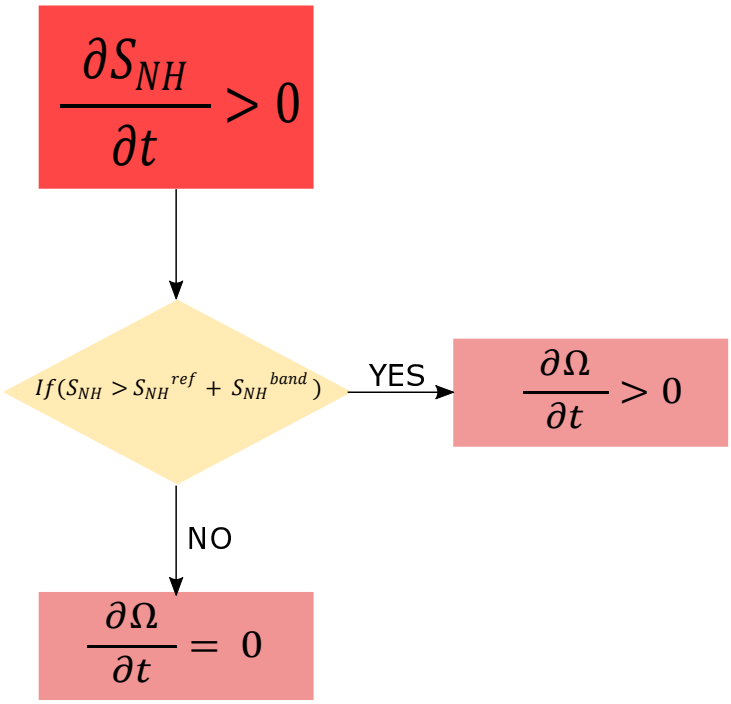

Figura C.8: Ammonium-ammonia concentration increase case.

It should be noted that the rotational speed of the next rotor increases when the rotational speed of the current rotor reaches the maximum value, as can be observed in Figure C.7. The aforementioned statement is valid for the second, third and fourth rotor (D, B and C).

The other operating case is defined as decrease in the concentration of ammonium-ammonia in the third reactor. In this case, the rotational speed performance is presented in Figure C.9.

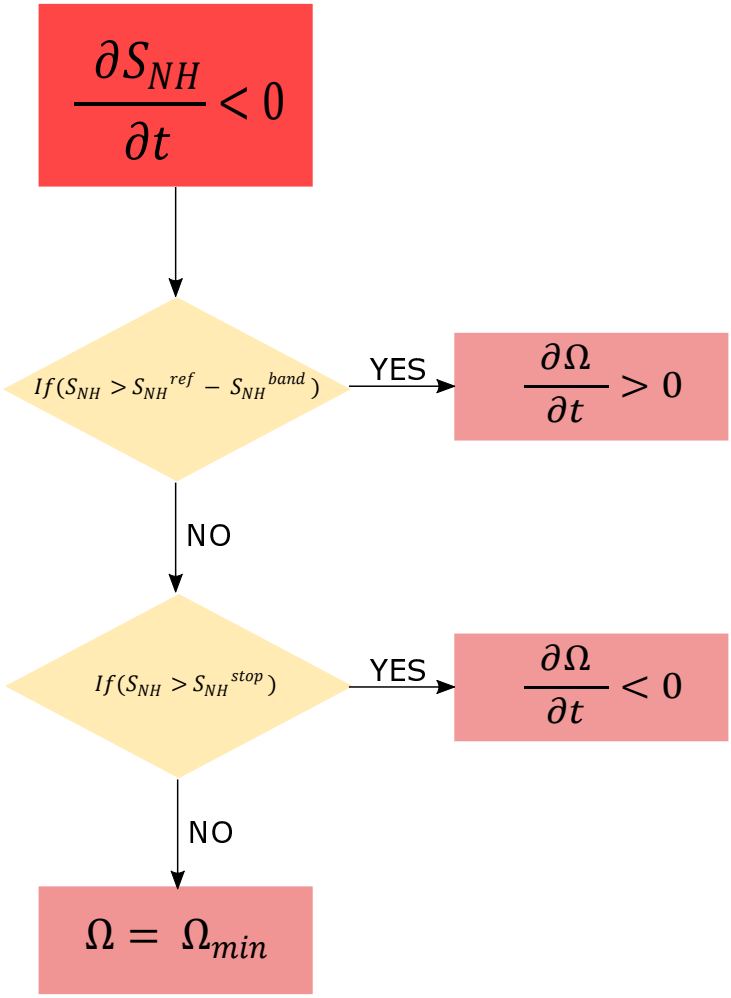

Figura C.9: Ammonium-ammonia concentration decrease case.

It should be noted that the rotational speed of the previous rotor decreases when the rotational speed of the current rotor reaches the minimum value, as can be observed in Figure C.7. The aforementioned statement is valid for the first, second and third rotor (A, D and B).

As can be observed, the upper the ammonia-ammonium concentration, the upper the rotational speed of the disk sets. If this occurs, the dissolved oxygen concentration increases. As can be observed in Figures A.5 and A.2, a dissolved oxygen increase causes the nitrification process, in presence ammonia-ammonium nitrogen. Hence, the ammonia-ammonium nitrogen diminishes in the effluent. Otherwise, the concentration of nitrite-nitrate increases.

C.3.1. Oxygen-ammonium alternative control

In this Subsection, an alternative control method is described. As has been mentioned in Section C.1, a manual control is usually carried out by the plant coordinator. It consists of minimize the rotational speed of the Orbals when the concentration of total nitrogen is over the above-mentioned threshold value (15 gN/m^3). The aforementioned control is carried out only when the total nitrogen excess is due to the increase of nitrite-nitrate concentration. If that occurs, the plant coordinator assesses the concentration of ammonia-ammonium in the influent and decides to apply or not the manual control described. In order to perform a complete automatic control of the wastewater plant, an alternative control method are described.

First of all, when the concentration of total nitrogen is over the threshold value, the rotational speed of the disk sets is decreased in the same way as has been described in Section C.3, instead of minimize the rotational speed of the disk sets, directly. At the same time, a nitrite-nitrate concentration set point is added in order to limit the disk sets rotational speed decrease. This is because when the Orbal's rotational speed is low, the concentration of ammonia-ammonium nitrogen increases due to the lack of oxygen.

The simulations are conducted for March in order to appreciate the improvement in concentration of total nitrogen. The results are presented in Figure C.10

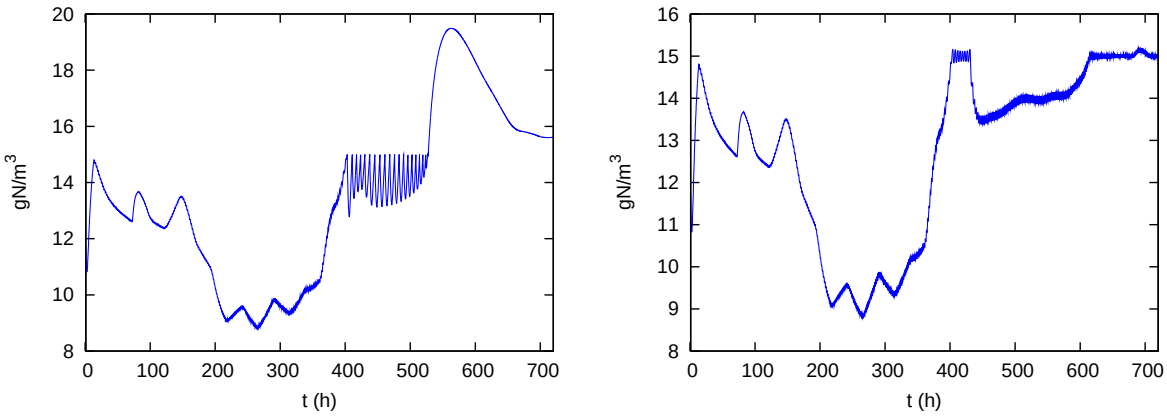

Figura C.10: Concentration of total nitrogen in third reactor using manual control (left) and automatic control (right).

As can be observed, in the case of using a manual control, the total nitrogen concentration is over the threshold value during almost 200 hours. However in the case of using the automatic control described, the total nitrogen concentration is over the threshold value during a few hours. Hence, the total nitrogen concentration is better controlled by the automatic control than by the manual control.

C.4. Models with automatic control

In this Section, the configurations of the simulations are presented. In Subsection C.4.1, a simulation imposing a constant clarifier performance is depicted. In Subsection C.4.2, a simulation imposing a constant clarifier performance and including the ASM1 processes within it is presented. In Subsection C.4.3, a simulation taking into account settling velocity of particulate components as well as ASM1 processes within the clarifier is depicted.

The elements which connect each reactor to themselves or each clarifier are the same to those described in Section —. Hence, the flow discharge between reactors is calculated in the same way as Equation B.1,

while the flow discharge which connects the third reactor with the clarifier and the reactor to the outside are calculated in the same way as Equation B.2.

C.4.1. Model simulation including mass storage

The layout of the wastewater plant which has been simulated is depicted in Figure C.11. As can be observed, this model recreates a wastewater plant with sludge recirculation and purge, in the same way as the Model 3 described in Section B.3. However, the recirculation flow is defined in different way, as described below. The real wastewater plant also includes a sludge thickener and two sludge dehydrators. The aforementioned components have not been included in the simulation due to the lack of real information about them. Nevertheless, the sludge thickener and the sludge dehydrator do not substantially affect the simulation results because they are mainly used to reduce the sludge volume, as has been mentioned in Subsection B.7.1. The aforementioned model also consists of three reactors, one clarifier, a recirculation line and purge discharge. The main variables included in the model are also summarized in Table C.3. Note that from the concentration and volumetric discharge, the mass flow can be defined as $\dot{m}_{(\cdot)} = X_{(\cdot)} \cdot q_{(\cdot)}$.

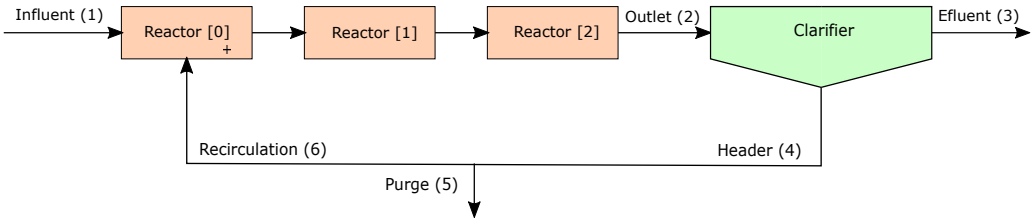

Figura C.11: Plant layout and nomenclature of the relevant points.

Concentration	Discharge or volume	Description
X_1, S_1	q_1	Influent of the plant
X_2, S_2	q_2	Outlet of the reactor (spillway)
X_3, S_3	q_3	Effluent of the plant
X_4, S_4	q_4	Header
X_5, S_5	q_5	Purge
X_6, S_6	q_6	Recirculation

Cuadro C.2: Table of variables in the model

In the model designed here, it is necessary to make the following assumptions:

- The recirculation discharge is defined as $q_6 = rq_1$, where r is the recirculation factor. The aforementioned factor is used in order to define the recirculation discharge instead of the header discharge (Model 3). This is because the plant coordinator controls the recirculation discharge using the aforementioned parameter, directly.
- The header discharge is defined as $q_4 = \frac{q_6}{(1-p)}$, where p is the fraction of header discharge purged.
- In the reactors, the first of them operates under anoxic conditions ([0]) and the remainder of them, under aerobic conditions ([1] and [2]). In order to represent both situations, the ammonium-oxygen control described in Section C.3 is carried out. Furthermore, the ASm1 processes are carried out within them.
- In the clarifier, the soluble components are considered to be homogeneously distributed within the volume. The clarifier is modelled in order to separate particulate components and soluble components. The concentration of the soluble components in both the effluent and the recirculation are considered to be the concentration of those components at the clarifier, $S_2 = S_3 = S_4$. It should

be noted that the concentration of all the components in the header, purge and recirculation do coincide.

- In the clarifier, the particulate components are considered to be partially deposited by sedimentation, which means most solids come out of the plant through the header. However, a small fraction of these solids come out of the plant through the effluent. The concentration of the particulate components in the effluent are calculated, as follows

$$X_3 = X_2(1 - \eta_c), \tag{C.8}$$

where η_c is the clarifier yield.

Once the assumptions have been made, it is necessary to determine the transfer function between the concentration of the particulate components in the recirculation and in the clarifier ($X_4 = f(X_2)$). For this purpose, two control volumes are defined and a mass balance for water and particulate components in the clarifier is made. It should be noted that the concentrations of the particulate components in both the purge and the recirculation are considered to be the concentration of those components in the header. The first control volume is depicted on the left side and the other is depicted on the right side of Figure C.12.

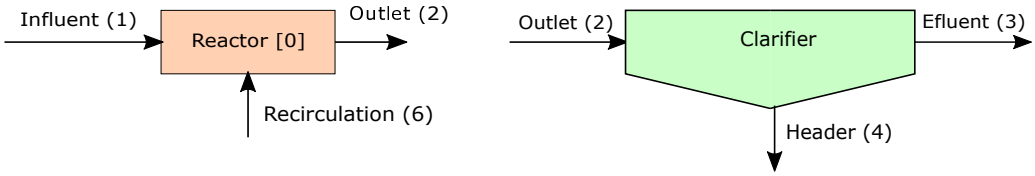

Figura C.12: Control Volumes.

Writing a water mass balance for the first control volume,

$$q_2 = q_1 + q_6, \tag{C.9}$$

and knowing that $q_6 = q_1 r$, it results

$$q_2 = q_1(1 + r). \tag{C.10}$$

Writing a water mass balance for the second control volume,

$$q_2 = q_3 + q_4, \tag{C.11}$$

and knowing that $q_4 = \frac{q_6}{(1-p)}$ and $q_6 = q_1 r$, it results

$$q_2 = q_3 + \frac{q_1 r}{1 - p}. \tag{C.12}$$

Combining both equations, (C.10) and (C.12), q_3 results

$$q_3 = \frac{q_1(1 - p - rp)}{1 - p}. \tag{C.13}$$

Writing a particulate components mass balance within the clarifier, it results

$$\dot{m}_2 = \dot{m}_4 + \dot{m}_3, \tag{C.14}$$

that can be written as

$$X_2 q_2 = X_4 q_4 + X_3 q_3. \tag{C.15}$$

Considering equation (C.10), $q_4 = \frac{r q_1}{1-p}$, equation (C.8) and (C.13), it results

$$X_2(1+r) = X_4 \frac{r}{1-p} + X_2 \frac{(1-\eta_c)(1-p-rp)}{1-p}. \tag{C.16}$$

Finally, the concentrations of the particulate components in the header are

$$X_4 = X_2 \left(\frac{r + \eta_c(1-p-rp)}{r} \right). \tag{C.17}$$

C.4.2. Model simulation including mass storage and ASM1 processes in the clarifier

The layout of the wastewater plant which has been simulated is depicted in Figure C.13. As can be observed, this model recreates a wastewater plant with sludge recirculation and purge. However, the real wastewater plant also includes a sludge thickener and two sludge dehydrators. The aforementioned components have not been included in the simulation due to the lack of real information about them. Nevertheless, the sludge thickener and the sludge dehydrator do not substantially affect the simulation results because they are mainly used to reduce the sludge volume, as has been mentioned in Subsection B.7.1. The wastewater plant which has been simulated consists of three reactors, one clarifier, a recirculation line and purge discharge. It should be noted that in this model the ASm1 processes are also carried out within the clarifier, which does not happen in the previous models. The main variables included in the model are also summarized in Table C.3. Note that from the concentration and volumetric discharge, the mass flow can be defined as $\dot{m}_{(\cdot)} = X_{(\cdot)} \cdot q_{(\cdot)}$.

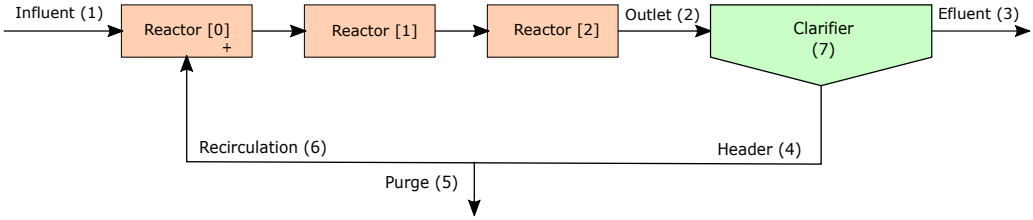

Figura C.13: Plant layout and nomenclature of the relevant points.

Concentration	Discharge or volume	Description
X_1, S_1	q_1	Influent of the plant
X_2, S_2	q_2	Outlet of the reactor (spillway)
X_3, S_3	q_3	Effluent of the plant
X_4, S_4	q_4	Header
X_5, S_5	q_5	Purge
X_6, S_6	q_6	Recirculation
X_7, S_7	V_7	Clarifier

Cuadro C.3: Table of variables in the model

In the model designed here, it is necessary to make the following assumptions:

- The recirculation discharge is defined as $q_6 = rq_1$, where r is the recirculation factor.
- The header discharge is defined as $q_4 = \frac{q_6}{(1-p)}$, where p is the fraction of header discharge purged.
- In the reactors, the first of them operates under anoxic conditions ([0]) and the remainder of them, under aerobic conditions ([1] and [2]). In order to represent both situations, the ammonium-oxygen control described in Section C.3 is carried out. Furthermore, the ASm1 processes are carried out within them.
- In the clarifier, the ASm1 processes are also carried out within it. The soluble components are considered to be homogeneously distributed within the volume. The clarifier is modelled in order to separate particulate components and soluble components. The concentration of the soluble components in both the effluent and the recirculation are considered to be the concentration of those components at the clarifier, $S_7 = S_3 = S_4$. It should be noted that the concentration of all the components in the header, purge and recirculation do coincide.
- In the clarifier, the particulate components are considered to be partially deposited by sedimentation, which means most solids come out of the plant through the header. However, a small fraction

of these solids come out of the plant through the effluent. The concentration of the particulate components in the effluent are calculated, as follows

$$X_3 = X_7(1 - \eta_c), \tag{C.18}$$

where η_c is the clarifier yield.

Once the assumptions have been made, it is necessary to determine the transfer function between the concentration of the particulate components in the recirculation and in the clarifier ($X_4 = f(X_7)$). For this purpose, two control volumes are defined and a mass balance for water and particulate components in the clarifier is made. It should be noted that the concentrations of the particulate components in both the purge and the recirculation are considered to be the concentration of those components in the header. The first control volume is depicted on the left side and the other is depicted on the right side of Figure C.14.

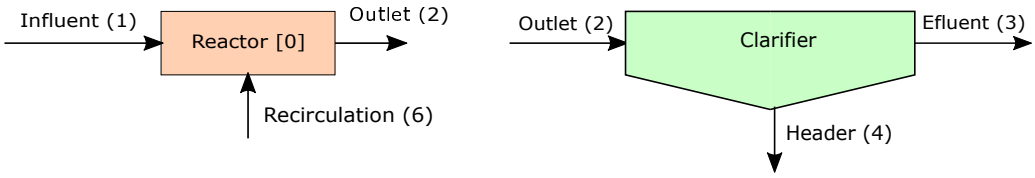

Figura C.14: Control Volumes.

Writing a water mass balance for the first control volume,

$$q_2 = q_1 + q_6, \tag{C.19}$$

and knowing that $q_6 = q_1 r$, it results

$$q_2 = q_1(1 + r). \tag{C.20}$$

Writing a water mass balance for the second control volume,

$$q_2 = q_3 + q_4, \tag{C.21}$$

and knowing that $q_4 = \frac{q_6}{(1-p)}$ and $q_6 = q_1 r$, it results

$$q_2 = q_3 + \frac{q_1 r}{1 - p}. \tag{C.22}$$

Combining both equations, (C.20) and (C.22), q_3 results

$$q_3 = \frac{q_1(1 - p - rp)}{1 - p}. \tag{C.23}$$

Writing a particulate components mass balance within the clarifier, it results

$$\dot{m}_2 = \dot{m}_4 + \dot{m}_3, \tag{C.24}$$

that can be written as

$$X_2 q_2 = X_4 q_4 + X_3 q_3. \tag{C.25}$$

Considering equation (C.20), $q_4 = \frac{r q_1}{1-p}$, equation (C.18) and (C.23), it results

$$X_2(1+r) = X_4\frac{r}{1-p} + X_7\frac{(1-\eta_c)(1-p-rp)}{1-p}. \tag{C.26}$$

Finally, the concentrations of the particulate components in the header are

$$X_4 = \frac{X_2(1-p)(1+r) - X_7(1-\eta_c)(1-p-rp)}{r}. \tag{C.27}$$

C.4.3. Model simulation taking into account clarifier characterization

The layout of the wastewater plant which has been simulated is depicted in Figure C.15, which is the same as the layout presented in Subsection C.4.2. As can be observed, it consists of three reactors, one clarifier, a recirculation line and purge discharge. It should be noted that in this model the clarifier characterizations takes into account the sedimentation velocity of the particalted components, as well as the reactions that are carried out within it. The main variables included in the model are also summarized in Table C.3. Note that from the concentration and volumetric discharge, the mass flow can be defined as $\dot{m}_{(\cdot)} = X_{(\cdot)} \cdot q_{(\cdot)}$.

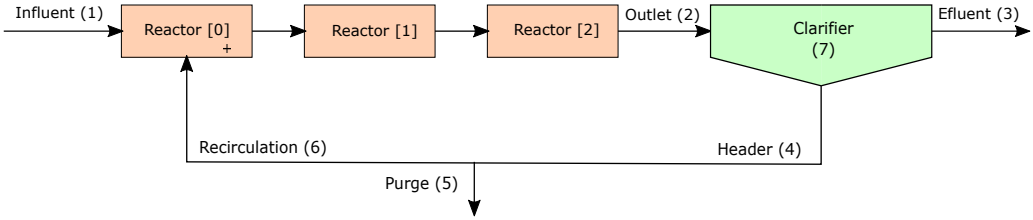

Figura C.15: Plant layout and nomenclature of the relevant points.

Concentration	Discharge or volume	Description
X_1, S_1	q_1	Influent of the plant
X_2, S_2	q_2	Outlet of the reactor (spillway)
X_3, S_3	q_3	Effluent of the plant
X_4, S_4	q_4	Header
X_5, S_5	q_5	Purge
X_6, S_6	q_6	Recirculation
X_7, S_7	V_7	Clarifier

Cuadro C.4: Table of variables in the model

In the model designed here, it is necessary to make the following assumptions:

- The recirculation discharge is defined as $q_6 = rq_1$, where r is the recirculation factor.
- The header discharge is defined as $q_4 = \frac{q_6}{(1-p)}$, where p is the fraction of header discharge purged.
- In the reactors, the first of them operates under anoxic conditions ([0]) and the remainder of them, under aerobic conditions ([1] and [2]). In order to represent both situations, the ammonium-oxygen control described in Section C.3 is carried out. All the components are considered to be homogeneously distributed within the volume, meaning that there are not differences between the concentration of any species within the reactors. Furthermore, the ASm1 processes are carried out within them.
- The ASm1 processes are also carried out within the clarifier. The clarifier volume is considered constant because of the volume variations of the clarifier are negligible as compared with the total volume. Hence, the clarifier spillway which allows to connect the clarifier to the outside is not applicable. Instead of defining a clarifier performance, as explained in Subsection C.4.2, Riemann's problem is solved in order to estimate the concentration of the particulate components in the effluent as well as the header. The aforementioned problem has been presented in Subsubsection C.4.3.

Clarifier characterization

In this Subsubection, a model used in order to simulate the clarifier performance considering the sedimentation velocity of the sludge are presented. The simulation of the clarifier performance allows to estimate the concentration of the suspended solids in the effluent and in the recirculation using experimental information which is provided by the plant coordinator. The aforementioned model is based on the theory of the solids flux and allows to simulate the continuous sedimentation process which is carried out in the clarifiers [24]. The simplest form which is used in order to describe the solid flux within the clarifier is presented in the Equation C.28 as

$$F(z,t) = F_{h,Z} + F_{s,Z}, \tag{C.28}$$

where $F_{h,Z}$ represents the downward bulk flux and $F_{s,Z}$ represents the gravity settling flux. The aforementioed parameters are defined as

$$\begin{cases} F_{h,Z} = V \cdot SS \\ F_{s,Z} = V_s \cdot SS \end{cases} \tag{C.29}$$

Considering the Equation C.29, the solid flux within the clarifier is defined as

$$F(z,t) = V \cdot SS + V_s \cdot SS = u \cdot SS, \tag{C.30}$$

where $F(z,t)$ represents the solid flux within the clarifier which is dependent on height z and time t. V represents the flow velocity in the clarifier. The aforementioned parameter depends on the z coordinate, as will be commented below. V_s represents the zonal sedimentation velocity of the activated sludge. SS represents the suspended solids concentration. u represents the total velocity in the clarifier.

The solid flux theory represents the mass balance model in the clarifier as follows

$$\frac{\partial(SS)}{\partial t} = -\frac{\partial(F)}{\partial z}. \tag{C.31}$$

However, it is necessary to consider a diffusion term. Considering that the direction of the sedimentation velocity is always downwards by gravity, the Equation C.30 is written as

$$F(z,t) = V \cdot SS - V_s \cdot SS - D_a \cdot \frac{\partial(SS)}{\partial z}, \tag{C.32}$$

where D_a is the pseudo-diffusivity coefficient. It is considered that the aforementioned parameter remains constant and takes a value of 0.54 m2/h [25].

In terms of the mass balance model, the diffusion term is second order derivative with respect to z. Considering the aforementioned term, Equation C.31 is written as

$$\frac{\partial(SS)}{\partial t} = -V\frac{\partial(SS)}{\partial z} + \frac{\partial(V_s \cdot SS)}{\partial z} + D_a \cdot \frac{\partial^2(SS)}{\partial^2 z}. \tag{C.33}$$

Once the solid flux theory has been described, the zonal sedimentation velocity of the activated sludge (V_s) is estimated. Considering that the aforementioned parameter only depends on the suspended solids concentration, the most common models which are used in order to determine the zonal sedimentation velocity of the activated sludge (V_s) are the exponential and the potential models [26]. The exponential model which has been chosen in order to simulate the clarifier performance is the Vesilind model. The aforementioned model defines the zonal sedimentation velocity of the activated sludge (V_s) as

$$V_s = ke^{-nSS}, \tag{C.34}$$

where k and n are parameters of the model. The aforementioned parameters are correlated with sedimentation parameters [27] as follows

References	Correlations k (m/h), n(l/g)
Pitman (1984)	$k = 10{,}4 - 0{,}0148SVI$ $n = 0{,}29exp(0{,}016SVI)$
Daigger and Roper (1985)	$k = 7{,}8$ $n = 0{,}148 + 0{,}0021SVI$
Ekama and Marais (1986)	$k/n = 39{,}32exp(-0{,}00518SVI)$ $n = 0{,}88 - 0{,}393log(k/n)$
Wahlberg and Keinath (1988)	$k = 18{,}2exp(-0{,}00602SVI)$ $n = 0{,}351 + 0{,}00058SVI$
Härtel and Pöpel (1992)	$k = 17{,}4exp(-0{,}0113SVI) + 3{,}3931$ $n = -0{,}9834exp(-0{,}00581SVI) + 1{,}043$
Daigger (1995)	$k = 6{,}5$ $n = 0{,}165 + 0{,}001586SVI$
Mines et al. (2001)	$k = 7{,}27$ $n = 0{,}0281 + 0{,}00229SVI$

Cuadro C.5: Correlations of sedimentation parameters.

where SVI represents the sludge volume index [28]. The aforementioned parameter is the most common index which is used in order to determine the sedimentability of the activated sludge. The SVI is defined as the volume (in milliliter units) occupied per gram of dry sludge after allowing the sediment to settle during 30 minutes, without stirring, in a graduated test tube. Mathematically, the SVI is expressed as

$$SVI = \frac{VF_{30}}{SS}\left[\frac{ml}{g}\right]. \tag{C.35}$$

A sedimentation test is carried out by the plant coordinator in order to estimate the above-mentioned parameter. For that purpose, the plant coordinator takes samples of the mixed liquor using a measuring cylinder and determines the SVI after allowing the sediment to settle during 30 minutes.

Another way to determine the sedimentation velocity is using the double-exponential settling velocity function of Takacs [29]. The aforementioned function is also based on the solid flux concept, as the Vesilind function. However, it is applicable to both hindered and flocculent settling conditions, unlike the standard Vesilind model, which is applicable only under hindered conditions. The sedimentation velocity using the Takacs model is written as

$$V_s = min(v_o^{'}, v_o e^{-r_h SS^*} - v_o e^{-r_p SS^*}), \tag{C.36}$$

where $v_o^{'}$ represents the maximum settling velocity and takes a value of $10{,}4\frac{m}{h}$, v_o represents the maximum Vessiling settling velocity and takes a value of $19{,}75\frac{m}{h}$, r_h represents the hindered zone settling parameter and takes a value of $0{,}000576\frac{m^3}{gSS}$, r_p represents the flocculant zone settling parameter and takes a value of $0{,}00286\frac{m^3}{gSS}$ and SS^* represents the suspended solids concentration, subject to a limiting condition defined as

$$SS^* = SS - SS_{min}, \tag{C.37}$$

where SS_{min} represents the minimum attainable suspended solids concentration calculated from

$$S_{min} = f_{ns} X_{in}, \tag{C.38}$$

where SS_{in} represents the mixed liquor suspended solids concentration entering the settling tank and f_{ns} represents the non-settable fraction and takes a value of 0,00228.

Finally, it is necessary to define two zones within the clarifier in order to determine the flow velocity in the clarifier [30]. The aforementioned zones are the clarification zone and the sedimentation zone, which are represented in Figure C.16

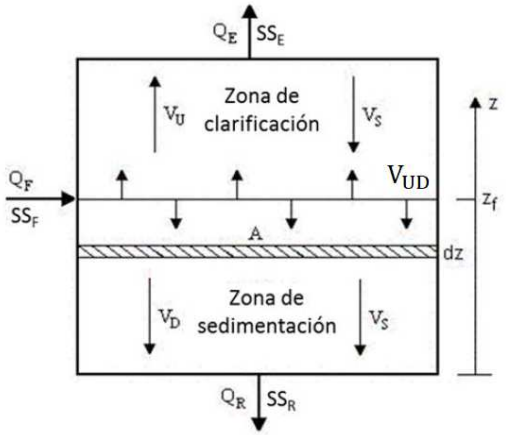

Figura C.16: Clarifier zones

where Q_F, Q_E and Q_R represent the inlet flow in the clarifier, the effluent flow and the header discharge, respectively; SS_F, SS_E and SS_R represent the suspended solids concentration in the clarifier inlet, in the effluent and in the recirulation, respectively; V_U, V_D and V_{UD} represent the flow velocity in the clarification zone, in the sedimentation zone and in the clarifier inlet, respectively; Z_f represents the height of the clarifier inlet. It should be noted that the suspended solids concentration in the clarifier inlet and in the outlet of the third reactor do coincide. Moreover, the inlet flow in the clarifier and the outlet flow of the third reactor do coincide.

As can be observed in Figure C.16, the height position of the clarifier inlet must be known in order to determine the height of the above-mentioned zones. The height position of the clarifier inlet, the top position of the sedimentation zone and the bottom position of the clarification zone do coincide. The characterization of the clarification and sedimentation zones is needed because the flow velocity in the clarifier depends on the z coordinate, as has been commented previously. The flow velocity which appears in Equation C.33 is determined as

$$V = \begin{cases} V_U = \frac{Q_E}{A} & \text{if } z > z_f \\ V_{UD} = \frac{Q_E}{A} - \frac{Q_R}{A} & \text{if } z = z_f \\ V_D = -\frac{Q_R}{A} & \text{if } z < z_f \end{cases} \tag{C.39}$$

where A is the surface area where the flow in the clarification and sedimentation zones are distributed, meaning the cross-sectional area of the clarifier.

Considering Equation C.34 and C.39, the mass balance model depends on the height z and using the Vesilind model can be written as

$$\begin{cases} \frac{\partial(SS)}{\partial t} = \left(-\frac{Q_E}{A} + k \cdot e^{-n \cdot SS}(1 - n \cdot SS)\right) \frac{\partial(SS)}{\partial z} + D_a \cdot \frac{\partial^2(SS)}{\partial^2 z} & \text{if } z > z_f \\ \frac{\partial(SS)}{\partial t} = \left(\frac{Q_R}{A} - \frac{Q_E}{A} + k \cdot e^{-n \cdot SS}(1 - n \cdot SS)\right) \frac{\partial(SS)}{\partial z} + D_a \cdot \frac{\partial^2(SS)}{\partial^2 z} & \text{if } z = z_f \\ \frac{\partial(SS)}{\partial t} = \left(\frac{Q_R}{A} + k \cdot e^{-n \cdot SS}(1 - n \cdot SS)\right) \frac{\partial(SS)}{\partial z} + D_a \cdot \frac{\partial^2(SS)}{\partial^2 z} & \text{if } z < z_f \end{cases} \tag{C.40}$$

Once all the variables of the model have been described, the clarifier is divided into a number of layers of equal thickness Δz, even though the volume of the clarifier could change due to the inflow and outflows. However, the problem is simplified considering that the volume of the clarifier is constant. This is because the volume variations are very small against the total volume. The number of layers is a parameter of the numerical integration. From the author's experience, 100 layers are suitable to trade off convergence and calculation time [31]. The aforementioned discretization using N number of layers is presented in Figure C.17

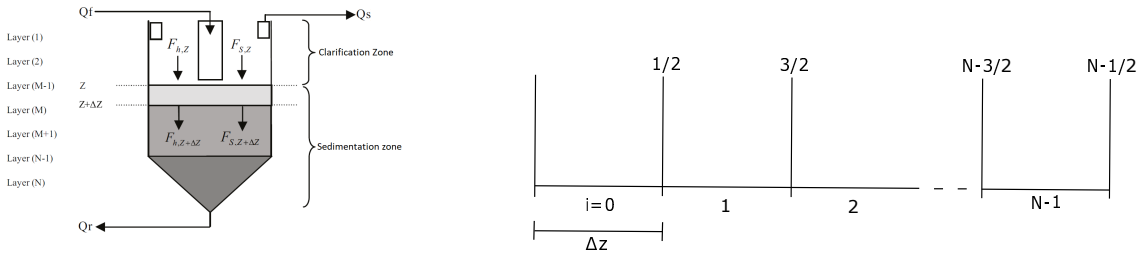

Figura C.17: Clarifier discretization

The time discretization is carried out using a time step which must not be less than the following calculation

$$\Delta t_{min} = \frac{CFL \cdot \Delta z}{\left|\lambda_{i+1/2}\right|}, \tag{C.41}$$

where CFL is the $Courant - Friedrichs - Lewy$ condition and takes a value of 1. $\lambda_{i+1/2}$ represents the velocity through the cell wall [32] and is written as follows

$$\lambda_{i+1/2} = \frac{F_{i+1} - F_i}{u_{i+1} - u_i}, \tag{C.42}$$

Once both discretizations have been presented, the numerical integration is detailed. It should be noted that the Equation C.40 is solved through an explicit method using Riemann's solver, with the exception of the diffusion term. The aforementioned term is integrated implicitly. The explicit integration without taking into account the diffusion term is carried out by integrating both members of the Equation C.31 [32], as follows

$$\int\int \left(\frac{\partial(SS)}{\partial t}\right) dzdt = -\int\int \left(\frac{\partial(F)}{\partial z}\right) dzdt, \tag{C.43}$$

where F represents the solid flux without taking into account the diffusion term, same as Equation C.28. Equation C.43 is evaluated in i cell and can be written as

$$SS_i^{n+1} = SS_i^n - \frac{\Delta t}{\Delta z}\left(F_{i+1/2}^- - F_{i-1/2}^+\right), \tag{C.44}$$

where SS_i^{n+1} represents the suspended solids concentration of i cell at a time corresponding to $n+1$. $F_{i+1/2}^-$ represents the solid flux from i-1 cell entering into the cell i and $F_{i-1/2}^+$ represents the solid flux from i+1 cell entering into the cell i, as follows

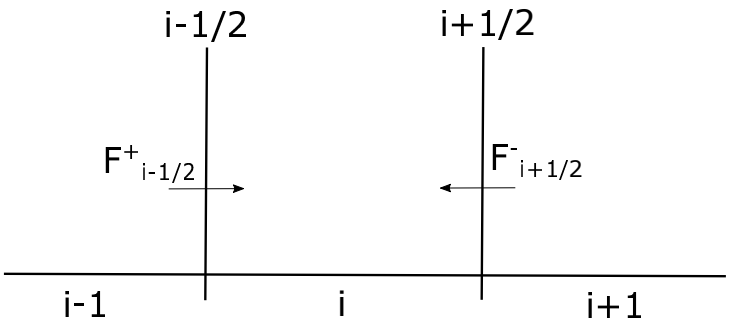

Figura C.18: Solid flux

The solid flux through the wall can be written as

$$\begin{cases} F^{-}_{i+1/2} = SS_i u_i + u^{-}\left(SS_{i+1} - SS_i\right) \\ F^{+}_{i-1/2} = SS_i u_i - u^{+}\left(SS_i - SS_{i-1}\right) \end{cases} \tag{C.45}$$

where u^{-} and u^{+} are

$$\begin{cases} u^{-} = \frac{1}{2}\left(\lambda_{i+1/2} - \left|\lambda_{i+1/2}\right|\right) \\ u^{+} = \frac{1}{2}\left(\lambda_{i-1/2} + \left|\lambda_{i-1/2}\right|\right) \end{cases} \tag{C.46}$$

The boundary conditions express the absence of settling at the top and at the bottom of the clarifier [33], meaning that the solid flux is equal to zero at the system boundaries. Moreover, an extra boundary condition can be imposed at the inlet of the clarifier. The aforementioned boundary condition represents the concentration change of the inlet cell due to the inlet of the solid flux, considering that the inlet cell does not change his volume. The aforementioned conditions are represented as

$$\begin{cases} V_s \cdot SS = 0 & \text{if } z = H \text{ or } z = 0 \\ SS^{n+1} = SS^{n} + \frac{Q_F SS_F \Delta t}{A \Delta z} & \text{if } z = z_f \end{cases} \tag{C.47}$$

where SS_F represents the suspended solids concentration at the inlet of the clarifier and H represents the maximum height of the clarifier. Considering that there is no flow velocity at the inlet of the clarifier, effluent and header and the inlet cell has an initial concentration that takes a value of $100\frac{g}{m^2}$, the distribution of the concentration throughout the clarifier in time is presented in Figure C.19. The aforementioned Figure represents the evolution of the concentration within the clarifier from 1400 seconds to 2300 seconds, meaning that the time difference between consecutive graphics is 100 seconds

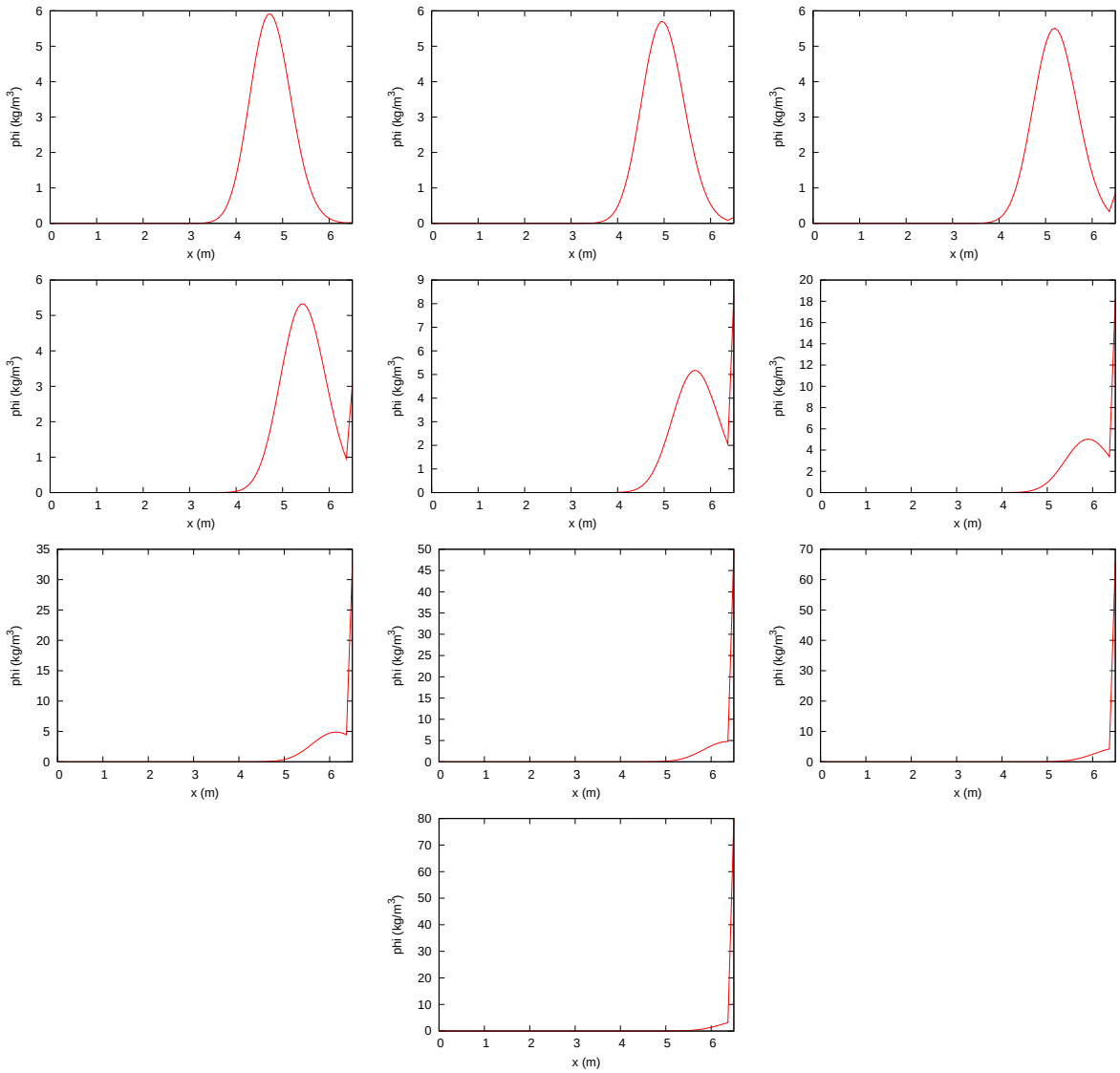

Figura C.19: Distribution of the concentration throughout the clarifier from 1400 to 2300 seconds.

The diffusion term must be implemented in the model in order to simulate the clarifier performance as real as possible. For that purpose, it is necessary to integrate the Equation C.40 again, but in this case is solved through a implicit method using Thomas' algorithm [34]. This is because the solid flux is defined in a different way, as follows

$$\begin{cases} F_{i+1/2} = \left(D_a \frac{\partial(SS)}{\partial z}\right)_{i+1/2} = (D_a)_{i+1/2} \frac{(SS_{i+1} - SS_i)}{\Delta z} \\ F_{i-1/2} = \left(D_a \frac{\partial(SS)}{\partial z}\right)_{i-1/2} = (D_a)_{i+1/2} \frac{(SS_i - SS_{i-1})}{\Delta z} \end{cases} \tag{C.48}$$

On basis of the aforementioned definition of solid flux, Equation C.44 is evaluated in i cell and can be written as

$$-\Delta t \frac{(D_a)_{i-1/2}}{\Delta x^2} SS_{i-1}^{n+1} + \left(1 + \Delta t \frac{(D_a)_{i+1/2}}{\Delta x^2} + \Delta t \frac{(D_a)_{i-1/2}}{\Delta x^2}\right) SS_i^{n+1} - \Delta t \frac{(D_a)_{i+1/2}}{\Delta x^2} SS_{i+1}^{n+1} = SS_i^n \tag{C.49}$$

As can be observed, the above-mentioned equation relates the concentration of the i cell at n time, which is known due to the convection, to the concentration of the $i-1$, i and $i+1$ cell at $n+1$ time, which are the unknown parameters. It should be noted that the value of diffusion term ($(D_a)_{i+1/2}$) depends on the z position of the wall where is being evaluated, as follows

$$(D_a)_{i+1/2} = \begin{cases} 0 \frac{m^2}{h} & \text{if } i = 0 \text{ or } i = N-1 \\ 0{,}54 \frac{m^2}{h} & otherwise \end{cases} \tag{C.50}$$

where the value of $0{,}54 \frac{m^2}{h}$ has been extracted from Hamilton's model, as has been commented. The aforementioned equation expresses the absence of diffusion at the top and at the bottom of the clarifier. In order to simplify the naming, Equation C.49 can be written using constant coefficients as follows

$$a_i SS_{i-1}^{n+1} + b_i SS_i^{n+1} + c_i SS_{i+1}^{n+1} = SS_i^n \tag{C.51}$$

where a, b and c are the constant coefficients of Equation C.49. The aforementioned Equation can be written in matrix form as follows

$$A \cdot \begin{pmatrix} SS_0 \\ SS_1 \\ . \\ . \\ . \\ SS_{N-2} \\ SS_{N-1} \end{pmatrix}_{n+1} = \begin{pmatrix} SS_0 \\ SS_1 \\ . \\ . \\ . \\ SS_{N-2} \\ SS_{N-1} \end{pmatrix}_{n} \tag{C.52}$$

where A is a tridiagonal matrix which can be written as

$$A = \begin{pmatrix} b_0 & c_0 & . & . & . & 0 & 0 \\ a_1 & b_1 & c_1 & . & . & . & 0 \\ . & . & . & . & . & . & . \\ . & . & . & . & . & . & . \\ . & . & . & . & . & . & . \\ 0 & . & . & . & a_{N-2} & b_{N-2} & c_{N-2} \\ 0 & 0 & . & . & . & a_{N-1} & b_{N-1} \end{pmatrix} \tag{C.53}$$

The derivation of the Thomas' algorithm is a special case of Gaussian elimination of the aforementioned matrix [34]. The first step consists of eliminating the lower diagonal (a_i coefficients). For that purpose,

it is necessary to multiply the first row by a_3 , the second row by b_2, subtract both equations and divide by b_2. Once all these operations have been made, the second equation is written as

$$\left(b_3 - \frac{a_3 c_2}{b_2}\right) SS_3^{n+1} + c_3 SS_4^{n+1} = SS_3^n - \frac{a_3}{b_2} SS_2^n \tag{C.54}$$

The above-mentioned equation can be written as

$$b_3^{'} SS_3^{n+1} + c_3 SS_4^{n+1} = SS_3^{n'} \tag{C.55}$$

The above-mentioned equation can be evaluated in all the rows running through the system of equations. For that purpose, the next equation must be evaluated in all the rows

$$b_i^{'} SS_i^{n+1} + c_i SS_{i+1}^{n+1} = SS_i^{n'} \tag{C.56}$$

However, the definition of the parameters $b_i^{'}$ and $SS_i^{n'}$ depends on the row which is being evaluated, as follows

$$b_i^{'} = \begin{cases} b_i & \text{if } i = 0 \text{ or } i = N-1 \\ b_i - \frac{a_i c_{i-1}}{b_{i-1}} & otherwise \end{cases} \tag{C.57}$$

$$SS_i^{n'} = \begin{cases} SS^n & \text{if } i = 0 \text{ or } i = N-1 \\ SS_i^n - \frac{a_i}{b_{i-1}} SS_{i-1}^n & otherwise \end{cases} \tag{C.58}$$

Once Equation C.56 has been evaluated in all the rows, the lower diagonal of the matrix A, which has been presented at Equation C.53, is eliminated. Hence, the resulting matrix is written as

$$A^{'} = \begin{pmatrix} b_0 & c_0 & . & . & . & 0 & 0 \\ . & b_1^{'} & c_1 & . & . & . & 0 \\ . & . & . & . & . & . & . \\ . & . & . & . & . & . & . \\ . & . & . & . & . & . & . \\ 0 & . & . & . & . & b_{N-2}^{'} & c_{N-2} \\ 0 & 0 & . & . & . & . & b_{N-1}^{'} \end{pmatrix}, \tag{C.59}$$

so that the matrix-equation, which has been presented at Equation C.52, is written as

$$A^{'} \cdot \begin{pmatrix} SS_0 \\ SS_1 \\ . \\ . \\ . \\ SS_{N-2} \\ SS_{N-1} \end{pmatrix}_{n+1} = \begin{pmatrix} SS_0 \\ SS_1^{'} \\ . \\ . \\ . \\ SS_{N-2}^{'} \\ SS_{N-1}^{'} \end{pmatrix}_{n} \tag{C.60}$$

The latest equation of the aforementioned matrix-equation just contains one unknown parameter, SS_{N-1}^{n+1}, which can be solved directly as follows

$$SS_{N-1}^{n+1} = \frac{SS_{N-1}^{n'}}{b_{N-1}^{'}}, \tag{C.61}$$

The rest of unknown parameters can be solved running through the system of equations in the opposite direction. For that purpose, it is necessary to solve the next equation for all the rows, with exception of the first row, as follows

$$SS_i^{n+1} = \frac{SS_i^{n'} - c_i SS_{i+1}^{n+1}}{b_i'}. \tag{C.62}$$

Considering that there is no flow velocity at the inlet of the clarifier, effluent and header, the inlet cell has an initial concentration that takes a value of $100\frac{g}{m^3}$ and the diffusion mechanism is present, the distribution of the concentration throughout the clarifier in time is presented in Figure C.20. The aforementioned Figure represents the evolution of the concentration within the clarifier from 1400 seconds to 2300 seconds, meaning that the time difference between consecutive graphics is 100 seconds

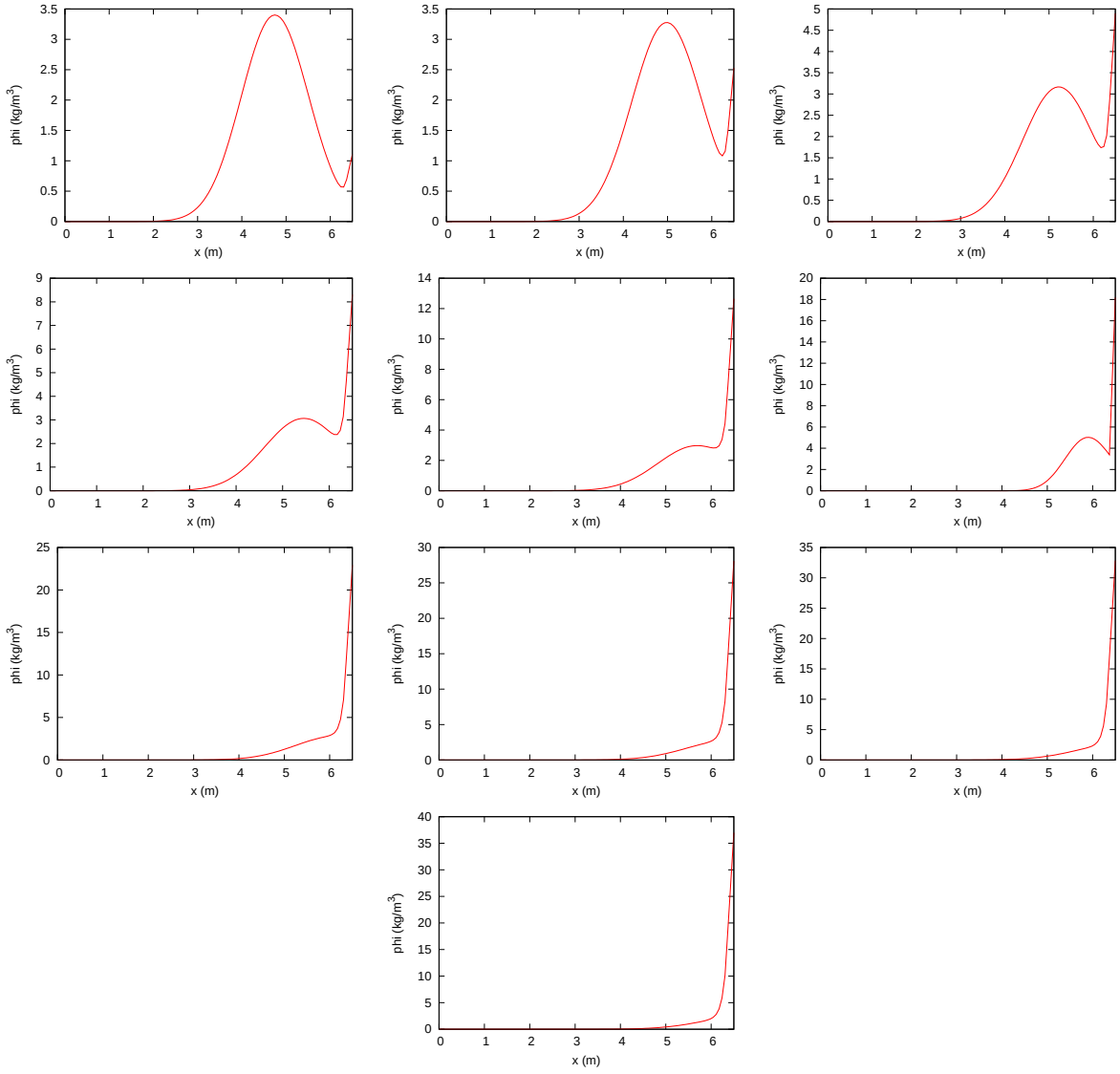

Figura C.20: Distribution of the concentration throughout the clarifier taking into account the diffusion term, from 1400 to 2300 seconds.

C.5. Initial conditions

In this Section, the initial conditions are set in order to simulate the Models which have been described in Subsections C.4.1, C.4.2 and C.4.3. The initial conditions are the influent flow and the recirculation ratio, depicted in Figure C.21; the concentrations of the influent, presented in Figure C.22; and the initial concentration of the 13 species in the reactors and in the clarifier, depicted in Tables C.6 and C.7. It should be noted that the initial conditions of all Models are the same, except the initial concentration of the 13 species in the reactors and in the clarifier, where applicable.

First of all, the influent flow and the recirculation ratio are estimated. For this purpose, the evolution over time of the influent flow and recirculation ratio, which have been presented in Figure C.4, are used as a reference. The evolution over time of the aforementioned parameters are presented in Figure C.21.

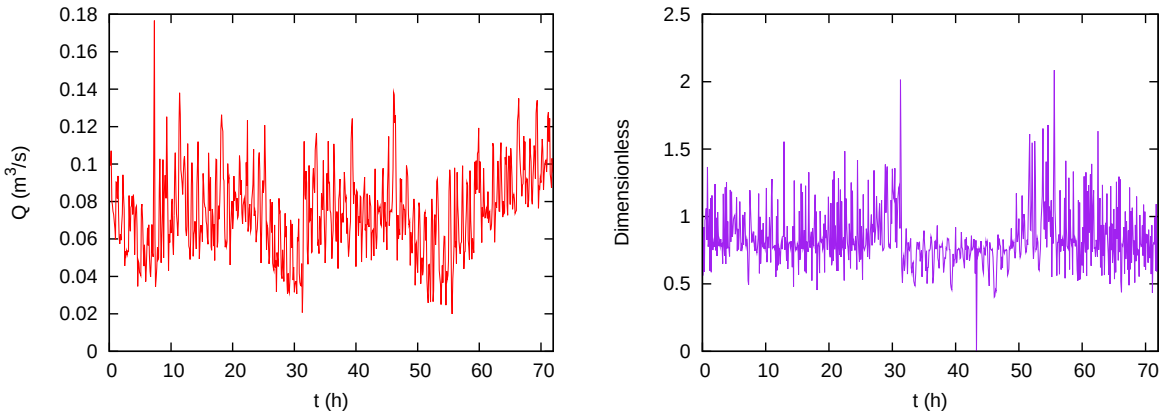

Figura C.21: Influent (—) and recirculation ratio (—).

The concentrations of the influent are set. For this purpose, the evolution over time of the DBO, DQO, total nitrogen, ammonium and nitrate concentrations, which have been presented in Figure C.3, are used as a reference. However, the daily averages of these measured values are also used in order to interpolate the remaining values and reduce the input data. Besides, experimental ratios are set in order to estimate the remaining concentrations. The aforementioned ratios are

- Slowly biodegradable substrate concentration over readily biodegradable substrate (X_s/S_s). This ratio takes a value of 5.13.
- Particulate inert organic matter over soluble inert organic matter (X_i/S_i). This ratio takes a value of 20.82.
- Particulate biodegradable organic nitrogen over soluble biodegradable organic nitrogen (X_{nd}/S_{nd}). This ratio takes a value of 14.26.

By using these ratios and the above-mentioned daily averages, the daily concentration of the 13 species in the influent are estimated. Hence, the aforementioned concentrations during 17th, 18th and 19th April are presented in Figure C.22.

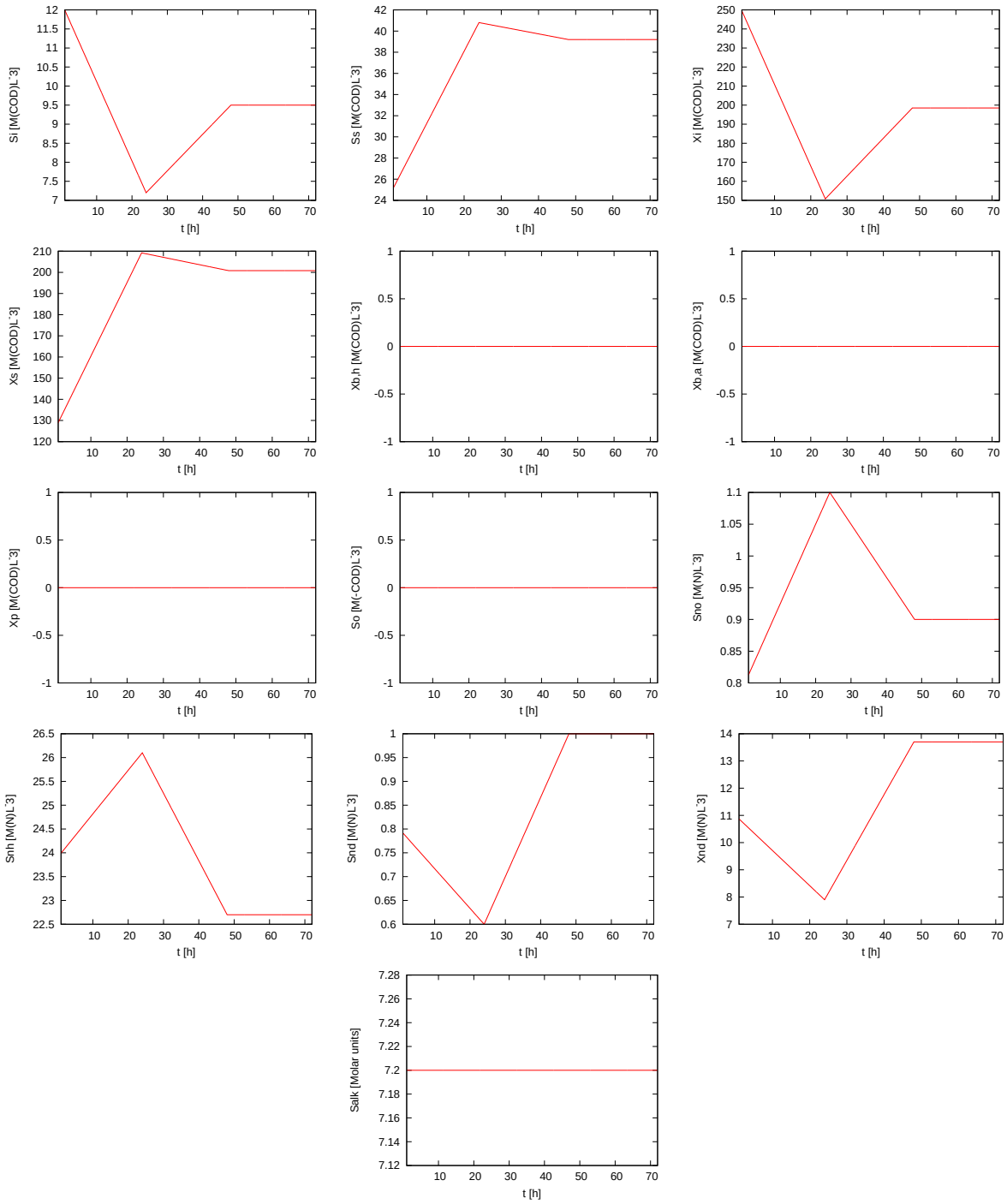

Figura C.22: Concentration of the 13 species in effluent.

Finally, the initial concentration of the 13 species in the reactors and in the clarifier are set. For that purpose, the daily concentrations of the influent provided by the company during 16th April are used as inputs in order to carry out a simulation. The aforementioned simulation is carried out until the concentrations in the effluent reach the steady-state. The concentrations in the reactors at that time are used as initial concentrations in the reactors for the wastewater plant simulations, as well as in the clarifier. The initial concentration of the 13 species in the reactors used in the Model presented in Subsection C.4.1 are presented in Table C.6

Component	First Reactor	Second Reactor	Third Reactor	Dimensions
S_S	6.88	5.274	4.096	$M(COD)L^{-3}$
S_I	4.6	4.6	4.6	$M(COD)L^{-3}$
S_O	0.0	0.3773	0.3048	$M(O_2)L^{-3}$
S_{NO}	0.0686	2.7225	4.107	$M(N)L^{-3}$
S_{NH}	14.55	9.235	6.916	$M(N)L^{-3}$
S_{ND}	0.2013	1.291	1.2898	$M(N)L^{-3}$
S_{ALK}	3.898	3.33	3.065	$mol(HCO_3^-)L^{-3}$
X_I	210.58	2609.845	2610.624	$M(COD)L^{-3}$
X_S	135.514	61.85	25.8	$M(COD)L^{-3}$
$X_{B,H}$	495.4	530.18	544.73	$M(COD)L^{-3}$
$X_{B,A}$	32.757	33.608	34.09	$M(COD)L^{-3}$
X_P	480.3	483.479	485.998	$M(COD)L^{-3}$
X_{ND}	9.316	4.516	2.0	$M(N)L^{-3}$

Cuadro C.6: Initial concentration of the 13 species in the reactors.

The initial concentration of the 13 species in the reactors and in the clarifier used in the Model presented in Subsection C.4.2 are presented in Table C.7

Component	First Reactor	Second Reactor	Third Reactor	Clarifier	Dimensions
S_S	13.577	6.368	5.234	2.92	$M(COD)L^{-3}$
S_I	4.6	4.6	4.6	4.6	$M(COD)L^{-3}$
S_O	0.0	0.614	0.4358	0.0006	$M(O_2)L^{-3}$
S_{NO}	0.00598	1.886	2.544	0.285	$M(N)L^{-3}$
S_{NH}	15.591	10.048	7.899	8.9625	$M(N)L^{-3}$
S_{ND}	0.0657	1.364	1.458	0.4703	$M(N)L^{-3}$
S_{ALK}	3.977	3.447	3.247	3.484	$mol(HCO_3^-)L^{-3}$
X_I	2879.408	2878.8	2879.707	2234.479	$M(COD)L^{-3}$
X_S	168.87	95.35	53.32	61.547	$M(COD)L^{-3}$
$X_{B,H}$	490.5	528.86	547.42	477.808	$M(COD)L^{-3}$
$X_{B,A}$	33.274	34.07	34.498	30.328	$M(COD)L^{-3}$
X_P	530.388	533.6	536.06	402.52	$M(COD)L^{-3}$
X_{ND}	11.764	6.97	4.068	5.136	$M(N)L^{-3}$

Cuadro C.7: Initial concentration of the 13 species in the reactors and in the clarifier.

The aforementioned initial concentration of the 13 species in the reactors and in the clarifier are also used in the Models presented in Subsection C.4.3, where Takacs and Vesilind's definition are used. This is because the steady state cannot be achieved due to the number of parameters which must be calibrated. It should be noted that the concentrations of the 13 species in the clarifier are the same for all cells.

C.6. Results

In this section, numerical results of the simulation for the models described in Subections C.4.1, C.4.2 and C.4.3 are presented. It has been noted that the aforementioned simulation has been carried out during

3 days (72 hours). The evolution over time of the volumetric flow of the effluent and the purge for the Models described in Subections C.4.1, C.4.2 and C.4.3 are presented in Figures C.23, C.24, C.25 and C.26, respectively. The evolution over time of the concentration of the components in the effluent for the Models described in Subections C.4.1, C.4.2 and C.4.3 are depicted in Figures C.27, C.28, C.29, C.30, C.31, C.32, C.33 and C.34 .

The diffusion coefficient used in the Models described in Subsection C.4.3 are different with regard to the diffusion coefficient set by Hamilton. This is because the Hamilton's coefficient is an experimental value that does not apply to the Models described in Subsection C.4.3. Hence, the aforementioned coefficient has been calibrated for each simulation. For the simulation where Vesilind's model is used in order to estimate the sedimentation velocity of the particulate components, the diffusion term takes a value of 2.15 m^2/h. However, for the simulation where Takacs' model is used in order to estimate the sedimentation velocity of the particulate components, the diffusion term takes a value of 0.15 m^2/h. This discrepancy is due to the difference of the definition of both velocities. While Takacs' definition takes into account the hindered and the flocculent velocity of the particulate components, Vesilind's model only takes into account one exponential velocity. Moreover, Takacs' model has a maximum limit velocity, while Vesilind's definition has not.

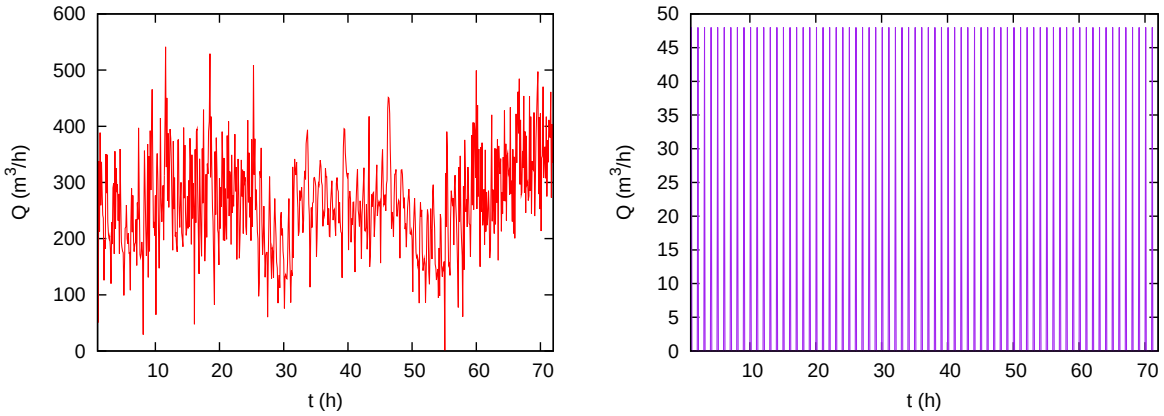

Figura C.23: Volumetric flow of the effluent (—) and purge (—) using the Model described in Subsection C.4.1.

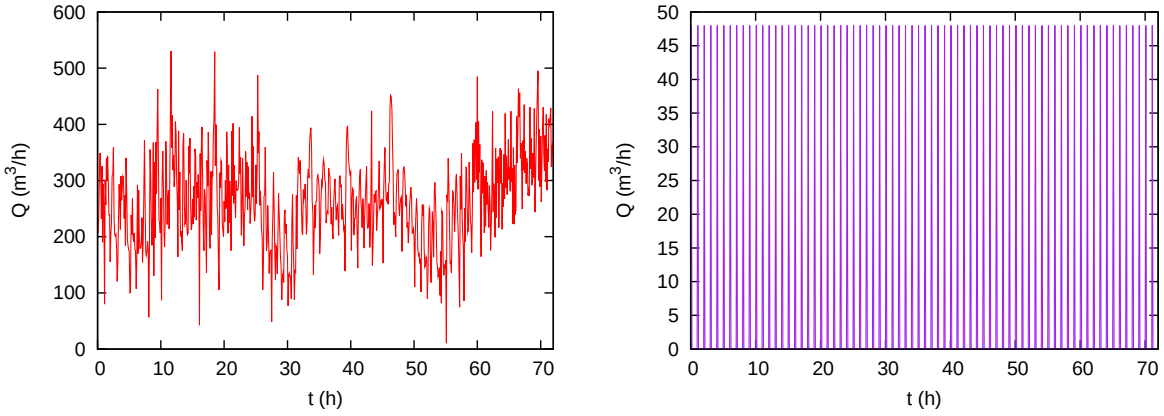

Figura C.24: Volumetric flow of the effluent (—) and purge (—) using the Model described in Subsection C.4.2.

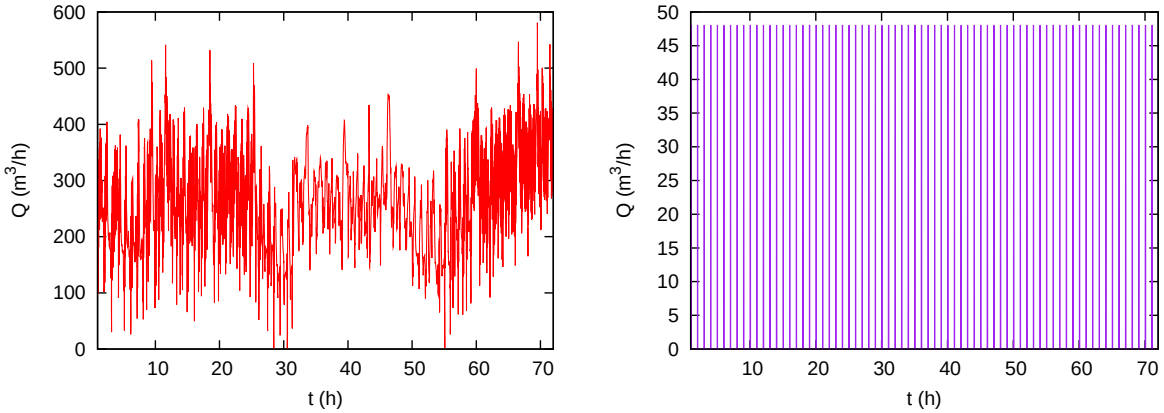

Figura C.25: Volumetric flow of the effluent (—) and purge (—) using the Model described in Subsection C.4.3 (Takacs).

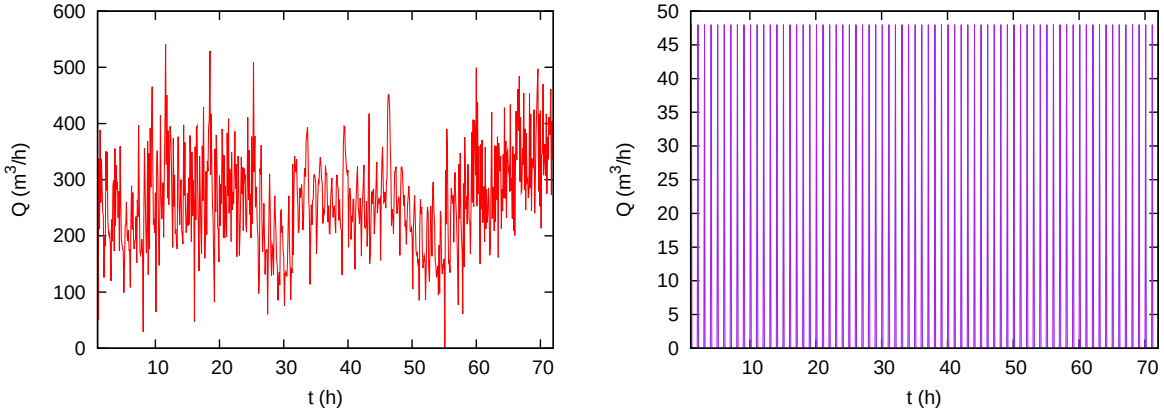

Figura C.26: Volumetric flow of the effluent (—) and purge (—) using the Model described in Subsection C.4.3 (Vesilind).

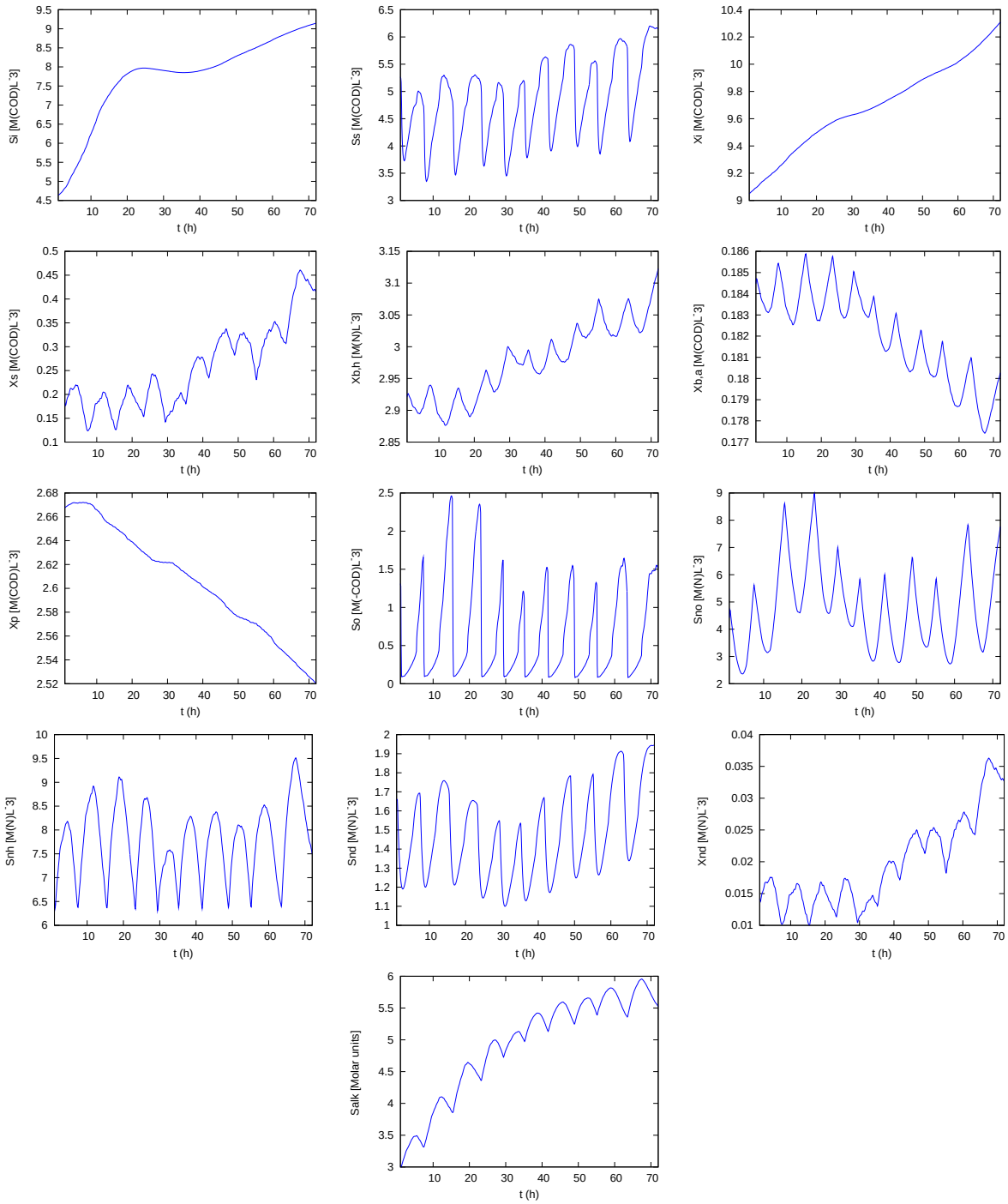

Figura C.27: Concentration of the 13 species in the effluent using the Model described in Subsection C.4.1.

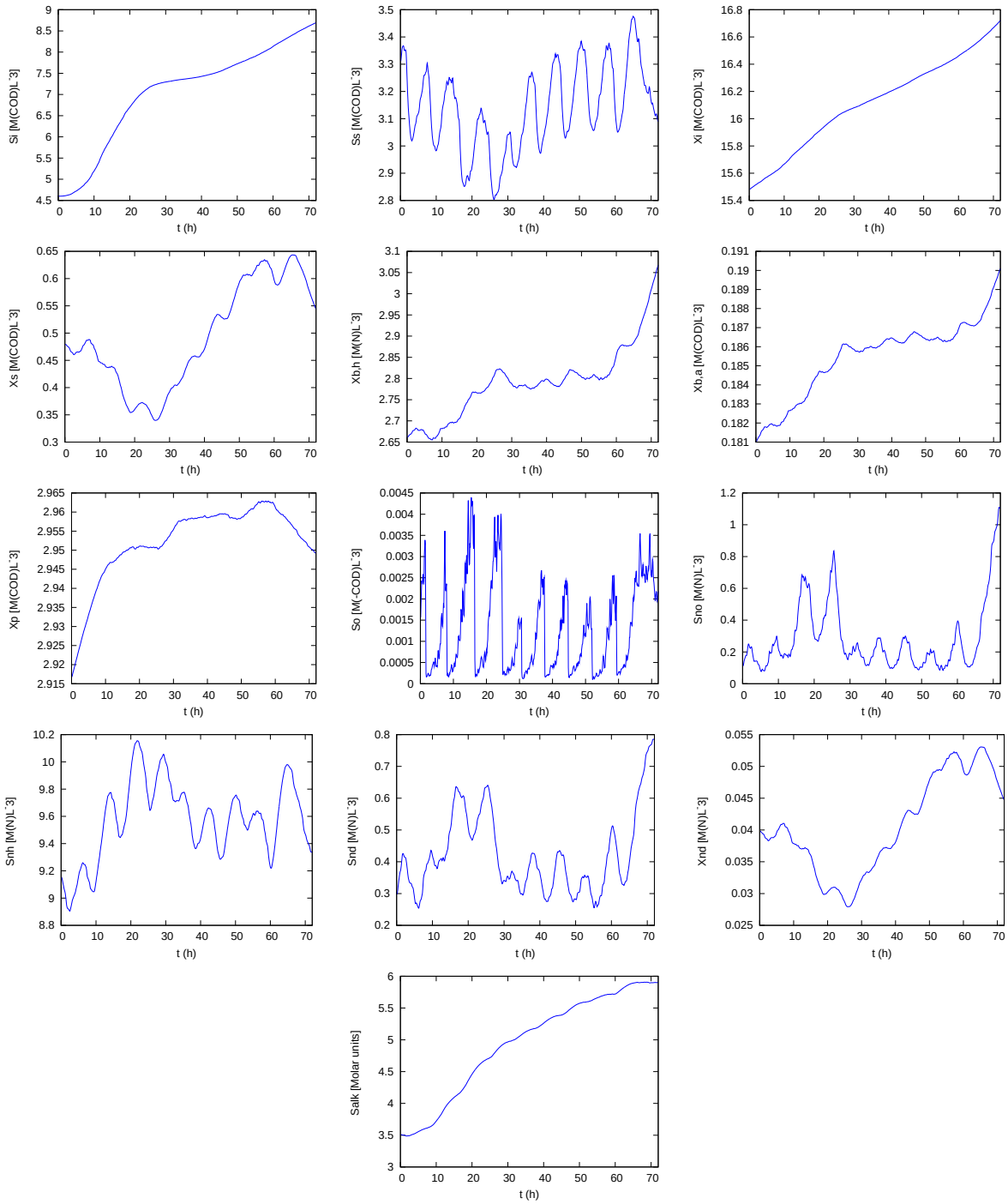

Figura C.28: Concentration of the 13 species in effluent using the Model described in Subsection C.4.2.

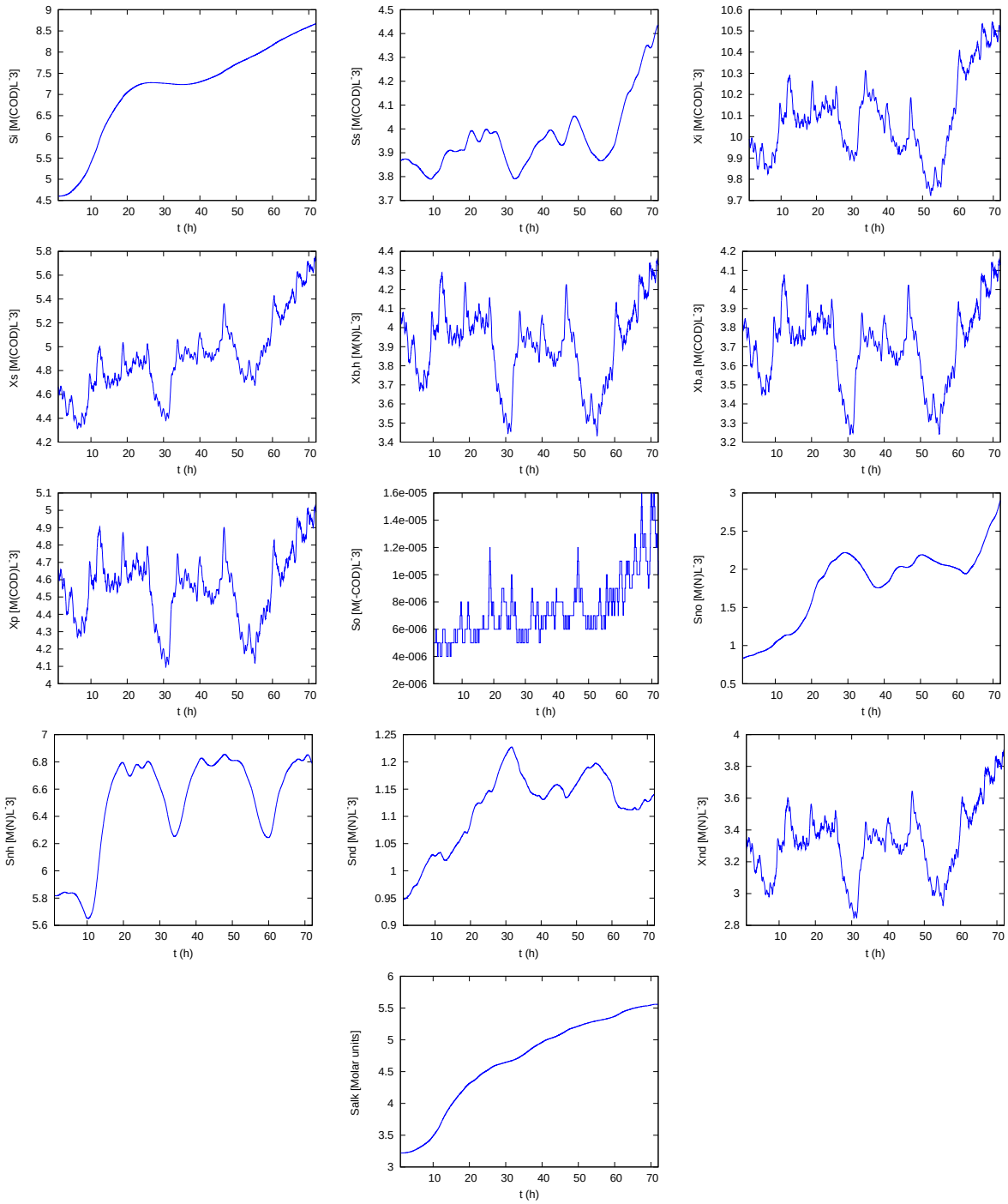

Figura C.29: Concentration of the 13 species in effluent using the Model described in Subsection C.4.3 (Takacs).

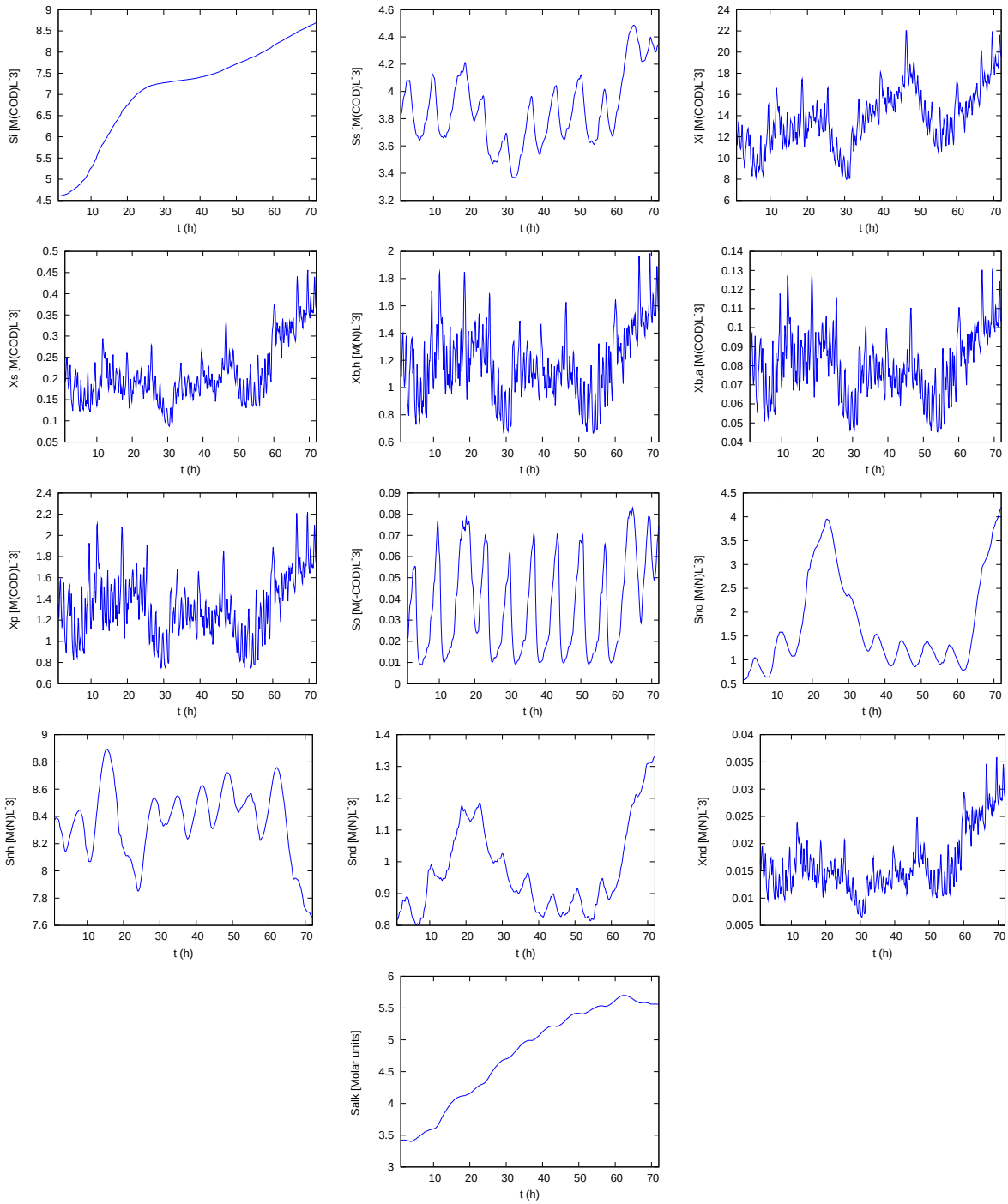

Figura C.30: Concentration of the 13 species in effluent using the Model described in Subsection C.4.3 (Vesilind).

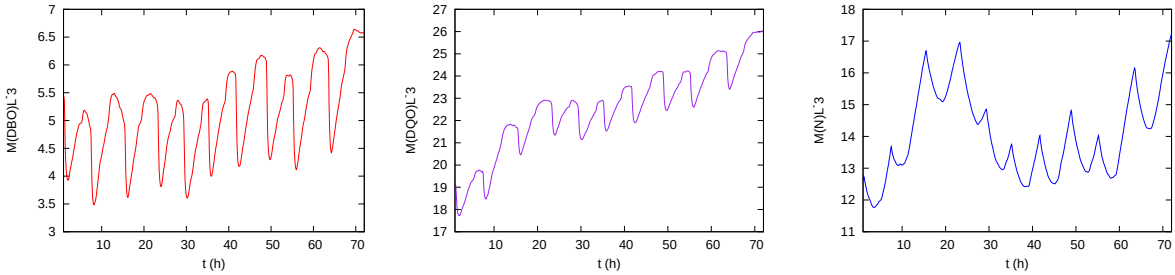

Figura C.31: Concentration of DBO (—), DQO (—) and total nitrogen (—) in the effluent using the Model described in Subsection C.4.1.

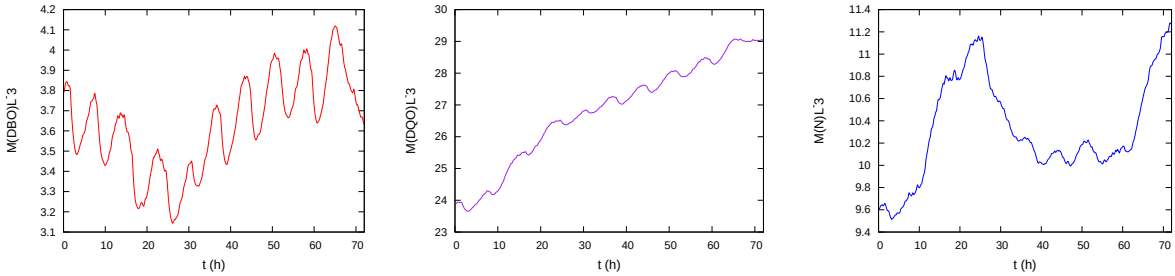

Figura C.32: Concentration of DBO (—), DQO (—) and total nitrogen (—) in the effluent using the Model described in Subsection C.4.2.

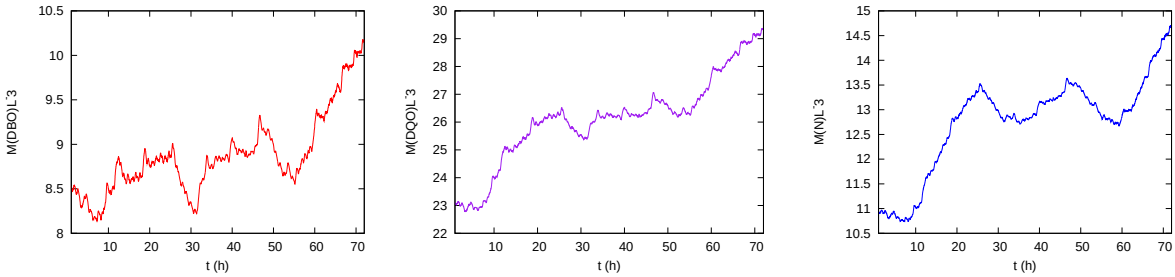

Figura C.33: Concentration of DBO (—), DQO (—) and total nitrogen (—) in the effluent using the Model described in Subsection C.4.3 (Takacs).

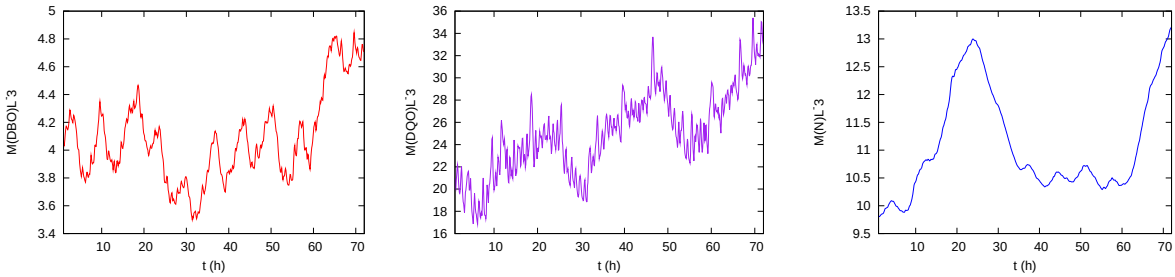

Figura C.34: Concentration of DBO (—), DQO (—) and total nitrogen (—) in the effluent using the Model described in Subsection C.4.3 (Vesilind).

C.7. Conclusions

In this Section, a comparison between the results of the simulations and the provided infomation are described.

The real concentrations of DBO, DQO and total nitrogen in the effluent and the results of the simulation described in Subsection C.4.1 are depicted in Figure C.35

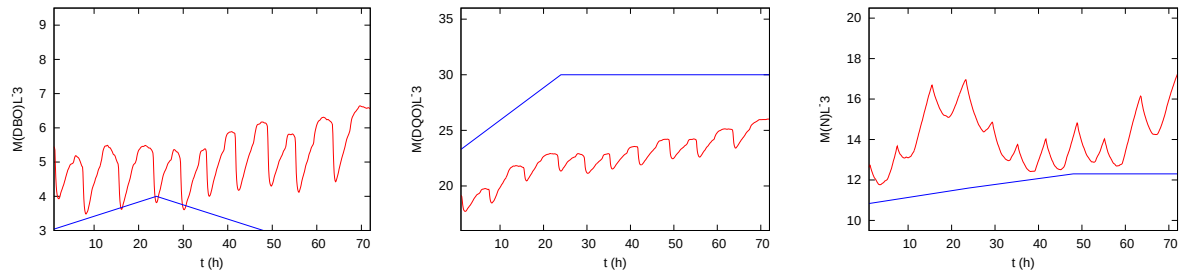

Figura C.35: Results of the simulation described in Subsection C.4.1 (—) and real concentrations in the effluent (—).

Firstly, there are many discrepancies between the DBO concentration of the simulation and the real DBO concentration in the effluent. As can be observed, the evolution over time of the DBO concentration of the simulation differs with regard to the evolution over time of the real DBO concentration. Besides, the maximum and minimum values which have been reached in the simulation are different from the real concentration values. Furthermore, the DQO concentration of the simulation and the real DQO concentration in the effluent do not converge to a similar value. Moreover, the evolution over time of the real DQO concentration has steeper slope than the evolution over time of the DQO concentration of the simulation. Finally, in terms of total nitrogen concentration, there are discrepancies between the real measured values and the results of the simulation. On the one hand, the evolution over time of the total nitrogen concentration of the simulation differs with regard the evolution over time of the real total nitrogen concentration, especially in the intervals between 20 and 40 hours and between 60 and 70 hours. On the other hand, the maximum and minimum values which have been reached in the simulation are upper than the real concentration values.

The real concentrations of DBO, DQO and total nitrogen in the effluent and the results of the simulation described in Subsection C.4.2 are depicted in Figure C.36

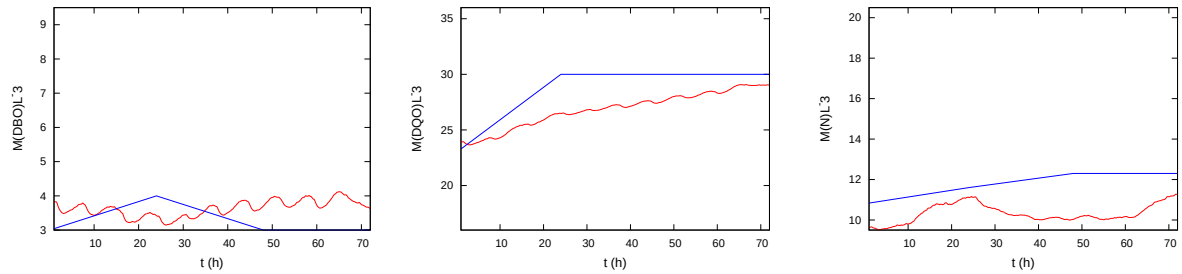

Figura C.36: Results of the simulation described in Subsection C.4.2 (—) and real concentrations in the effluent (—).

There are some discrepancies between the DBO concentration of the simulation and the real DBO concentration in the effluent. As can be observed, the evolution over time of the DBO concentration of the simulation differs with regard to the evolution over time of the real DBO concentration. However, the maximum and minimum values which have been reached in the simulation are similar to the real

concentration values. Furthermore, the DQO concentration of the simulation and the real DQO concentration in the effluent do converge to the similar value. Moreover, the evolution over time of the real DQO concentration has steeper slope than the evolution over time of the DQO concentration of the simulation. Finally, in terms of total nitrogen concentration, there are discrepancies between the real measured values and the results of the simulation. As can be observed, the evolution over time of the total nitrogen concentration of the simulation differs with regard the evolution over time of the real total nitrogen concentration, especially in the intervals between 20 and 40 hours and between 60 and 70 hours. Besides, the maximum and minimum values which have been reached in the simulation are lower than the real concentration values.

The real concentrations of DBO, DQO and total nitrogen in the effluent and the results of the simulation described in Subsection C.4.3 using Takacs' definition of sedimentation velocity are depicted in Figure C.37.

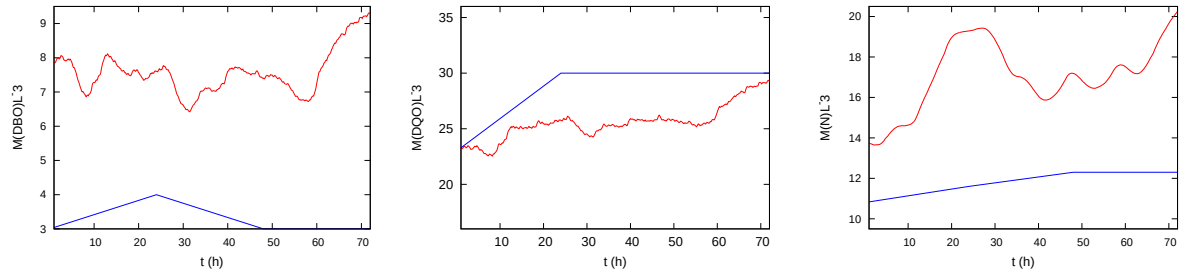

Figura C.37: Results of the simulation described in Subsection C.4.3 (—), using Takacs' definition of settling velocity, and real concentrations in the effluent (—).

On the one hand, there are many discrepancies between the DBO concentration of the simulation and the real DBO concentration in the effluent. As can be observed, the evolution over time of the DBO concentration of the simulation differs with regard to the evolution over time of the real DBO concentration. Besides, the maximum and minimum values which have been reached in the simulation are different from the real concentration values. On the other hand, the DQO concentration of the simulation and the real DQO concentration in the effluent do converge to the similar value. Moreover, the evolution over time of the real DQO concentration has steeper slope than the evolution over time of the DQO concentration of the simulation. Finally, in terms of total nitrogen concentration, there are many discrepancies between the real measured values and the results of the simulation. Firstly, the evolution over time of the total nitrogen concentration of the simulation differs with regard the evolution over time of the real total nitrogen concentration, especially in the intervals between 10 and 30 hours. Secondly, the maximum value which have been reached in the simulation are much higher than the real concentration values.

The real concentrations of DBO, DQO and total nitrogen in the effluent and the results of the simulation described in Subsection C.4.3 using Vesilind's definition of sedimentation velocity are depicted in Figure C.38.

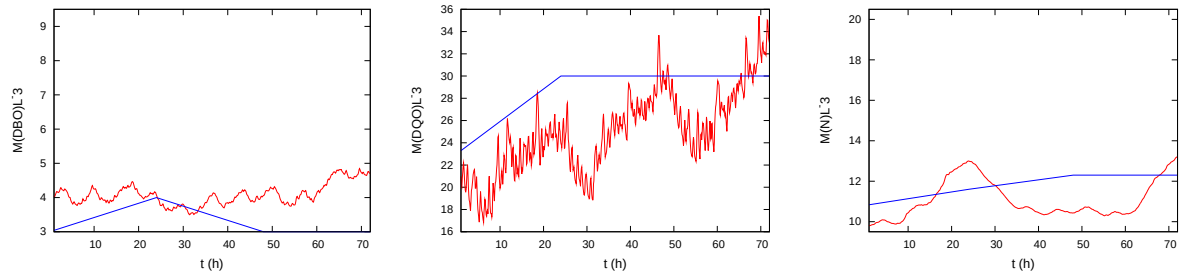

Figura C.38: Results of the simulation described in Subsection C.4.3 (—), using Vedilind's definition of settling velocity, and real concentrations in the effluent (—).

There are some discrepancies between the DBO concentration of the simulation and the real DBO concentration in the effluent. As can be observed, the evolution over time of the DBO concentration of the simulation differs with regard to the evolution over time of the real DBO concentration. However, the maximum and minimum values which have been reached in the simulation are slightly higher than the real concentration values. Furthermore, the DQO concentration of the simulation and the real DQO concentration in the effluent do converge to a higher but similar value. Moreover, the evolution over time of the real DQO concentration has steeper slope than the evolution over time of the DQO concentration of the simulation. Finally, in terms of total nitrogen concentration, there are discrepancies between the real measured values and the results of the simulation. As can be observed, the evolution over time of the total nitrogen concentration of the simulation differs with regard the evolution over time of the real total nitrogen concentration, especially in the intervals between 20 and 40 hours and between 60 and 70 hours. Besides, the maximum value which has been reached in the simulation are higher than the real concentration values, while the minimum value which has been reached in the simulation are lower than the real concentration values.

Adding to the Model described in Subsection C.4.1 the ASM1 processes within the clarifier, some improvements are achieved. The maximum and minimum values of the DBO concentration in the effluent are more alike to the real concentration values using the model described in Subsection C.4.2. Besides, the evolution over time and the maximum and minimum values of the DQO concentration in the effluent are also more alike to the real concentration values using the aforementioned model. Finally, the maximum and minimum values of the total nitrogen concentration in the effluent are more closer to the real concentration values, although the results of the Model described in Subsection C.4.1 as well as the results of Model described in Subsection C.4.2 differ with regard the real values.

Adding to the Model described in Subsection C.4.2 the clarifier caracterization, some differences are occurred. Using Takacs' definition of the settling velocity of particulate components, DBO and total nitrogen concentration are less alike to the real values than in the Model described in Subsection C.4.2. In terms of DQO, both models are similar. However, using Vesilind's definition of the settling velocity of particulate components, the concentrations are similar to the real values like in the Model described in Subsection C.4.2. In terms of DBO, the reached values are slighly higher than in the Model described in Subsection C.4.2. The concentration of DQO is also similar but the its variability is higher than in the Model described in Subsection C.4.2. Finally, the total nitrogen concentration values are more alike to the real values than in the Model described in Subsection C.4.2.

As conclusion, the evolution over time of the above-mentioned concentrations are slightly different between the results of the simulations and the reality. These discrepancies are fundamentally due to the average values which are used as boundary conditions in the simulation, as well as the experimental ratios which have been presented in Subsection C.5. In terms of boundary conditions, the initial concentrations of the 13 species in the reactors and in the clarifier have been set through a simulation described in Subsection C.5, as has been commented. Hence, the purge calculation as well as the aforementioned initial concentrations are surely different to the reality due to the discrepancy between the real sludge

quality and the sludge quality of the Models. Finally, the results of the simulation using a clarifier discretization are similar to the reality like the results of simulation where the aforementioned discretization is not include, although the clarifier discretization implies a larger number of parameters which must be calibrated. The aforementioned statement is true only if the Vesilind's definition of settling velocity is used. This is because Vesilind's model takes into account an experimental parameter (SVI) which has been determined by the plant coordinator, while Takacs' does not include any experimental parameter. Hence, it can be concluded that the clarifier discretization could be added to the model if the parameteres which have been used are calibrated properly.